Energy geostructures: The case of the Cleunay station in Rennes

Auteur : Sauvenier, Jeanne
Promoteur(s) : François, Bertrand
Faculté : Faculté des Sciences appliquées
Diplôme : Master en ingénieur civil des mines et géologue, à finalité spécialisée en géologie de l'ingénieur et de l'environnement
Année académique : 2022-2023
URI/URL : http://hdl.handle.net/2268.2/17716

University of Liège

Faculty of Applied Sciences

Energy geostructures : The case of the Cleunay station in Rennes

Master's Thesis completed by

Sauvenier Jeanne

in order to obtain the degree of Master of Science in Mine and Geology Engineering

Supervisors :
Mme Alice Di Donna
M. Bertrand François

Academic Year 2022-2023

Abstract

In 2023, the IPCC published its 6th synthesis report describing and assessing the current and future consequences of global warming. Like its predecessors, this report also raises the issue of greenhouse gases, which are one of the main causes of the problem. The sources of greenhouse gas emissions are many and varied. However, 45% of these emissions come from the combustion of fuels for electricity and heat. Combustion for schools, shops, public buildings and family homes accounts for 10.3% of these emissions. The study of shallow geothermal energy can offer an alternative to the 10.3% that comes from current methods of producing heating, cooling and domestic hot water. Energy geostructures are technologies that use the principle of shallow geothermal energy in a closed circuit. These structures, which are in contact with the ground, are equipped with heat exchangers to make use of the natural heat available on the soil. The particularity of these structures is that they have a dual role to play, both structurally and in terms of energy supply, which means that each project has to be studied in depth. This technology is expanding rapidly around the world, and the Cleunay metro station studied in this report is an example of this type of structure. Completed in 2020, the station is fully equipped with heat exchangers in both the slurry walls and the slab. The aim of the study of this station is to use a 3D digital model to determine the amount of heat that can be extracted from the soil through this structure. To do this, a thermal response test, carried out in the field in November 2019, will be used to calibrate the model. The type of building that has been studied with the model is a primary school building. The results obtained indicate a maximum energy that can be extracted from the ground using this structure. This value is equal to 100 MWh. This is enough to cover the heating needs of a school of approximately 9 300 m^2 under different hypothesis.

Résumé

Durant cette année 2023, le GIEC a publié son 6ème rapport de synthèse décrivant et évaluant les conséquences actuelles et futures du réchauffement climatique. Ce rapport de synthèse soulève, comme les précédents, la problématique des gaz à effet de serre, qui est une cause majeure du problème. Les sources d'émissions de gaz à effet de serre sont diverses, mais 45 % de ces émissions proviennent de la combustion de combustibles pour l'électricité et la chaleur. Parmi ces émissions, 10,3 % provient de la combustion pour les écoles, les commerces, les bâtiments publics et les résidences familiales. L'étude de la géothermie de faible profondeur peut proposer une alternative aux 10,3% venant des modes de production actuels de chauffage, climatisation et besoin en eau sanitaire. Les géostructures énergétiques sont des technologies qui vont utiliser le principe de la géothermie peu profonde en circuit fermé. En effet, ces structures en contact avec le sol sont équipées d'échangeurs de chaleur afin d'utiliser la chaleur naturelle du sous-sol présente. La particularité est que ces structures jouent un double rôle à la fois structurel et d'approvisionnement en énergie, ce qui nécessite une étude approfondie de chaque projet. Cette technologie est en pleine expansion dans le monde et la station de métro de Cleunay, étudiée dans ce rapport, est un nouvel exemple de ce type de structure. En effet, cette station, dont les travaux ont été terminés en 2020, est entièrement équipée d'échangeurs de chaleur que ce soit au niveau de ses parois moulées et de son radier. L'étude de cette station a pour but, via un modèle numérique 3D, de déterminer la quantité de chaleur qu'il est possible d'extraire du sol via cette structure. Pour ce faire, un test de réponse thermique, réalisé sur le terrain en novembre 2019, est utilisé afin de calibrer le modèle réalisé. Le type de bâtiment étudié grâce au modèle est une école primaire. Les résultats trouvés permettent d'obtenir une limite maximale de l'énergie qu'il est possible d'extraire du sol grâce à cette structure. Cette valeur est égale à 100 MWh c'est-à-dire à la possibilité de subvenir au besoin de chauffage d'une école de plus ou moins 9 300 m^2 sous certaines conditions.

Contents

Chapter 1

Introduction

1.1 Climate context and challenges

On March 20, 2023, the IPCC (Intergovernmental Panel on Climate Change) [1] released its new synthesis report describing the current state of knowledge on the extent of climate change and the consequences it will generate. This report, like all its predecessors, is alarming. Chapter 2 of this synthesis begins with the following sentence: "Human activities, principally through emissions of greenhouse gases, have unequivocally caused global warming, with the global surface temperature reaching 1.1°C above 1850-1900 in 2011-2020" [GIEC, 2023]. This sentence is clear: greenhouse gases are cited as one of the primary causes of global warming. The combustion of fossil fuels largely contributes to the emissions of greenhouse gases. The introduction of renewable technologies without fossil fuel combustion will contribute, in part, to the reduction of greenhouse gas emissions caused by humans [Laloui and A. F., 2020]. Indeed, 45% of these emissions come from the combustion of fuels for electricity and heat. Combustion for schools, shops, public buildings and family homes accounts for 10.3% of these emissions. The study of shallow geothermal energy can offer an alternative to the 10.3% that comes from current methods of producing heating, cooling and domestic hot water [Atlas climatique du Canada] [Ball, 2020].

Geothermal energy is a technology for producing renewable energy by utilizing the natural heat of the Earth. There are several types of geothermal energy: deep geothermal energy, which can be used for electricity generation, and shallow geothermal energy, which can be utilized for heating, cooling buildings, or producing domestic hot water [Laloui and A. F., 2020].

1.2 Geothermy

Shallow geothermal energy can be approached in two ways. The first is the open system. This method allows water to be extracted directly from existing aquifers in order to exploit this heat. This method requires two wells, a pumping well and a re-injection well. The water is pumped into the first well, cooled by passing through the heat pump, and then injected into the second well. During cooling, water is pumped into the cold well and then reinjected into the hot well [Brugeo].

The second way is a closed system. This method consists of circulating a heat transfer fluid in a closed circuit of pipes installed in the ground. The most common system uses a double set of U-shaped pipes. The heat carrier fluid, whose initial temperature is lower than that of the

1. "GIEC" in french

ground, heats up in the ground as it passes through the pipes in the circuit. At the outlet, the temperature of the heat carrier fluid is lowered by passing through the heat pump before it is returned to the closed circuit [Brugeo].

Energy geostructures are technologies that use the principle of shallow geothermal energy in a closed loop. These energy geostructures, such as foundation piles, cast walls, tunnels, etc., are equipped with heat exchangers in contact with the ground and have the characteristic of playing a dual role, both in terms of construction and energy supply [Di Donna et al., 2020].

1.3 Energy geostructures

One of the challenges associated with geothermal energy is the high financial cost of installation, including both the borehole and the heat pump [Clauser and Ewert, 2018]. Indeed, the financial cost of a geothermal system is marked by high fixed installation costs but relatively low operating and maintenance costs. Consequently, the financial benefit of geothermal systems is realized through long-term amortization. However, in the present circumstances of growing scarcity and rising costs of fossil fuels, geothermal energy also possesses the advantage of being solely reliant on electricity.

The specificity of energy geostructures comes from the fact that they are geothermal systems with a reduced cost thanks to the integration of heat exchangers directly into the structure under construction [Di Donna et al., 2020]. This characteristic can remove one of the fears of building construction using geothermal equipment, because the cost will be lower. If this is achieved, geothermal heating could become more accessible to the general public. Figure 1.1 shows the number of energy geostructures in the world. This number increase with time but stay to low. This figure also shows the amount of CO_2 "saved" with those geothermal projects. It is shown that in 2018, there were 180 projects of energy geostructures that were built and in operation in the world. This number resulted in 25 000 tons of CO_2 that were not released into the atmosphere. If this value is converted, it corresponds to an average distance of 109 000 000 km by plane [2]. This means 2700 times around the Earth if the plane follows the equator.

1.4 Objectives and content of the work

This work is done with the "THERMETRENNES" research program, the aim of which is to study the thermal behavior of four new metro stations equipped with heat exchangers, in the city of Rennes. The aim of this research program is to provide feedback on energy geostructures [SIGES]. The aim of this feedback is to provide more data and case studies that can help in the development of other projects.

In order to carry out this work, an internship was conducted at the 3SR laboratory in Grenoble, to produce a 3D digital model using COMSOL software of the Cleunay station. This station is fully equipped with heat exchangers at both the slab and the slurry wall. The model made is quite complex, as it includes all the pipes installed in both the slurry walls and the slab. The model's parameters were calibrated by an on-site thermal response test. This numerical model was then used to determine how much power could be extracted from the station and what types of buildings could be heated.

The first part of this work consists of a brief review of the various types of energy geostructures, describing their specific thermal and mechanical characteristics. It concludes with a summary

2. Conversion was made using this link: https://impactco2.fr/convertisseur

of the results obtained from the study of the Lancy-Bachet station, which is a station equipped with a geothermal system similar to the equipment in the Cleunay station.

The following section describes the geological and hydrogeological context of the Cleunay station and the thermal response test performed.

The third chapter describes the numerical model, describing the governing equations, the parameters introduced and the initial and boundary conditions. This chapter also provides a word about the model mesh used, as well as the solver and time step used by the software.

The fourth chapter describes the calibration of the model and the sensitivity of the various parameters. These results will enable to obtain a model that best reproduces the thermal behavior of the Cleunay station, based on current measurements.

The final chapter uses the numerical model to study the station's behavior when heating an elementary school. The aim of this chapter is to give an idea of the power that can be extracted from the ground with cooling and heating it. This simulation will be divided into two parts. The first part consists of the heating period, while the second part consists of the cooling period, which will also be divided into two scenarios. The first scenario studies the behavior of the station without the use of the geocoolig. The second scenario involves the study of station cooling with the use of geocooling. These two scenarios will be compared and an order of magnitude in the power that can be extracted from the station will be provided.

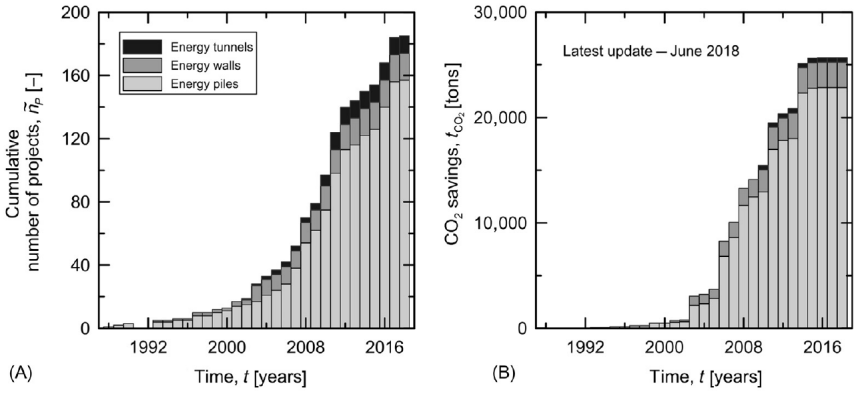

Figure 1.1 – At the left (A): cumulative number of energy geostructures worldwide. At the right (B): CO_2 savings thanks to these projects.[Laloui and Rotta Loria, 2020]

Chapter 2

State of the art

2.1 Energy geostructures

Energy geostructures are structures in contact with soil, such as pile foundations, basement walls and tunnel linings, that are equipped to exchange heat with the ground. Those technologies are geothermal systems with a low-grade heat energy present in the shallow earth surface. These applications are often used to extract energy from the ground through the use of a heat pump [Bayer et al., 2019] [Kawuwa Sani et al., 2019]. This is an innovative technology that combines the structural support role of conventional geostructures with the heat exchange role of shallow geothermal systems in a closed system for any type of built environment [Laloui and Rotta Loria, 2020]. The emergence of energy structures is driven by the need to find solutions to the ecological problems that humans face.

2.1.1 Functioning of energy geostructures

Figure 2.1 represents a typical operating system of an energy geostructure. The heat of the ground is extracted thanks to heat carrier fluid circulating into the pipes embedded within a geostructure (piles,tunnel,wall). Therefore, the working principle is the same as a closed geothermal system, but it is integrated into a geotechnical structure.

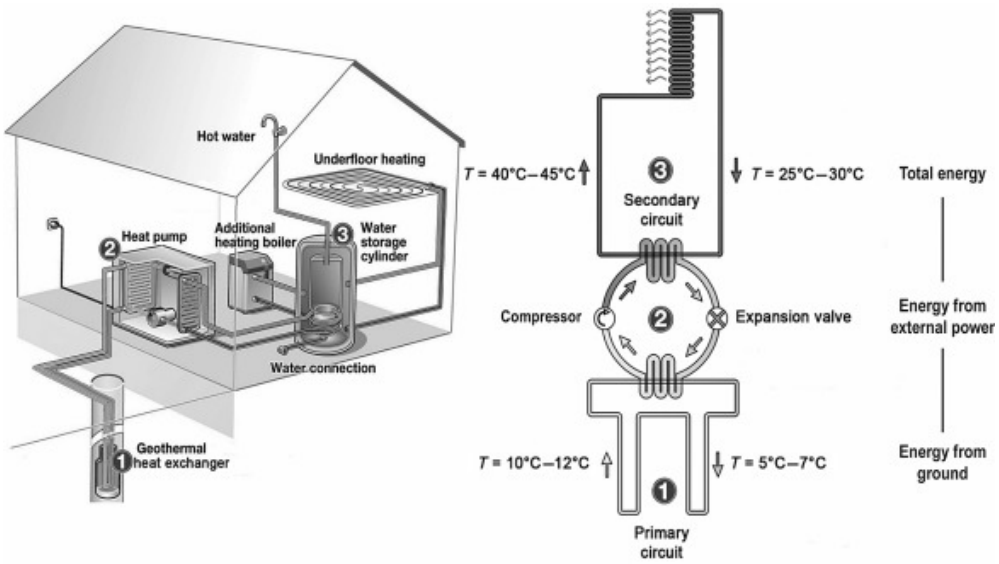

Figure 2.1 – Operation of an energy geostructure [Laloui and Rotta Loria, 2020]

Operation of an heat pump The heat pump is based on the concept that the temperature of a fluid is higher when the fluid is compressed into a smaller volume. It converts mechanical work (compression) into heat through electricity. A basic heat pump is schematized on Figure 2.2. It works with a fluid, called "refrigerant". This fluid circulated into a closed loop and is subjected to four different stages : (1) In the evaporator, the refrigerant comes into contact with heat carrier fluid which comes from the ground and is transformed into a gas. The heat carrier fluid decreases his temperature and so is reinjected into the soil to warm up again. (2) In the compressor, the gas is at low pressure and at relatively low temperature. It is compressed by using electricity to increase its temperature. After this stage, the refrigerant has a high temperature and high pressure. After the compressor comes the condenser (3), this stage has the aim to transfer the heat of the refrigerant to a heat carrier fluid present in a secondary circuit (see section below). The last stage is eventually the passage to an expansion valve (4) that decreases the temperature and the pressure to its initial condition to reentering to the evaporator phase and start with a new cycle. This process can also be reversed to cooling instead of heating [Laloui and Rotta Loria, 2020].

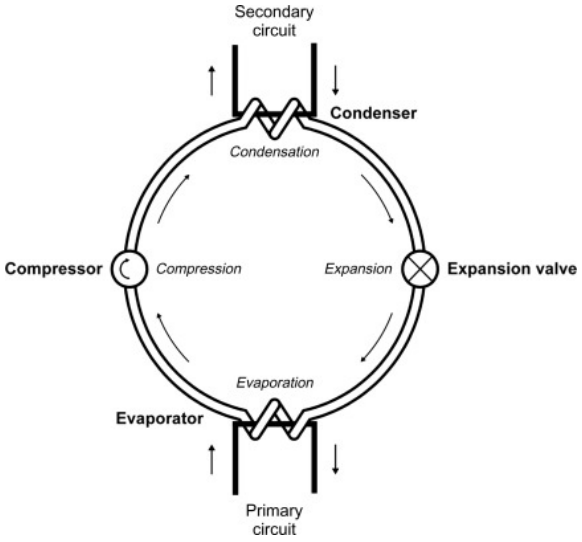

Figure 2.2 – Heat pump [Laloui and Rotta Loria, 2020]

Coefficient of performances The efficiency of heat pumps is defined by a coefficient of performance, COP. This describes the ratio between the energy required to operate and the energy produced [Brandl, 2006].

$$COP = \frac{\text{Energy output after heat operation [kW]}}{\text{Energy input for heat pump operation [kW]}} \tag{2.1}$$

Free-cooling and seasonal storage Geothermal systems can also be used in summer, applying free cooling. This is the use of temperature of the ground to cool a building : it is the same procedure but the heat carrier fluid is not heated thanks to the heat pump. Indeed, if the underground temperature is around 12°C, this is sufficient to reduce the temperature of a building with a temperature of 25°C for example. Furthermore, if the geothermal system has been operating in winter this can lead to a decrease in temperature at the heat extraction point. The subsequent use in supper can be useful to recover to the initial temperature, improving long term efficiency. The Figure 2.3 shows an example of a ground source heat pump combining heating and cooling. The period using the ground temperature for cooling can lead to an increase in ground temperature of up to 3°C in this example [Wei et al., 2019].

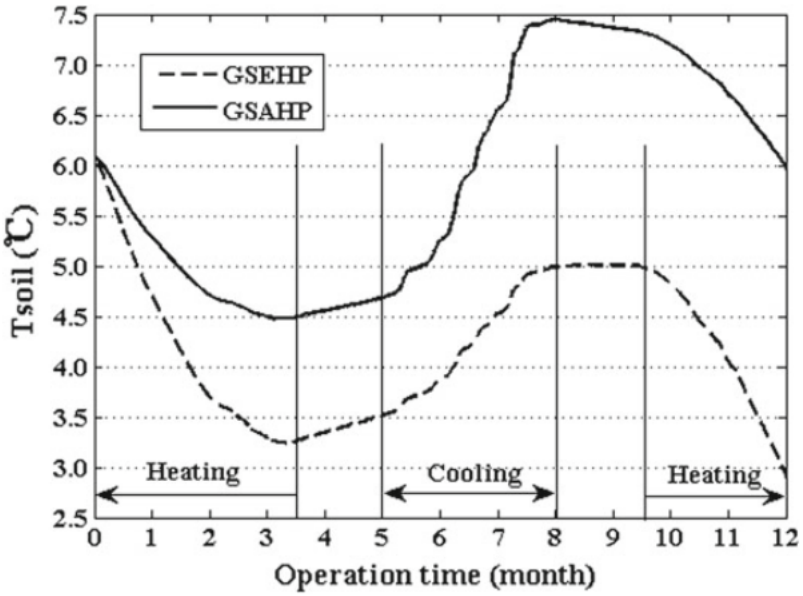

Figure 2.3 – Hourly average soil temperature in the first-year operation in Harbin [Wei et al., 2019]

2.1.2 Materials

The material used in the different energy geostructures is reinforced concrete because it is an ideal medium thanks to its good thermal conductivity and thermal storage capacity [Soga and Rui, 2016]. In energy geostructure, the pipes are fixed along the reinforcing cage or are placed within the filling material [Laloui and Rotta Loria, 2020]. Concerning the heat carrier fluid circulating into the pipes, it consists often of water with antifreeze or a saline solution. The antifreeze is often ethylene glycol or propylene glycol. Those products can be very toxic and has to be used carefully. Heat carrier fluid often contains an additive who allows to prevent corrosion [Laloui and Rotta Loria, 2020].

2.1.3 Coupling process

In energy geostructures the function of the structure is both carrying mechanical load and exchanger heat with the ground. As a result, this technologies needs to be studied considering thermo-hydro-mechanical interactions between the ground and the structure [Soga and Rui, 2016]. Figure 2.4 indicates the main interactions between pipes, structure and subsurface. Those interactions can be complex and is very dependant of the type of soil present. The first main process is the heat and fluid behaviour inside the pipes (the heat exchanger). The second is the thermomechanical coupling in the substructure. This is the impact of the temperature on the mechanical state of concrete structures. Like indicated in the Figure 2.4 it can create en expansion/contraction of the structure. The third process is the thermo-hydro-mechanical coupling of the soil. It refers to the interaction between the temperature field, the displacement field and the pore water pressure distribution in the soil [Soga and Rui, 2016].

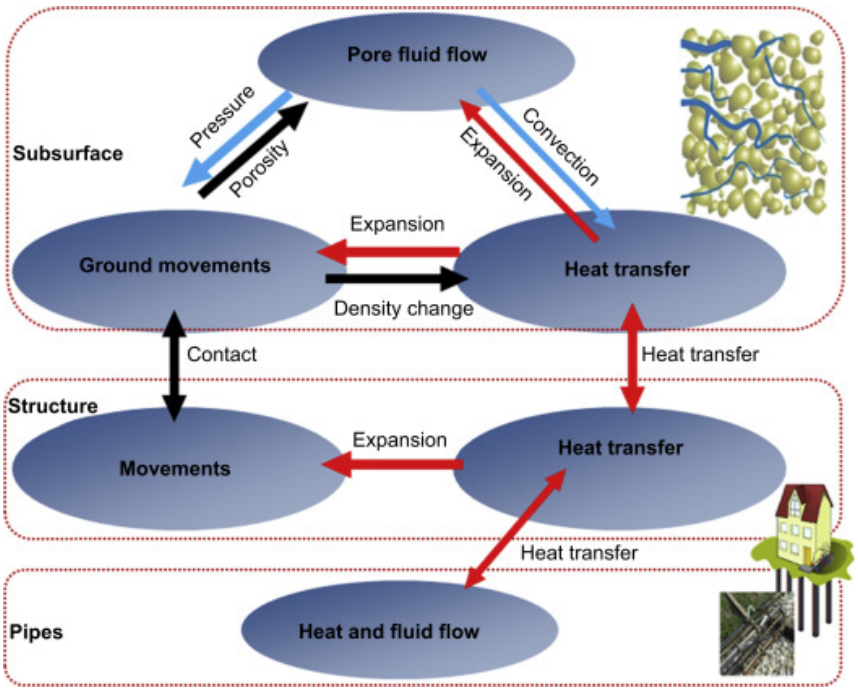

Figure 2.4 – Coupling process in energy geostructures [Soga and Rui, 2016]

2.1.4 Application of energy geostructures

There are various purposes of this technology. First of all, it can be a true alternative to cooling or/and heating infrastructure (houses, offices, retail spaces, ...) [Di Donna et al., 2020]. Moreover it can be used to contribute to the production of hot water for anthropogenic, agricultural or tank-farming use Laloui and Rotta Loria [2020]. Next, another application is to providing heat to prevent the icing of road, bridges, station platforms, airport runways. The last application is to store heat in the subsurface for a subsequent use [Laloui and Rotta Loria, 2020]

2.1.5 Advantages

Energy geostructures are a renewable energy source and they represent a good opportunity to reduce the need of fossil energy. This technology is characterised by being remarkably stable to provide energy compared to other renewable energies, wich makes it an interesting complementary choice [Bayer et al., 2019]. Moreover, energy geostructure possesses advantages in comparison with traditional geothermal systems. For example, the utilisation of concrete has more favourable thermal properties than the filling materials like bentonite [Laloui and Rotta Loria, 2020]. Another advantage is to decrease the cost of the initial installation of a geothermal process thanks to the use of structure that would be built in any case [Di Donna et al., 2020].

2.2 Different kind of energy geostructure

2.2.1 Energy foundation piles

The first studied kind of energy geostructure are energy foundation piles. The general principle is the utilisation of piles as heat exchangers between the heat transfer fluid and the soil. Figure 2.5 illustrates the behaviour of this technology [Kawuwa Sani et al., 2019]:

1. The primary unit consist of heat exchangers installed in piles
2. The secondary unit is the pipe network that delivers the heat energy in or out the building
3. The heat pump unit adapt the temperature to the need of the building

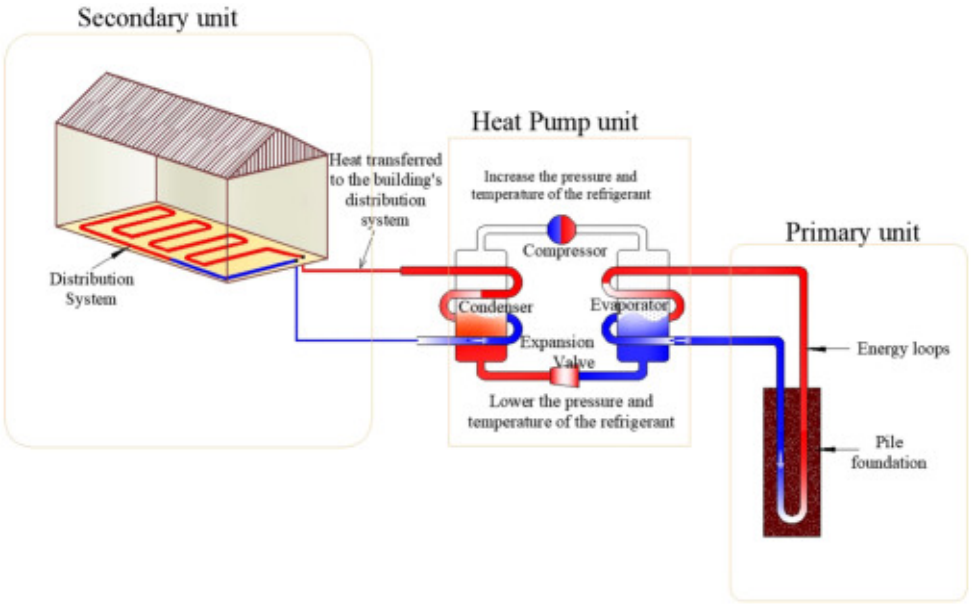

Figure 2.5 – Geothermal energy pile system [Kawuwa Sani et al., 2019]

Structure of the energy piles The pipes are made of high-density polyethylene and are fixed to the reinforcement cage if this is a bored pile. For a contiguous flight or auger piles, heat exchanger pipes are plunged into the center of the pile after placing the concrete [Soga and Rui, 2016].

Forms of the pipes The pipe can have various forms: U-shape, double U-shape, triple U-shape, W-shape, spiral or helical shape, direct double-pipe type, ... The different forms of the pipe inside the piles are show on Figure 2.6. Each form has their own advantages and disadvantages. Inside those pipes, the heat transfer fluid can be chosen between pure water or pure water with a biocide and/or an anti freezing solution, in the pipe the fluid can be in laminar or turbulent conditions [Kawuwa Sani et al., 2019], [Soga and Rui, 2016].

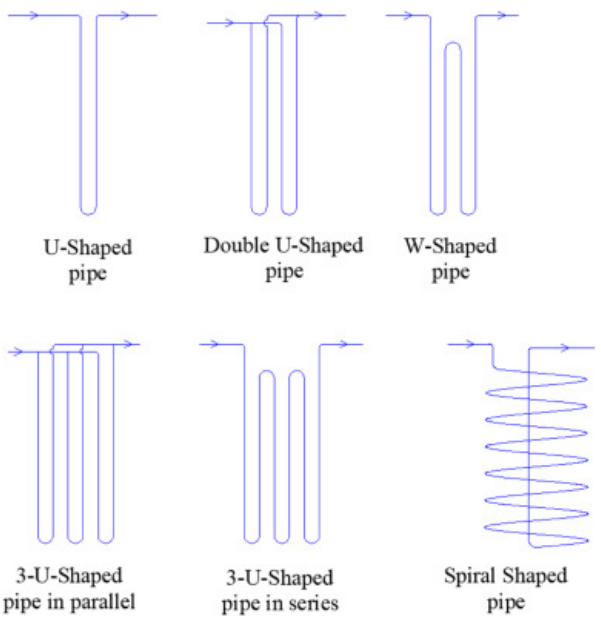

Figure 2.6 – Various configurations of energy loops within a geothermal energetic piles [Kawuwa Sani et al., 2019]

Thermo-mechanical behaviour Figure 2.7 summarises the behaviour of a pile (a) under stress without heating/cooling (b) heating/cooling and free expansion of the piles (c) heating/-cooling with end constraints.

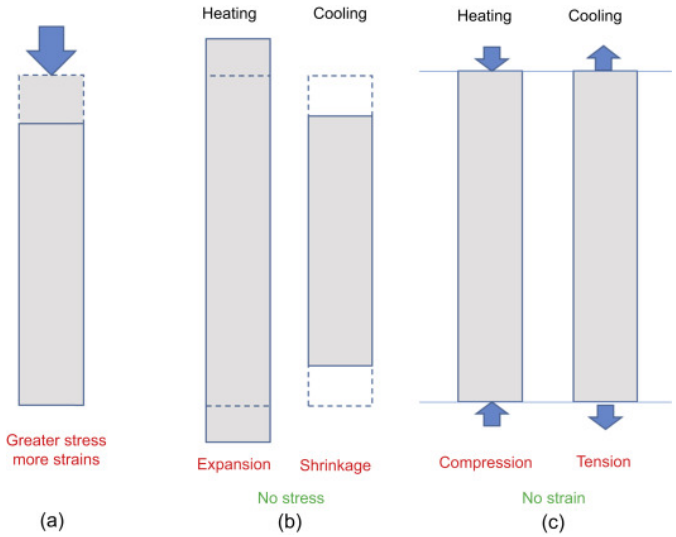

Figure 2.7 – Mechanical behaviour of piles subjected to a) Only stress b) Only heat c) Stress and heat [Soga and Rui, 2016]

(a)The first case is a conventional geostructure (without heating/cooling). The piles are compressed and stress is generated in the structure. Strain increases with stress [Soga and Rui, 2016]. (b) When the piles is heated/cooled with free expansion the structure expands/shrinks. The amplitude of the phenomenon is related to the temperature variation and the thermal expansion coefficient of the material (see equation below). Therefore, if the material is heated or cooled and there is no soil around it, it will expand vertically and radially. This will cause thermal strain [Soga and Rui, 2016].

$$\varepsilon_t = \alpha \Delta T \tag{2.2}$$

(c) When displacement is not allowed, there is stress formation within the pile. The equation of this stress is [Soga and Rui, 2016]:

$$\sigma_t = E(\varepsilon_{T-real} - \alpha\Delta T) \tag{2.3}$$

With,

— E Young's modulus of the pile mateiral;

— ε_{T-real} the actual strain inside the structure due to thermal changes. If the two sides are fixed, it is equal to zero. The thermal stress becomes $\sigma_t = -E\alpha\Delta T$. This stress is negative which mean that it's a compression when the pile is heated (ΔT >0) ;

— α the linear thermal expansion coefficient of the pile material.

The thermo-mechanical behaviour is also impacted by the type of piles. Two types of piles are presented to understand the interaction between heat/stress and strain. Figure 2.8 indicates the distribution of stress and strain without thermal variation [Soga and Rui, 2016] for :

— **Friction pile** the pile resists to the load thanks to the shaft friction only.

— **End-bearing pile** the pile resists to the load thanks to end-bearing and some resisted by side friction.

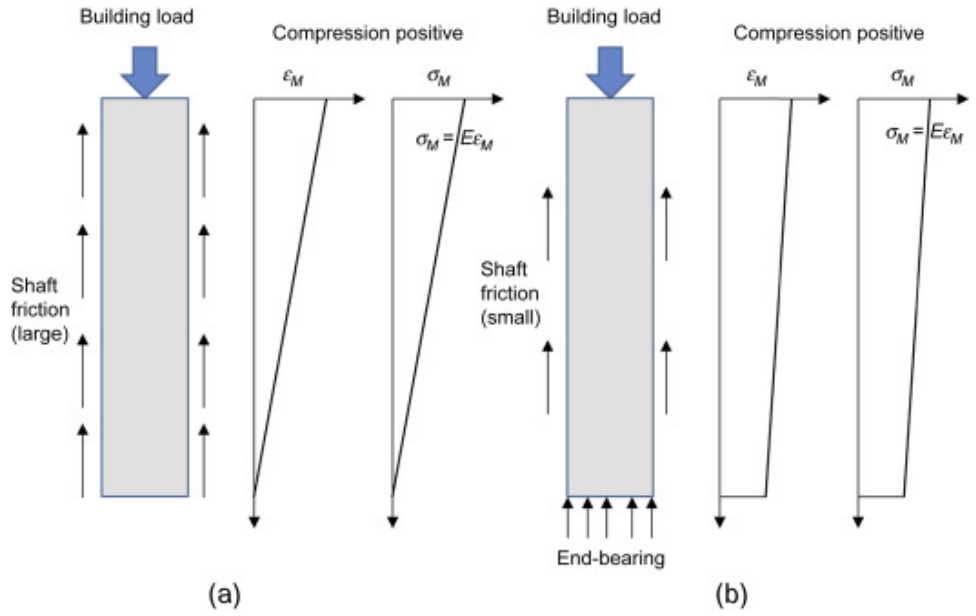

Figure 2.8 – (a) Friction pile (b) end-bearing pile [Soga and Rui, 2016]

Figure 2.9 shows the expected reaction of a pile due to the impact of (a) heating and (b) cooling on a friction pile. When the pile is heated and the two ends are free, the top half move upward and the bottom half move downwards. This behaviour creates additional friction on the pile (red arrow on the Figure). On the bottom, the additional friction has the same direction and the same magnitude of friction increase. At the top it is the contrary: the direction of the additional friction is on the other sens of the friction created by mechanical load and so the magnitude of friction decreases. When the pile is cooled, it is the same mechanism but in the other direction. Here some part of the pile are going in tension and must be check in the design considerations [Soga and Rui, 2016].

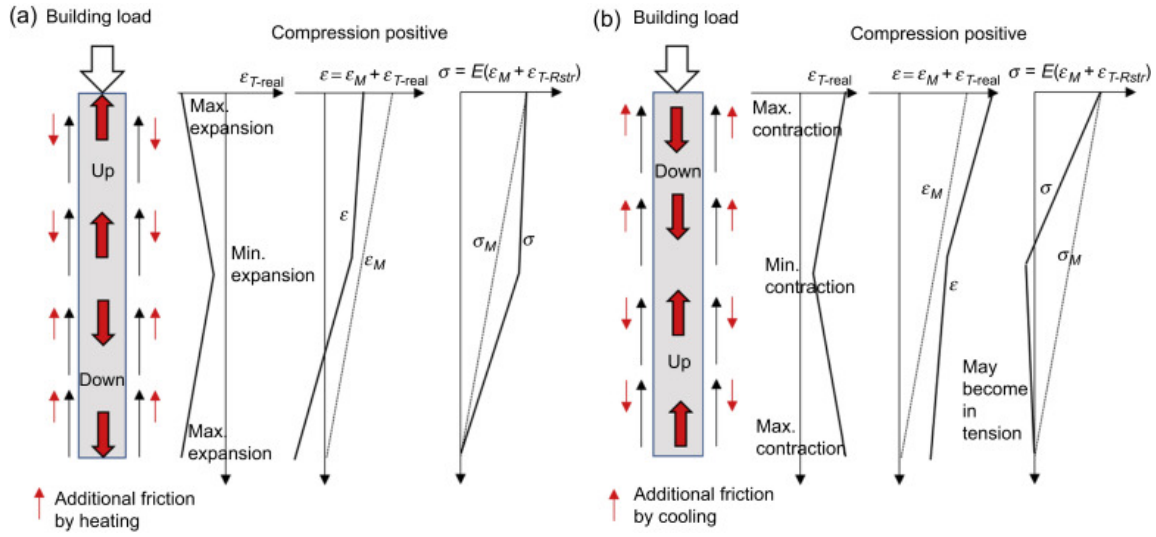

Figure 2.9 – (a) Heated friction pile (b) Cooled friction pile [Soga and Rui, 2016]

Figure 2.10 represents the expected behaviour of a end-bearing pile heated or cooled. By definition the end of the pile can only have limited movement. First, when the pile is heated there is only a displacement of the pile to the top and this created addition friction like with the friction pile. The thermal stress is compressive and increases with depth. The shaft friction reduces and hence more load is transferred to the bottom. When the pile is cooled, and apposite trend is observed. However, in this case no tension behaviour is attempt [Soga and Rui, 2016].

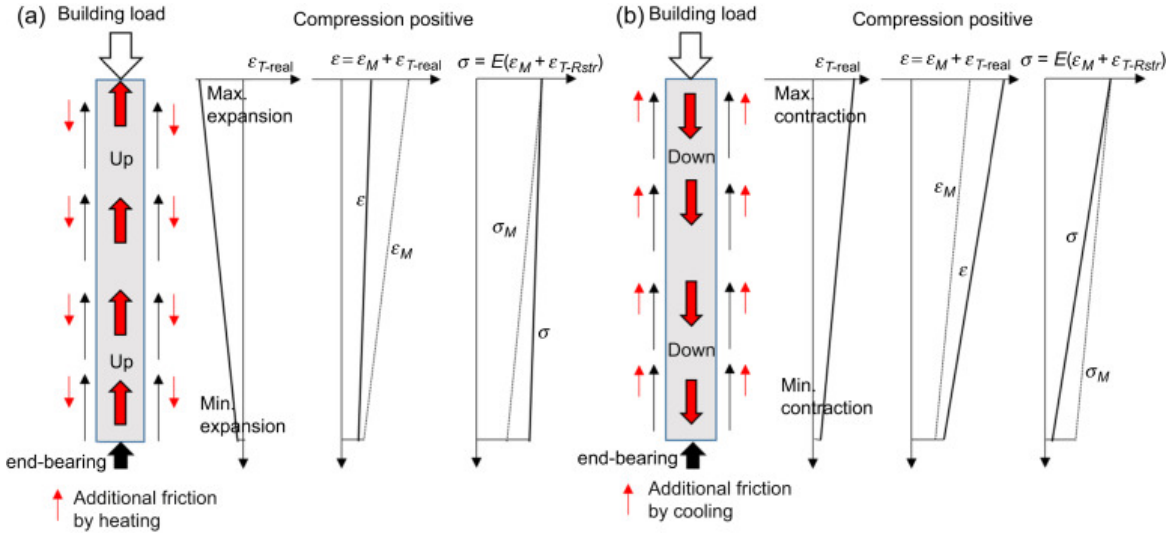

Figure 2.10 – (a) Heated end-bearing pile (b) Cooled end-bearing pile [Soga and Rui, 2016]

Another effect is the impact of heating on the soil. It may be subject to heaving or settling due to the contraction or expansion of the soil and in particular the pore fluid. This leads to a change in the earth pressure exerted by the soil on the pile. This effect can also be problematic for adjacent buildings.

Design consideration The behaviour of the different pile types studied above has shown the importance of the pile behaviour at these ends. As a consequence it is really important to evaluate the thermo-mechanical response of the pile during heating or cooling. Moreover, those results are under the assumptions of a homogeneous soil in the reality the response will be much more complex [Soga and Rui, 2016].

2.2.2 Energy walls

Another application is the utilisation of underground basement structure or railway station boxes as heat exchangers. In this case, the heat exchangers are installed into the walls and so response to two roles: they provide energy for above ground buildings and are structurally load-bearing. In comparison with energy piles, the volume of ground used has heat exchanger can be larger due to the structure and so can be more performing. For underground railway station there is also a possibility to extract heat in winter from both sides of the wall (station and soil) because stations often have an excessive heat generated by train operation, which is also an advantage [Soga and Rui, 2016].

Structure of energy wall Figure 2.11 represents different kind of structure of energy walls. Like with energy piles, heat exchangers are fixed to the structural steel reinforcement cage. It exists different scenario of structure according to the application. In the first case (A), pipes are installed on both side (groundside and airside). On (B) they are only on the airside, (C) they are only on the the groundside and (D) they are only the groundside with an insulated airside [Laloui and Rotta Loria, 2020]. Usually, the pipes are put as close as possible to the soil to decrease the thermal resistance of concrete and so improving the performance. The side of the wall in contact with the basement is sometimes insulated to ensure that the heat from the heat exchanger transfers into the soil rather than into the basement [Soga and Rui, 2016].

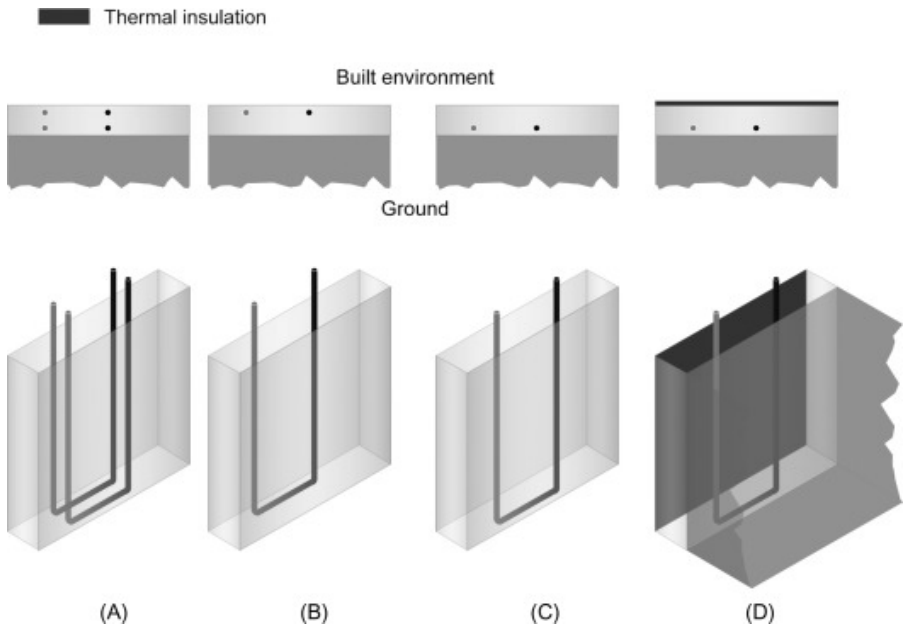

Figure 2.11 – Different position of pipes into an energy wall. Considering a U-shaped pipe [Laloui and Rotta Loria, 2020]

Configuration of energy wall Figure 2.12 shows the different configuration of pipe in an energy wall: (a) U-shaped pipe (b) bent U-shaped pipe, (c) W-shaped pipe, (d) bent pipe. Each configuration has a difference in the heat exchange surface. It has an impact both in the performance of the energy geostructure and pressure reduction [Laloui and Rotta Loria, 2020].

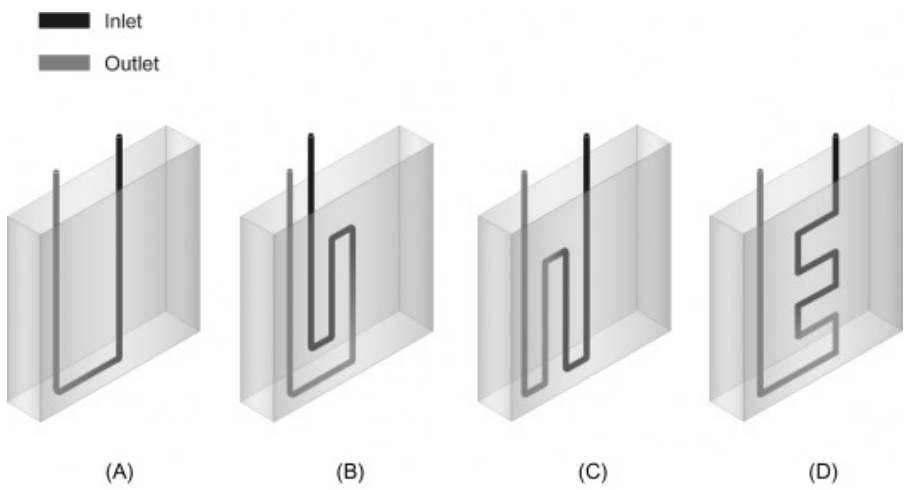

Figure 2.12 – Different kind of configuration of energy wall [Laloui and Rotta Loria, 2020]

Thermo-mechanical behaviour of energy wall The variations of temperature inside the wall can impact the structural performance of the wall. Figure 2.13 summarises the different effects of temperature on an energy wall. One of these effects is the impact on the soil. Indeed, in the same way as with the pile, it may be subject to heaving or settling due to contraction or expansion of soil and particularly of pore fluid. This effect leads to a change in earth pressure applied to the wall. In comparison with energy piles, energy walls have only one side of the wall exposed the soil, the other is free. Therefore, the stress distribution will be vastly different and can create an additional bending movement inside the wall. It has to be taken into account into the design operation to not deteriorate the concrete structure during the operation. Another effect due to the heaving or settling of the ground is the effect on adjacent building. As a consequence, in the design procedure the long-term ground deformation due to cyclic thermal change has to be evaluated [Soga and Rui, 2016].

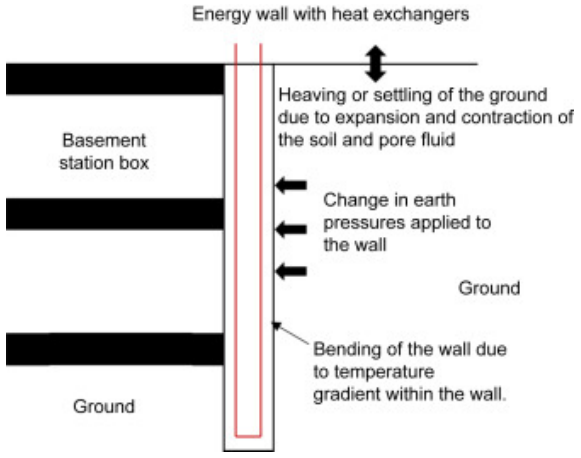

Figure 2.13 – Effect on variation of temperature on energy wall [Soga and Rui, 2016]

Particularity of energy wall There are few applications using energy walls used as shallow geothermal heat exchanger. Two studies was made by [Bourne-Webb et al., 2016, Di Donna et al., 2021] to determine which parameters influence the performance. The interaction between the air and the interactions between the wall and the soil of the wall was studied. It seems that there is an important impact of the temperature inside the structure. This temperature is influenced by the humidity and the air velocity inside the railway station (influence by number of tracks). Concerning the interaction of walls and soil few studies exists, but it seems that if

the soil is saturated the hypotheses of heat transfer purely convective seems not too far from the reality. However this is less true if the soil is dried [Bourne-Webb et al., 2016]

2.2.3 Energy tunnels

The experience of the London Underground informs about the heat problems that a subway railway can encounter [Waboso and Gilbey, 2007, Soga and Rui, 2016]. Indeed, in underground metro there is a large amount of heat which can be used. To give an order of idea the motors in a London Crossrail emit about 1 MW of heat and there is one train every 2.5 min during peak times [Nicholson et al., 2013, Soga and Rui, 2016]. Moreover, air conditioning and braking add additional heat even if the main heat source is still the soil. On this application, the heat exchanger pipes are embedded in the tunnel linings. It can be pre-casted in a factory or installed on site. Like the other applications the heat exchanger is connected to the reinforcement cage of tunnel linings [Soga and Rui, 2016] in the case of precast tunnels.

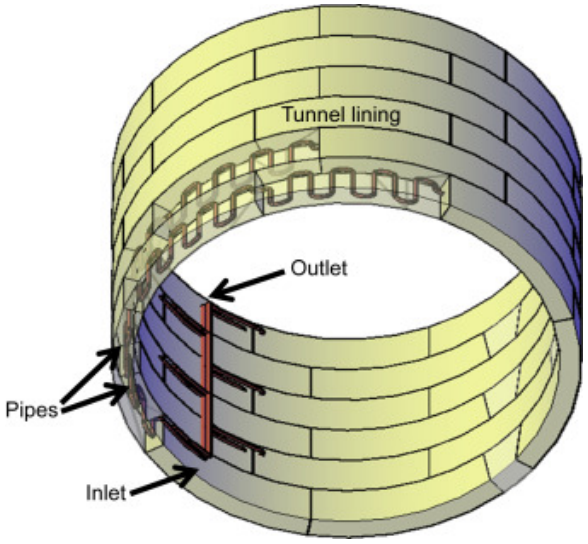

Figure 2.14 – Basic structure of an energy tunnel [Soga and Rui, 2016]

Distribution of the temperature inside the tunnel A particularity of energy tunnel is that soil is not the only source of heat, the air inside the tunnel can also be used in certain case. There are two types of tunnels. A cold tunnel is when the air inside the tunnel is controlled by the surface air temperature, it is short-running tunnel. The second type of tunnel is the hot tunnel. It is when the temperature inside the tunnel is higher than the surface air temperature [Soga and Rui, 2016]. According to the kind of tunnel studied, the application could be very different.

Operational modes A first mode is the utilisation of soil as heat storage medium between summer and winter seasons. In this case it is necessary to have insulation inside the section of the tunnel to avoid air temperature variation inside the tunnel. This mode is often use when the application is with a cold tunnel. A second mode is when the energy tunnel is used for heat extraction. In summer, the heat is extracted from the heat exchanger to supply hot water for above ground structures and heating buildings. In winter the heat is extracted to cool down the soil side which is useful for cooling the tunnel in the following summer [Soga and Rui, 2016].

Thermo-mechanical behaviour Figure 2.15 shows the different mechanical behaviour of a tunnel due to a variation of temperature. Foremost, one of the most important design aspects is

the thermal expansion/contraction of the segments. Indeed, the distribution of temperature can be complex, and it is significant to make a good estimation of those phenomena to avoid damage of the tunnel. Moreover, the local stresses at the joint sections are also very important because it can influence the water tightness of the lining and therefore creates additional movement in joint sections. Another consequence of the expansion/contraction of the soil is to lead to a change in earth pressure acting on the tunnel lining [Soga and Rui, 2016].

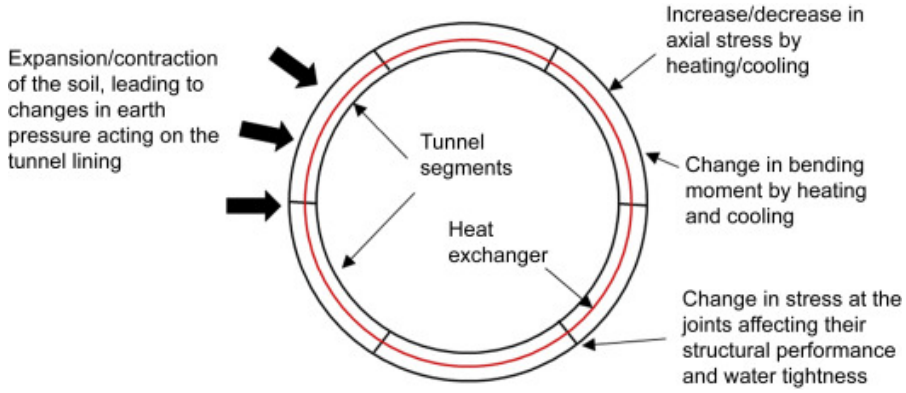

Figure 2.15 – The different thermo-mechanical behaviour of an energy tunnel [Soga and Rui, 2016]

2.3 Ground heat flow mechanism

There are three main modes of heat transport: heat conduction, heat convection and heat radiation. Each mode has not the same impact in the thermal distribution. These three modes are briefly presented below.

Heat conduction refers to heat movement between bodies in contact because of the difference in kinetic energy of atomic particles [Kawuwa Sani et al., 2019]. The driving force is the gradient of temperature between the two bodies. Equation 2.4 is the Fourier's law. It indicates indicates the conductive heat flux through a body in a one dimension:

$$Q = \lambda A \frac{dT}{dx}(W) \tag{2.4}$$

with, λ the thermal conductivity ($\mathrm{W}m^{-1}K^{-1}$), A the area (m^2), $\frac{dT}{dx}$ the temperature gradient ($\mathrm{K}m^{-1}$). Different values of the thermal conductivities are shown on Figure 2.16. These values are variable with the presence of water inside the porous medium and with the degree of compaction of the soil [Dassargues, 2020].

Lithologie*	λ_b (Wm^{-1} °K^{-1})
granites et gneiss	3,2 – 4,4
basaltes	3,0 – 3,5
quartzites	4,0 – 6,5
shales	1,5 – 3,5
micaschistes et ardoises	1,3 – 3,0
calcaires et dolomies	2,5 – 4,5
craies	1,5 – 2,5
grès	2,5 – 5,0
siltites	2,0 – 4,0
tuffs volcaniques	1,0 – 1,5

Lithologie*	λ_b (Wm^{-1} °K^{-1})
graviers	2,5 – 4,5
sables	3,0 – 5,5
silts	2,0 – 4,0
limons, loess et argiles	2,0 – 3,0
air	0,024 – 0,026
eau	0,57 – 0,60
matière organique	0,25 – 0,40

* valeurs pour conditions sèches (air dans les pores et les fissures). Les valeurs en conditions saturées ou partiellement saturées seront légèrement plus élevées en fonction de la teneur en eau. Sur un site donné, les données mesurées sont à privilégier.

Figure 2.16 – Thermal conductivity values of dry soil from different geological environments [Dassargues, 2020]

Heat convection It occurs by the movement of fluid from one point to another through pore space that exists with the soil mass [Kawuwa Sani et al., 2019]. The heat flux by convection is defined by:

$$q_{convec} = C_w \rho_w U_w (T - T_r)(W/m) \tag{2.5}$$

with, C_w (J K^{-1} kg^{-1}) the specific heat capacity of soil water, ρ_w (kg m^{-3})the water density, T (K) the applied temperature, T_r is the reference temperature and U_w (m s^{-1}) the velocity vector of water.
Heat convection is directly linked with the groundwater flow. It has an impact on the soil temperature because the heat is transferred by the water due to advection. This is significant only if the permeability is not too low [Kawuwa Sani et al., 2019]. Moreover, it allows a continuous thermal recharge of the ground [Di Donna et al., 2021]

Heat radiation It is due to heat propagation through electromagnetic waves. In soil, heat transfer thanks to radiation is negligible [1] To give an order in sandy soil under normal atmospheric temperature the heat radiation contribute to less than 1% of magnitude [Kawuwa Sani et al., 2019].

2.3.1 Ground initial temperature

Up to 10m below ground level, the temperature in the underground is affected by the seasonal weather cycles, but below this depth the temperature can be considered has constant [Kawuwa Sani et al., 2019]. This parameter will be of major importance as it will be directly linked to the performance coefficients of the heat pump. One advantage of geothermal energy is that it

1. except some exception in coarse aggregates. For more explication see Noriaki and Koichi [1969]

offers a constant temperature to the heat pump, if this is no longer the case the performance will be directly affected.

2.4 An example of in-situ application: The Lancy-Bachet station

A short summary of an in-situ application similar to the one studied in this report is provided. This project is located in the south of Geneva and aims to link Geneva to Annemasse in France. The station has been fully equipped with geothermal heat exchangers, representing a thermoactive surface of 5000 m^2. The structure of the station can be seen in Figure 2.17 [Zannin et al., 2020].

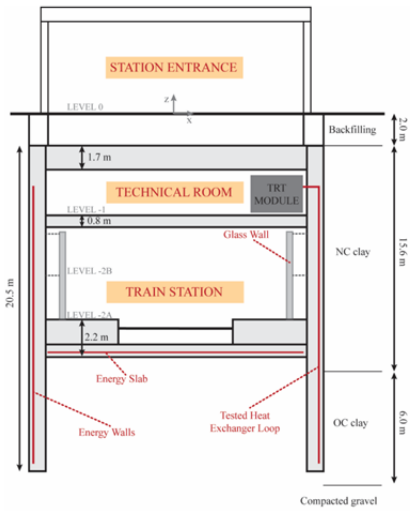

Figure 2.17 – Section of the Lancy-Bachet station with the location of the heat exchangers [Zannin et al., 2020]

Geothermal equipement The Lancy-Bachet station is fully equipped with geothermal exchangers within its cast walls and invert. Figure 2.17 shows a cross-section of the station with the location of the heat exchangers. The cast walls are fitted with U-shaped loops spaced at 0.25m. These pipes have an external diameter of 25 mm and an internal diameter of 23 mm. They are placed at a distance of 20 cm from the ground and 80 cm from the inside of the station. The total length of each loop is 36 m. The invert is equipped with heat exchangers in loops spaced 0.5 m apart. Each loop has a pipe length of 200 m and occupies an area of 96 m^2. These loops are located at a distance of 40 cm from the ground and 1.75 m from the interior of the station [Zannin et al., 2020].

Energy performance A thermal response test was performed to characterise the soil from a thermal point of view. The figure 2.18 shows the results obtained with this test. Firstly, the test starts with a circulation phase over a period of 2 days. This part shows that there is no fluctuation in the temperature of the fluid; the temperature reached the constant value of 17.34 °C. This temperature is, therefore, the average temperature of the wall. The second phase i.e. the heating phase, can be divided into a transient phase and an equilibrium phase. In the transient phase, the temperature increases rapidly over a period of 5-7 days and is followed by an equilibrium phase. These results were used to calibrate a numerical model and to approximate the values of the thermal conductivities of concrete and soil. The best result

was a thermal conductivity of the concrete of $\lambda_c = 1.7$ (m/WK) and a thermal conductivity of the soil of $\lambda_c = 1.4$ (m/WK). These results lead to an absolute error between the numerical model and the experimental data of 0.014°C [Zannin et al., 2020].

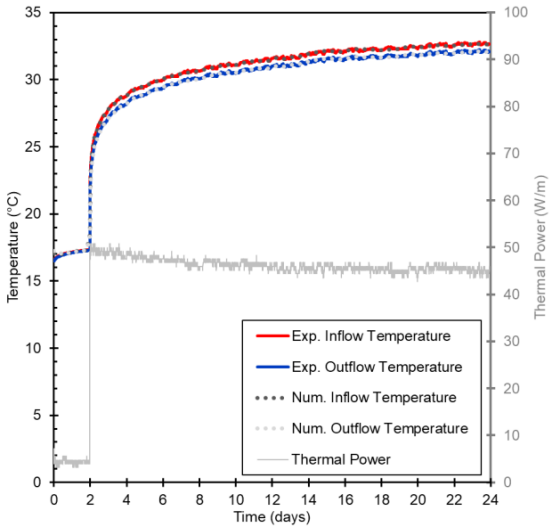

Figure 2.18 – Experimental temperature values in comparison with numerical results obtained with the model [Zannin et al., 2020]

Mechanical performance After this first model, a study about the thermo-hydro-mechanical behavior of the structure was made in order to complete the first model. To begin with, a heating and cooling test was carried out to understand how the station reacted to these temperature variations. These results, shown in Figure 2.19, were also used to improve the numerical model.

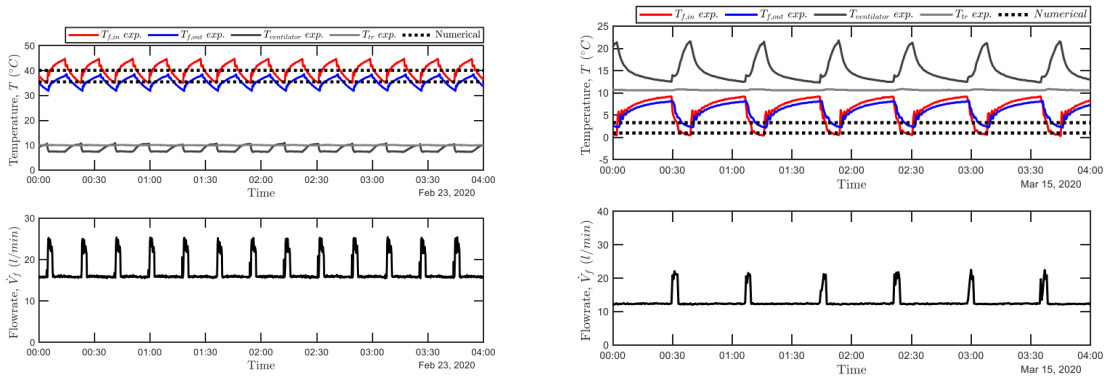

(a) Results of the heating part

(b) Results of the cooling part

Figure 2.19 – Variation of temperature and flowrate for the heating and cooling test [Zannin et al., 2020]

Next, a study of the mechanical behaviour of the station under the maximum temperatures recorded was carried out. This study was divided into two parts. The first part focused on the tunnel and the second on the cast walls. The results obtained show that the temperature in the tunnel is much more variable than in the case of the cast walls. This is justified by the fact that the effect of the wind tunnel causes a decrease in the temperature in the tunnel. The figure 2.20 shows the results obtained with the temperature measured in the slurry wall. It can be noted that the values of the vertical and longitudinal deformations are reasonably acceptable [Zannin et al., 2020].

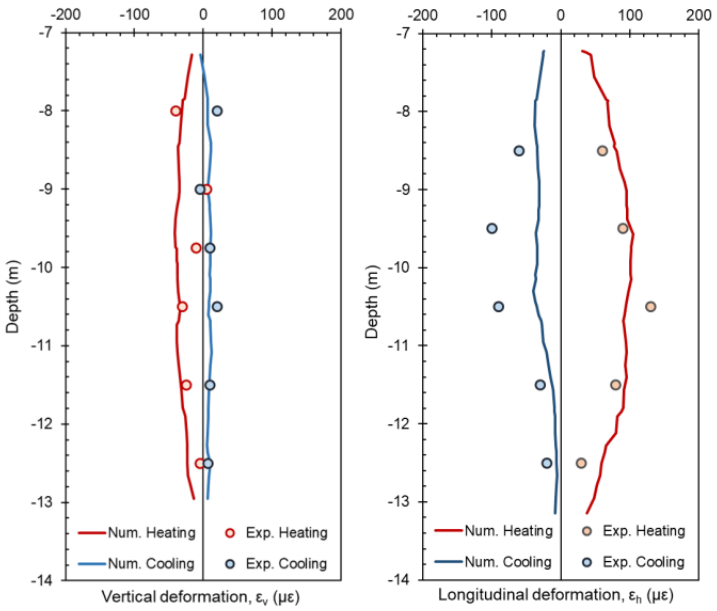

Figure 2.20 – Vertical and longitudinal deformation of cast wall [Zannin et al., 2020]

Chapter 3

Cleunay station

3.1 Description of the project

In 2003, the city of Rennes decided to equip the city with a new metro line in addition to the existing one. The arrival of this metro is part of a process to meet the challenges of sustainable development. Consequently, it has also been decided that four new stations will be equipped with heat exchanger. Those stations are: Jules-Ferry, Saint-Anne, Saint-Germain and Cleunay stations. These stations can be seen on Figure 3.1b. The studied station in this report is the Cleunay station located at the west of the city [RennesMétropole]. Figure 3.2 shows an aerial view of Cleunay station during the works. In the centre is the entrance to the underground station.

3.2 Localisation

The metro station studied is located in Rennes, a city in the northwest of France in the department of "Ille-et-Vilaine" in the region of Bretagne see Figure 3.1a.

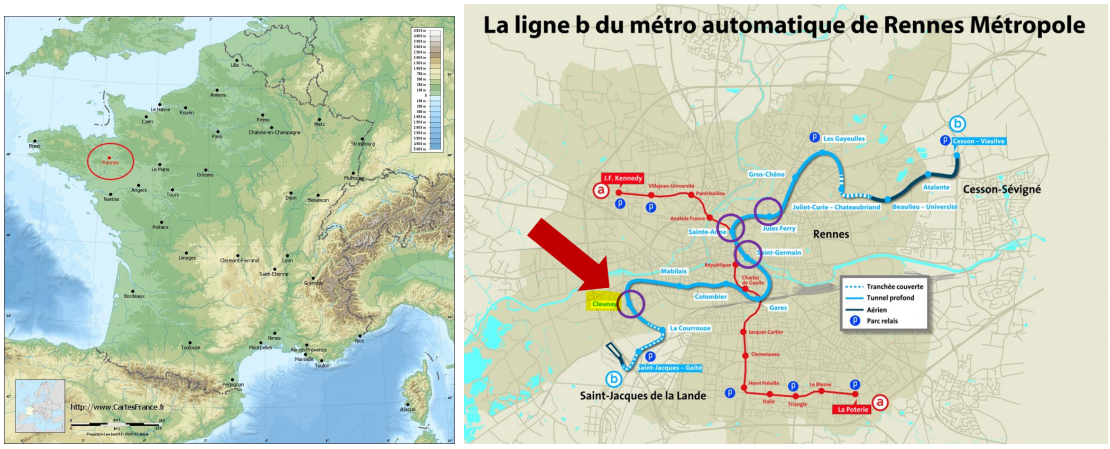

(a) Localisation of Rennes in France [CartesFrance]

(b) Rennes metro line. Cleunay station is located to the west. [RennesMétropole]

Figure 3.1 – Localisation of the Cleunay station

Figure 3.2 – Cleunay station worksite [Personal communication]

3.3 General context

3.3.1 Geological context

Rennes is located in the Armorican massif. This massif is divided into three parts due to major shear zones: the northern - central domain and the southern domain. Rennes is located between the northern and central domains, which means that it is divided by a shear zone [Pinson and Bault, 2019]. In Rennes, the general geology is characterised by a bedrock with embankments, colluvium and alluvium.

The embankments There are made of various materials. Highly heterogeneous. The thickness is between 0.4 and 0.6 m. Mainly made of gravelly sands and silts sandy-gravelly [Terrasol, 2015].

Colluvium and alluvium Sedimentary materials have the form of colluvium and alluvium. It can be more or less coarse facies without being entirely sandy or clayey. This layer lies below the embankments at a depth of 4.5-6 m from the surface. Two facies can be studied:

— Fine facies in the upper part: thickness around 2 to 3 m. Made of sand fine silty and sandy loam sometimes clayey.

— Coarse facies in the lower part: medium to coarse sands coarse and gravels

On this layer, a Lefranc test gives permeability around 1.310^{-6} m/s [Terrasol, 2015].

Brioverian substratum According to the bedrock, it is a Brioverian substratum. This is mainly made of briverian shale. These shales have been folded and altered. There are more or less friable, altered or fractured from the alterites to the healthy bedrock [Terrasol, 2015].

— Alterites come from the alteration of the bedrock. It is mainly clayey and silty but rarely sandy. It can be found up to 20m deep in some areas. But on average it is found at a depth of about 8-9m. This layer has a thickness around 0.5m.

— Sandstone and shale. Classified into 4 categories depending on their nature and state of fracturing.

— Local meeting of quartz veins.

Faults Figure 3.3 represents the presence of faults in Rennes. It is useful to know in advance the presence of faults in order to anticipate potential water flows with particular directions. This figure shows that the Cleunay station appears to be far enough from the faults to have a significant effect on the groundwater flow.

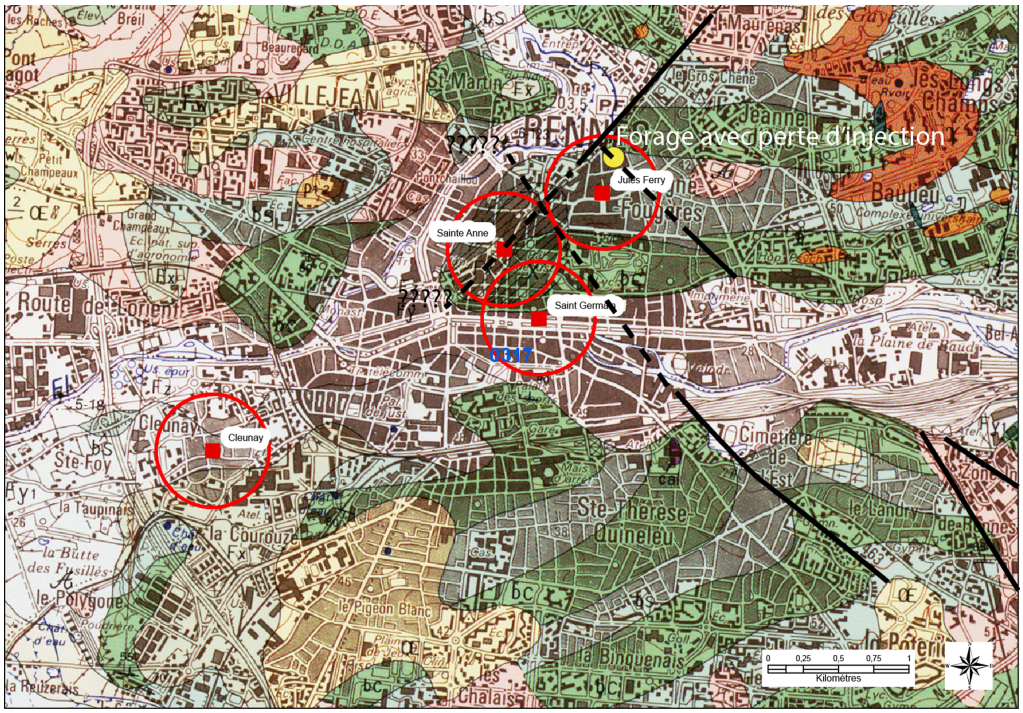

Figure 3.3 – Geological fault in Rennes (modified) [InfoTerre]

3.3.2 Hydrogeological context

In the region of Bretagne, there is an absence of long aquifers but the presence of small independent aquifers (no more than 10 hectares in surface area) [Pinson and Bault, 2019]. Three types of aquifer have been found [Terrasol, 2015] :

— Perched aquifers : found punctually and small size. They are found in the embankments. Present thanks to local clayey alterites. They do not communicate with other aquifers and they are feed thanks to rainfall.

— Alluvial groundwater : present in the alluvions and made of clayey alterites. The flow direction is linked with the axes of the valley.

— Fractured bedrock aquifers. This is on equilibrium with the alluvial groundwater. The flow direction is linked with the fractures.

Figure 3.4 indicates the global direction of the water flow in Rennes. At Cleunay station, the flow is mainly directed to the North due to the draining river "la Vilaine".

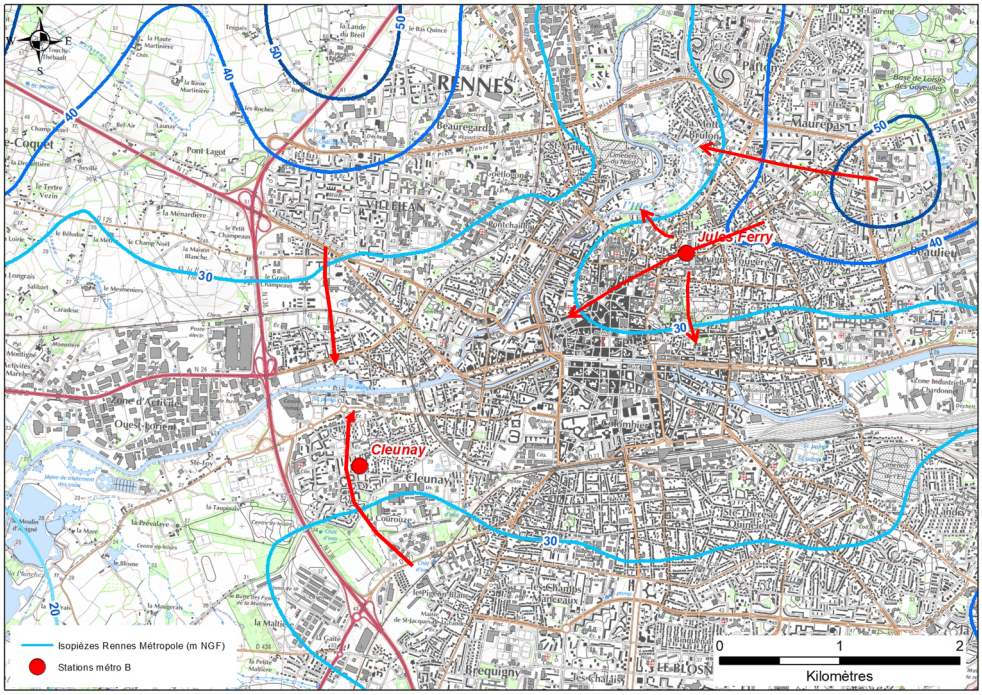

Figure 3.4 – Piezometric maps in Rennes with water flow direction [InfoTerre]

3.4 Local context

3.4.1 Field data

Four drilling campaigns were carried out between 2008 and 2013. The localisation of this campaign can be observed in Figure 3.5. A short description of obtains results is given.

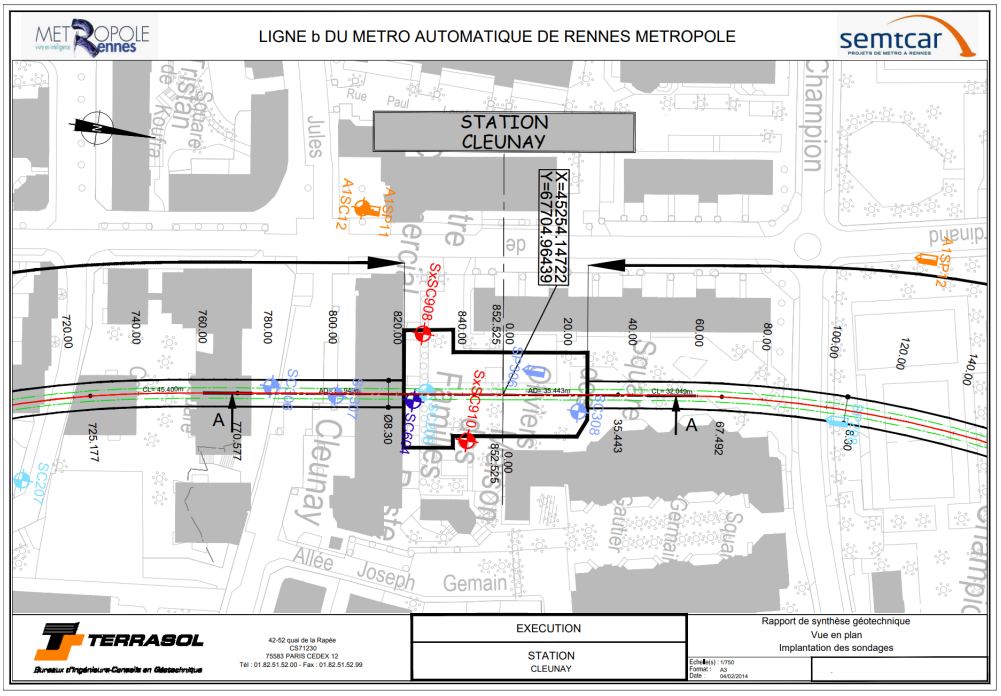

Figure 3.5 – Visualisation of the boreholes [Terrasol, 2015]

— A1-SC12 :

- Core drilling carried out in 2008-2009 (before the start of construction work);
- Depth of drilling equal to 26m;
- Presence of 1 m of embankments followed by 5 m of alluvium. Brioveruan substratumm (bedrock more or less fractured) at a depth of 6 m from the ground;
- Lefranc test indicates a permeability between 2.22 10^{-7} m/s and 2.14 10^{-7} m/s in the alluvium;
- Piezometric survey for 70 days (from 16/07/2007 to 25/09/2008) → Piezometric height between 3.16 and 5.13 m/ground (See Annex A.1);
- log present on Annex A.2.

— SC207 :
- Core drilling carried out in 2010;
- Depth of drilling equal to 30 m;
- 1 m of embankments - 1 m of alterite before bedrock.

— SC208 :
- Core drilling carried out in 2010;
- Depth of drilling equal to 25.9 m;
- 6 m of alluvium - 1 m of alterite before bedrocks;
- Lefranc test in alluvium indicates a permeability around 1.3 10^{-6} m/s.

— SC306 :
- Core drilling carried out in 2011;
- Depth of drilling equal to 26.3 m;
- 6 m of alluvium before bedrock.

— SC307 :
- Core drilling carried out in 2011;
- Depth of drilling equal to 26 m;
- 6 m of alluvium - 1 m of alterite before bedrock.

— SC308 :
- Core drilling carried out in 2011;
- Depth of drilling equal to 26 m;
- 1 m of embankments - 4 m of alluvium - 1 m of alterite before bedrock.
- Lefranc test in alluvium indicates a permeability around 1.3 10^{-6} m/s.

— SC604 :
- Core drilling carried out in 2012;
- Depth of drilling equal to 25 m;
- 1 m of embakments - 5 m of alluvium - 1 m of alterites before bedrocks.

A summary of those information lead to the geological section of Cleunay station see on Figure 3.6. The cutting line can be seen in the Figure 3.5. And so, in average, the geology on the site is as follows:

— between 4 and 6 m of alluvium (yellow on Figure 3.6)

— 1 m of alterite (blue on Figure 3.6)

— bedrock made of shale with more or less sandstone (green on Figure 3.6, the different variations of green indicate the various degrees of alteration of the bedrock)

With a piezometric height between 3.16 and 5.13 m/ground.

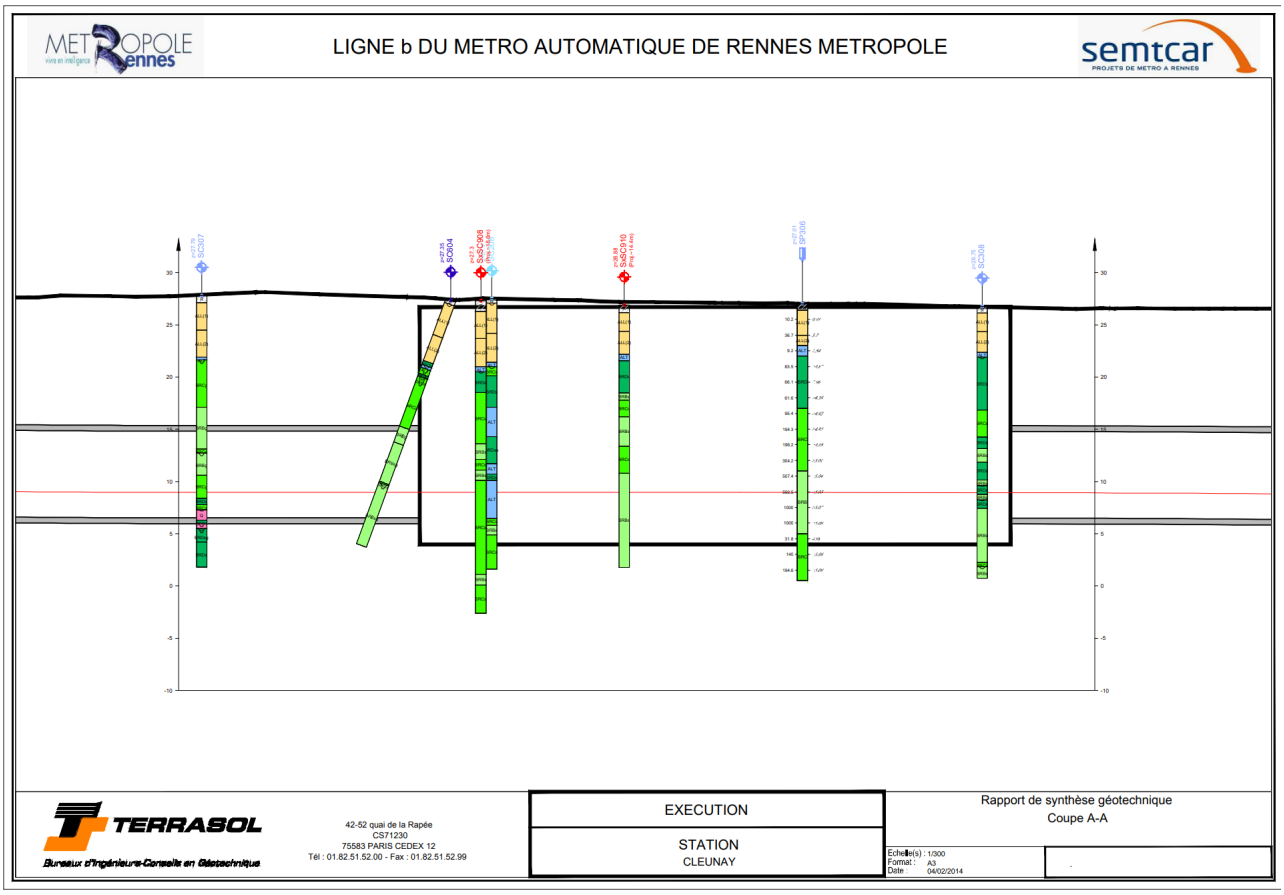

Figure 3.6 – Section A-A of the station [Terrasol, 2015]

3.5 Geothermal equipment

Regarding the station circuit, the station is equipped at both the slurry wall and slab level. Figure 3.7 shows the position of the pipes in the slab and the panels of the slurry wall.

The slurry walls There are 1.2 m thick and the pipes inside are placed as close to the ground as possible. The pipes are U-shaped and in each loop there are 6 or 8 vertical pipes. The height of these loops is not homogeneous and is between 10.9 and 12.8 m. There are 44 loop in the wall, which lead to a total equipped surface equal to 1532 m^2.

About the slab It has a thickness of 2 m and is made of both reinforced concrete and protective concrete that prevents the waterproofing layer from being pierced. The surface of the slab equipped with pipes is corresponding to 1394 m^2. 72 loop are installad and each loop contains 8 vertical pipes. The length of pipe in s loop is between 76 and 78 m.
The pipes used in these geothermal exchangers have an internal diameter of 20.4 mm and an external diameter of 25 mm.

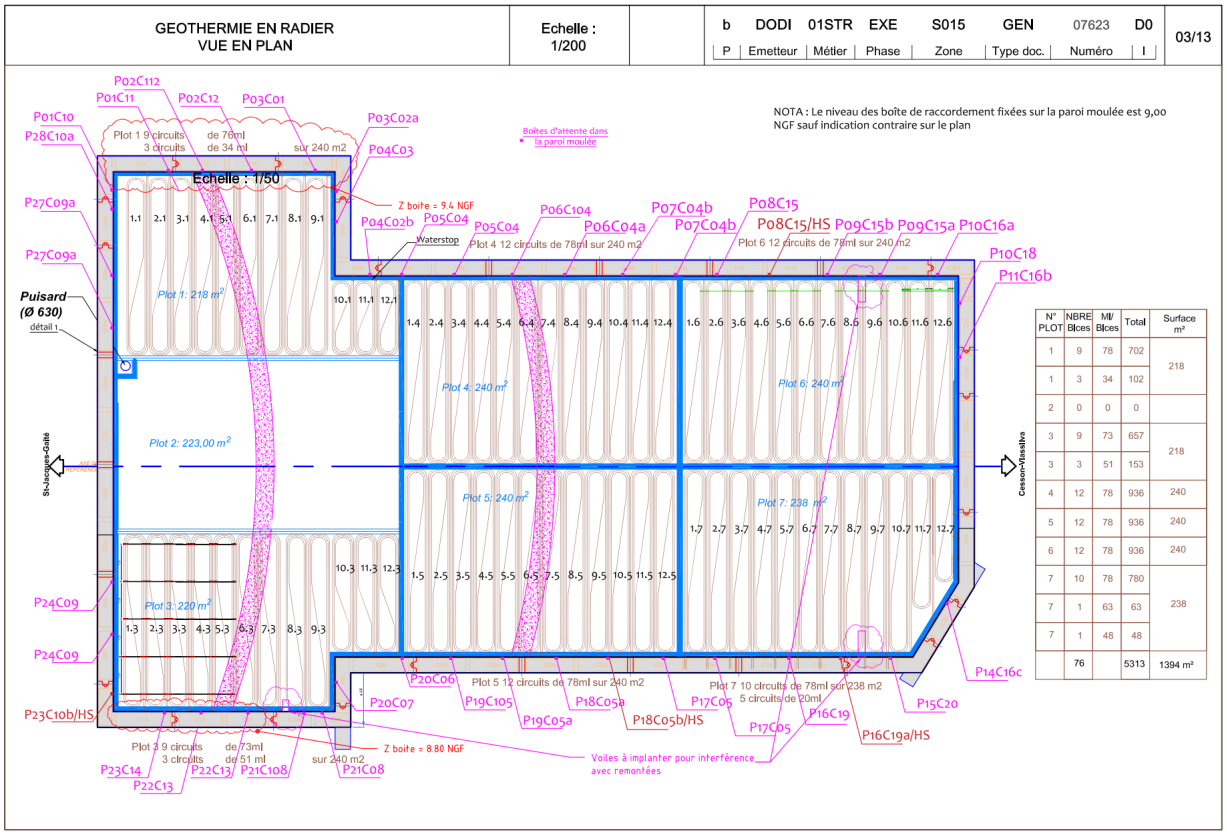

Figure 3.7 – Plan of the position of the geothermal probes in the foundation and illustration of the panels used in the cast walls [personal communication]

Figure 3.8 – Photo of the pipe cages used in the slurry walls [personal communication]

3.6 Thermal response test

In 2019, a 49-day thermal response test was conducted by AQUASSYS. The recording took place from 7/10/2019 to 25/11/2019. This test consists of evaluating the behaviour of the soil to the extraction of a certain amount of energy through the geothermal circuit of the station. To do this, a heat transfer fluid at a certain temperature is injected into the circuit. This fluid circulating in the pipes will be affected by the temperature of the ground. The temperature at the outlet is then measured. Then, this outlet water is subjected to the effect of a cooling unit before being reinjected into the circuit. The aim of this test is to reproduce the behaviour of the heat pump with the cooling unit.

Conduct of the test The test was carried out in four phases, depending on the active area of the circuit. The first phase consisted of the activation of the slurry wall and slab in the western part of the station (plot 1-4-6) . This led to an activation of 1463 m^2. The second phase activates only the western part of the slab, 697 m^2. The third phase has the same activation area as the first. The last phase, where both the slab and the slurry wall are active, corresponds to half of the western part (plot 1 and half of the 4).

	Phase 1	Phase 2	Phase 3	Phase 4
Slurry wall active	West part	/	West part	Half of the west part
Slab active	West part	West part	West part	Half of the west part
Area active (m^2)	1463	697	1469	731.5

Table 3.1 – Description of the active area of the different phases

3.6.1 Results

Inlet and outlet temperature Figure 3.9 represents the measure of the temperature of the heat carrier fluid on inlet and outlet and the ambient temperature of the Cleunay station. The green line represents the four different phases of the test. The initial temperature is 12°C and after 50 days of extraction the temperature drops to 5.3°C. The outlet temperature starts at 13.5°C and ends at 7.4°C. When the active surface area decreases during a phase change, there is a local decrease in temperature. Similarly, if the active surface area increases during a phase change, there is a local increase in temperature. 2 power outages were recorded during the test period, on days 9 and 36. In addition, the water flow was interrupted between days 26 and 27. The ambient temperature ranged from 17°C to 10°C and stabilised at around 13°C at the end of the test. The average value of this ambient temperature is 13.83°C.

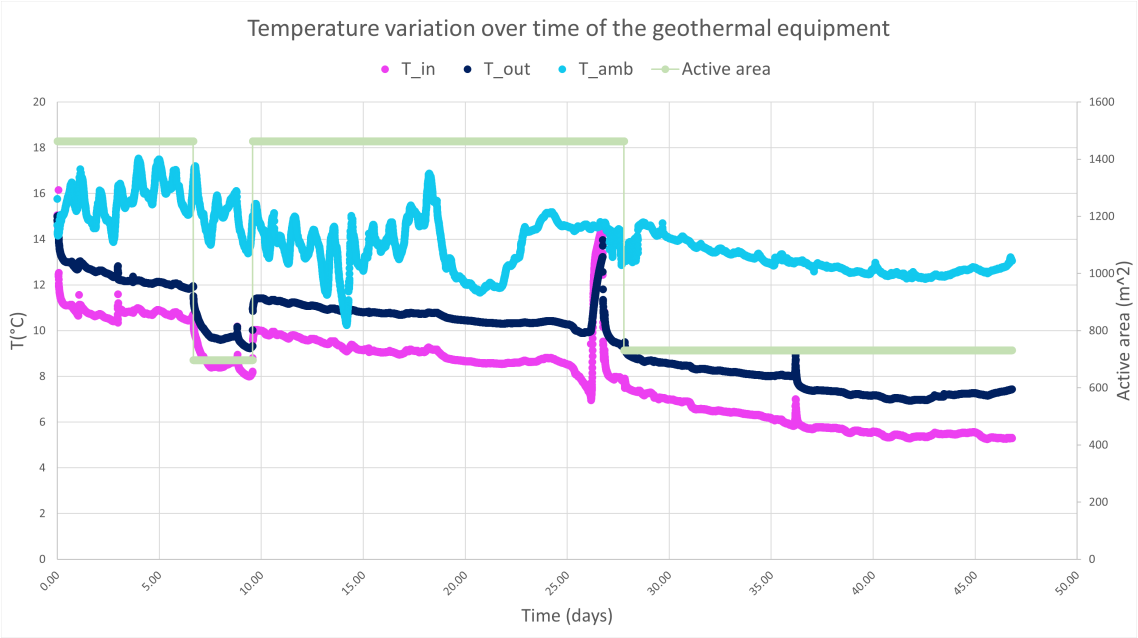

Figure 3.9 – Inlet, outlet and ambient temperature values during the thermal test period

Difference between inlet and outlet temperatures Figure 3.10 shows that the values of the $\Delta T_{(output-input)}$ is relatively constant excepted some outliers. These outliers are due to power outages in the station or stoppages in the water circulation. The average value of this ΔT is 1.6°C.

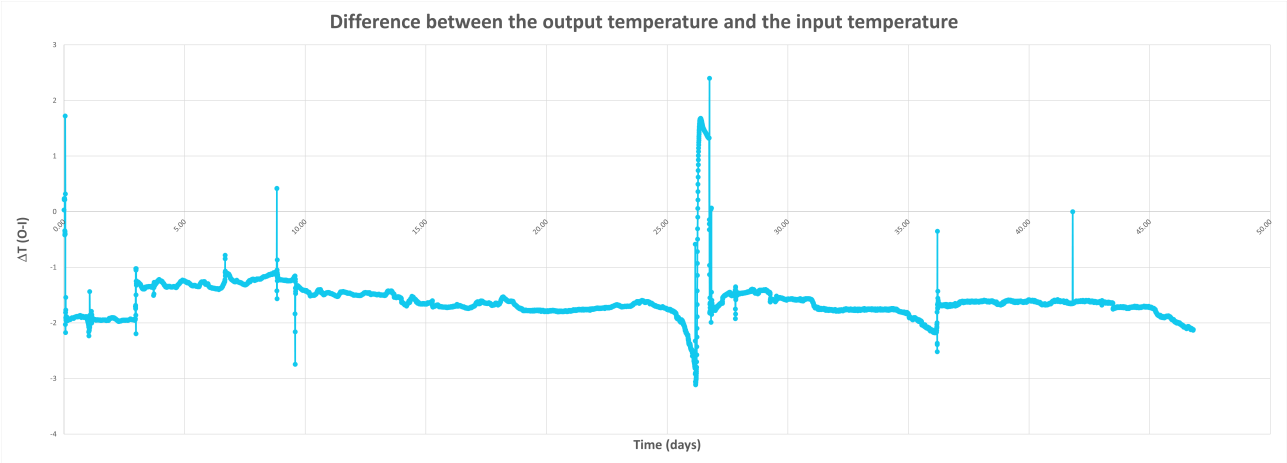

Figure 3.10 – Variation of the temperature difference between the inlet and outlet during the thermal test period

Flow rate and fluid velocities Figure 3.11 allow to see the recorded flow rate from the test. This flow rates decrease slightly with time and varies between 12 m^3/h and 9 m^3/h. The other two curves show the fluid velocity inside the pipes within the primary and secondary circuits.

To do this, the value of the flow rate is divided by the internal surface of the circuit. This makes it possible to determine the fluid velocity in the primary circuit but not in the secondary circuit. This value must be further divided by the number of loops through which the fluid passes. This determines the value of the fluid in each loop of the circuit.

These values of fluid velocities will be used as input to the model as will be described in the next chapter which consists of the description of the model performed.

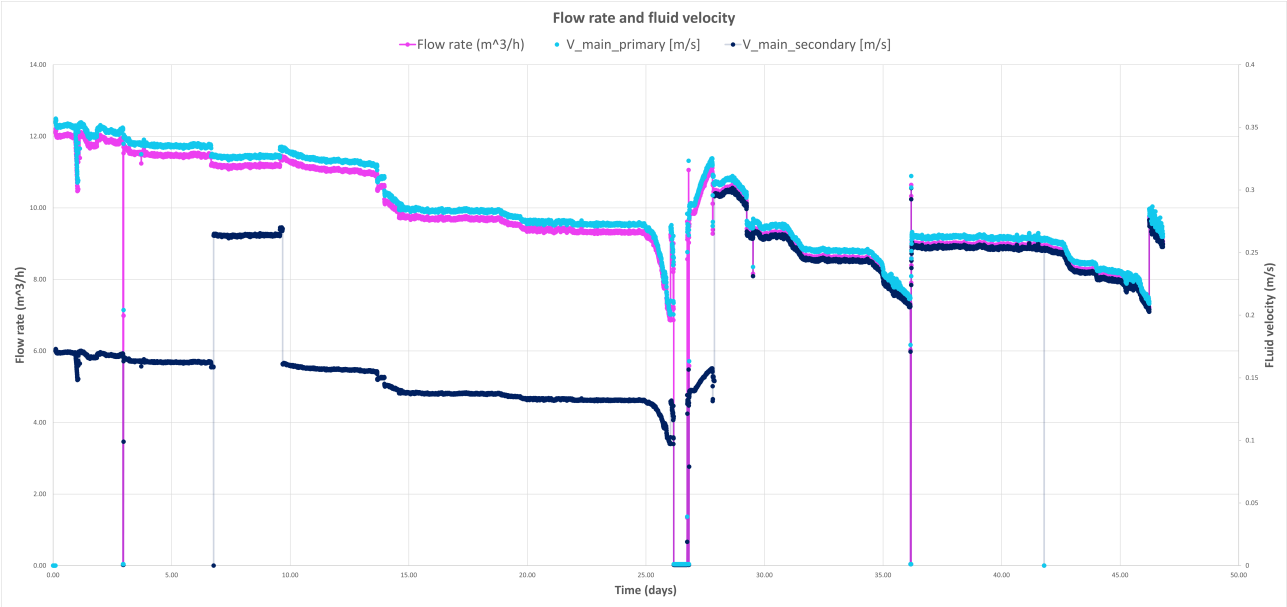

Figure 3.11 – Visualisation of the flow rate and fluid velocity inside the pipes during the thermal test period

Extracted power With those data, the equation 3.1 can be used in order of calculate the power that can be extracted with the present ΔT between the input and output. This calculated power is presented on Figure 3.12.

$$P = \Delta T \cdot Q \cdot 1.16 \tag{3.1}$$

With,

- P, calculated extracted powers in kW
- ΔT, the difference of temperature between the inlet and outlet (measured)
- Q, the mean flow rate in m^3/s
- 1.16 a coefficient for units. It it the heat capacity of water devided by 3600 wich allow the passage of the hours in secondes.

$$\frac{\rho \cdot C_p}{60 \cdot 60 \cdot 1000} = 1.16 \tag{3.2}$$

The extracted power, like the ΔT, is relatively constant over time. The average extracted power is 18.10 kW, except at the beginning of the simulation when it is closer to 28 kW.

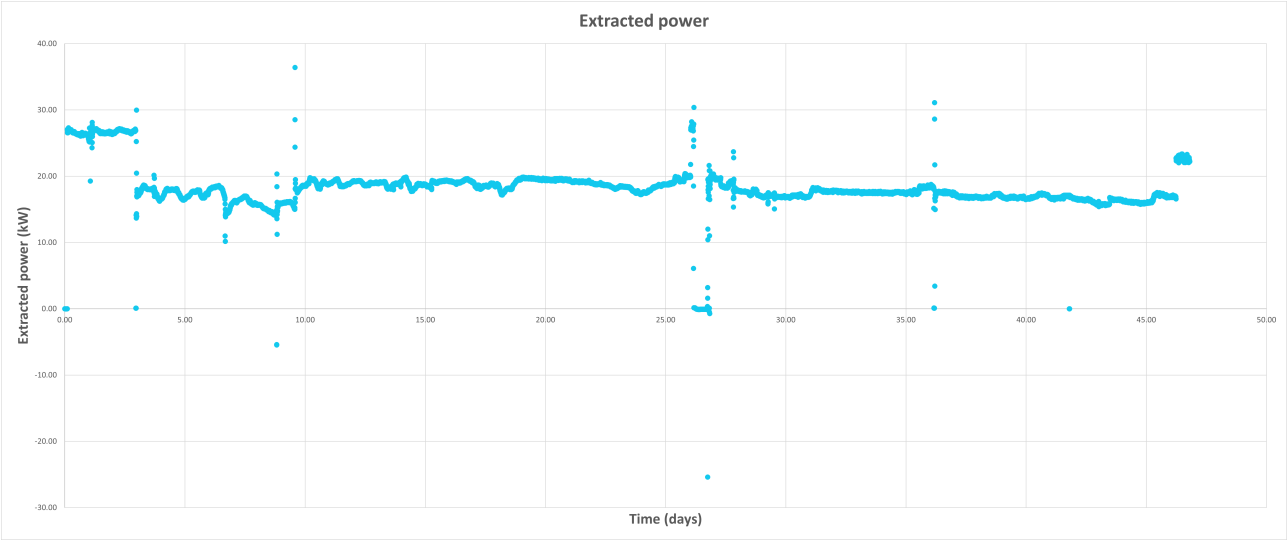

Figure 3.12 – Extracted power thanks to the present ΔT

Extracted power per active area If attention is focused to the power per active area of the geothermal circuit, it is observed on Figure 3.13 and Table 3.2 that in phases 2 and 4 this power per unit is much higher because the active area is much smaller.

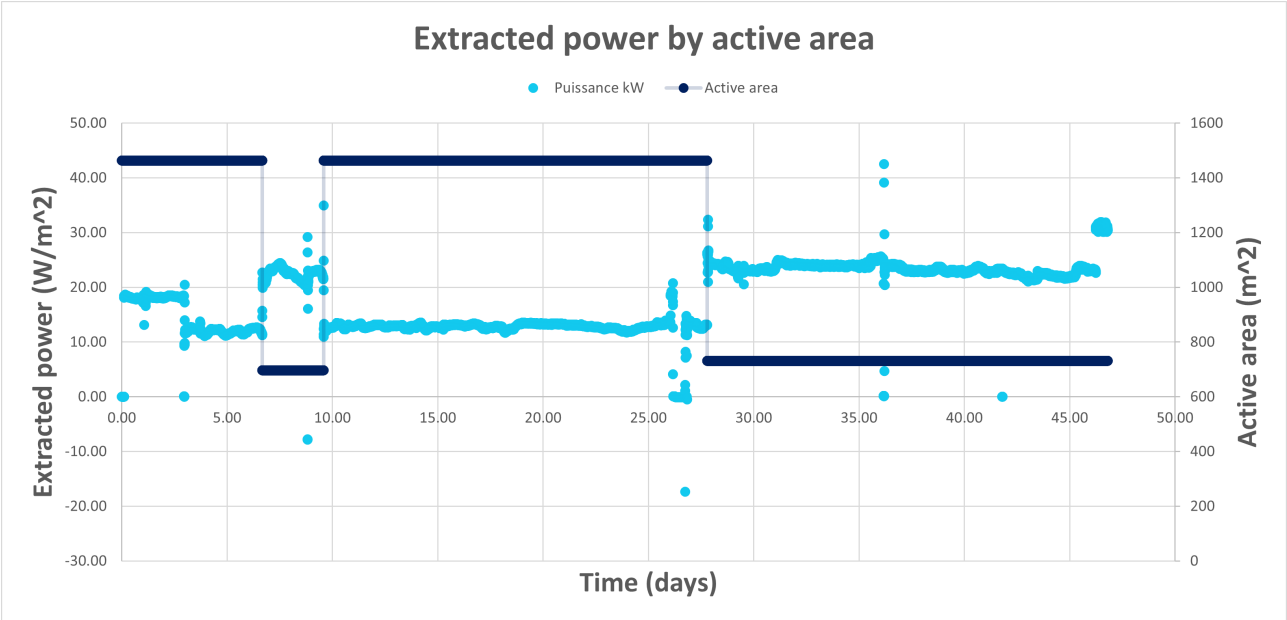

Figure 3.13 – Extracted power by active area thanks to the present ΔT

	Phase 1	Phase 2	Phase 3	Phase 4
Mean extracted power by active area (W/m^2)	14.45	22.40	13.46	23.53

Table 3.2 – Summary of the mean power extracted by active area

Chapter 4

Numerical model

This part consists of the presentation of the model carried out to study the thermal behavior of Cleunay station. The structure of this section is as follows: Firstly, a description of the model geometry is presented. This description examines both the model and the pipes. Then, the equations governing the model are summarized, and all the parameters utilized to describe the different materials are presented. After that, a description of the boundary condition imposed on the model is described. Finally, a description of the mesh and the solveur used is proposed.

4.1 Description of the model

The software used to model the station and reproduce the thermal response test data is COMSOL. This software is used for numerical simulation with 3D finite element analysis and supports multiphysics. In this model, three physics are used: heat transfer in porous media (for the soil), heat transfer in pipes (for the heat exchanger) and heat transfer in solids (for the concrete). The physics of heat transfer in porous media allows a simple description of the groundwater flow.

4.1.1 Station geometry

The model is a box with a length of 80 m, a depth of 40 m, and a width of 55 m. The size is chosen in order to avoid boundary effects. Inside this box, the Cleunay station is created. The Cleunay station has an average depth of 25.5 m, a width between 25.5 and 36 m, and a length of 56.5 m [Terrasol, 2015]. Figure 4.1 give a general vieuw of this model.

Figure 4.2 represents more precisely the dimensions of this model. The 18.5 m represents the interior of the station. In the field, this area is made up of several floors with corridors, cash desks, connecting staircases, and so on. In the model, this zone is simplified as air. Below, the 4.5 m represents the sub-docks. This area is made of concrete. Furthermore, the 2 m below represents the slab, which consists of the loops of the geothermal circuit, this is also made with concrete. Additionally, the walls are 1.2 m thick."

To finish, a simplification has been made to the shape of the slab. In reality, it has a slightly circular shape, but in my model, the slab has been approximated with a rectangular shape.

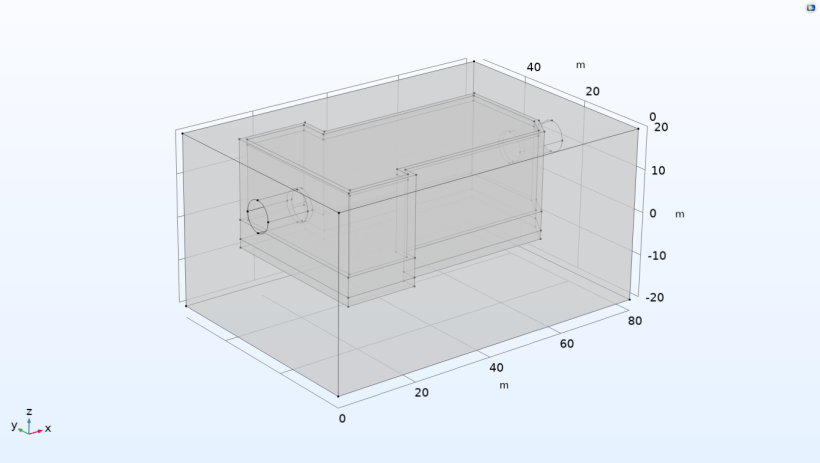

Figure 4.1 – General vieuw of the Cleunay station

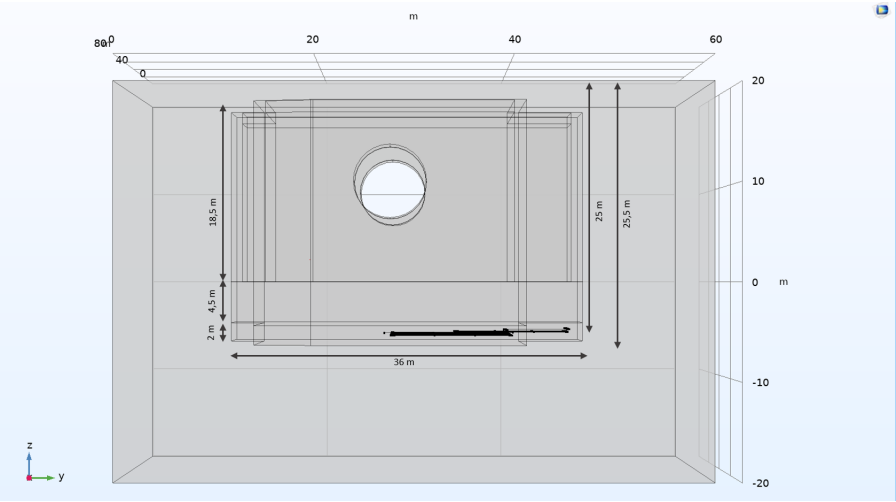

Figure 4.2 – Model dimensions scheme. Presence of circuit in the slab.

Pipe characteristics The geothermal circuit is formed of a primary and secondary circuit. The secondary circuit is composed of all the loops present in the circuit, and has an inner diameter of 20.4 mm. The primary circuit is the pipe that feeds and collects all the loops of the secondary circuit. It has an inner diameter of 105.4 mm. Both are made of PE-Xa tube (a plastic material resulting from the polymerization of ethylene). The primary and secondary circuits can be seen in Figure 4.3, where each input and output of the loop is connected to the primary circuit. During the rest of the report, the use of primary circuit and collector circuit will be considered synonymous.

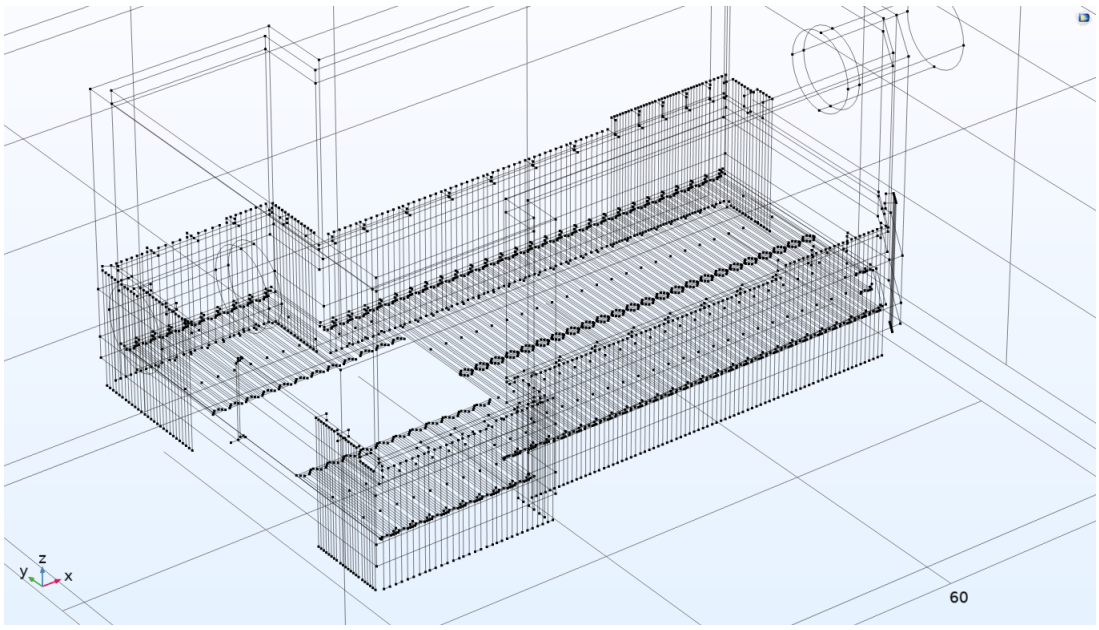

Figure 4.3 – Model with pipes

	Primary circuit	Secondary circuit
Outer diameter (mm)	25	110
Thickness of the tube	2.3	2.3
Inner diameter (mm)	20.4	105.4
Thermal conductivity (W/mK)	0.41	0.41

Table 4.1 – Characteristics of primary and secondary circuits

4.1.2 Pipes geometry

Characterization of the loop in the slab The pipe loops that make up the geothermal circuit in the slab have a "snail" shape, with the pipe in the loop winding around itself (see Figure 4.5). As seen in Figure 3.7 on page 28, the slab is divided into seven parts. The position of the pipes in the model has been optimized to best match the data received from the site installation. Table 4.2 shows the difference between the length of the loops on-site and the length of the loops in the field. Additionally, the length of the connection between the secondary circuit loops and the primary circuit is also included. This table allows us to observe that the length of the loops in the model corresponds to the provided data. The only exception is the length of the 7B and 7C plots, which are the loops located at the northeast corner of the station.

Regarding the location of these pipes in the station, they are placed at a depth of 25.5 m from the surface and 5.5 m from the interior of the station, as shown in Figure 4.2. The space between the pipes and the interior of the station is filled with concrete. The primary circuit is established 50 cm above the pipes. It is also positioned 1.2 m from the wall in contact with the ground. Refer to Figure 4.4 to vizualize the geometry.

Finally, the total length of the primary circuit, including the input and output pipes, is 181 m. The total length of the secondary circuit, comprising the 72 loops, is 5313 m. This results in an equipped area of 1394 m^2.

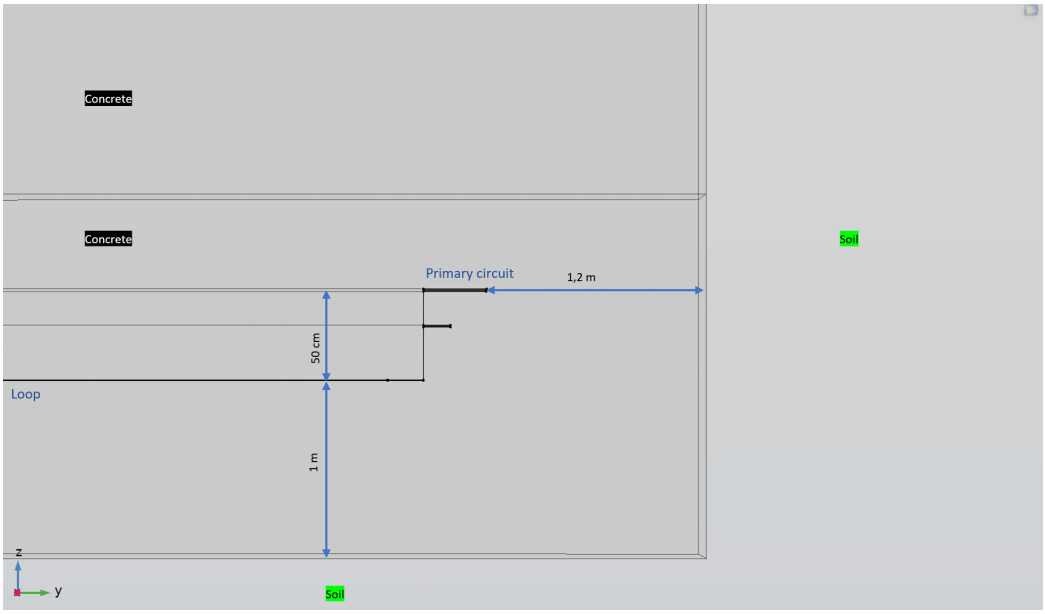

Figure 4.4 – Zoom of the geometry on the slab

	Theorical length (m)	Model length (m)	Length of link (m)
Plot 1A	78	78.0	1.3
Plot 1B	34	34.0	1.5
Plot 2	0	0	0
Plot 3A	73	73.0	1.52
Plot 3B	51	51.1	1.4
Plot 4	78	78.1	1.04
Plot 5	78	78.1	1
Plot 6	78	78.1	1.04
Plot 7A	78	78.1	1
Plot 7B	63	60.1	2.1
Plot 7C	48	45.1	1.5

Table 4.2 – Difference between the theoretical value and the numerical value for each loop

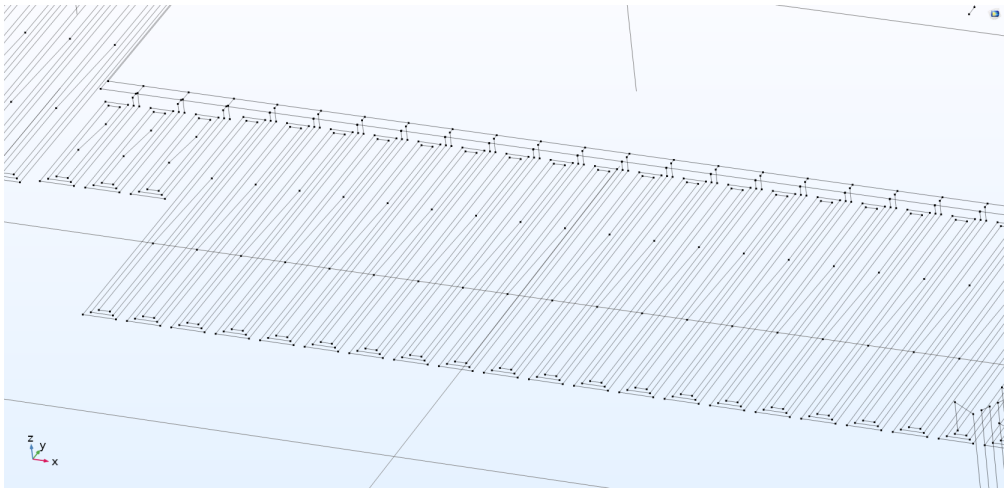

Figure 4.5 – Visualisation of the shape of the slab loops as well as the primary and secondary circuit

Characterization of the loops in the slurry wall The pipes in the slurry walls are made of the same material as the pipes in the slab, but their shapes and positions in the station are different. In the slurry walls, a loop is made up of 3 or 4 "U" shapes, as can be seen in Figure 4.6. In total, the slurry walls are composed of 44 loops, but 4 loops are out of order. The heights of these loops are not uniform, varying between 10.9 m and 12.8 m. However, each loop has a consistent maximum depth of 29 m from the surface. Figure 4.6 clearly illustrates that all the loops are aligned at the same level at the bottom but vary in height at the top. Therefore, what varies is the length of the wall in contact with the air in the station and the pipes in the loop. In the worst case, the pipes are 3.8 m long, with a wall in contact with the interior of the station.

Figure 4.7 summarizes the geometry of the primary and secondary circuits on the wall. The loops are placed at a distance of 2 cm from the wall in contact with the ground and, thus, 1 m from the wall in contact with the interior of the station. The primary circuit is positioned at a height of 2.3 m above the station floor and 10 cm from the wall in contact with the station interior.

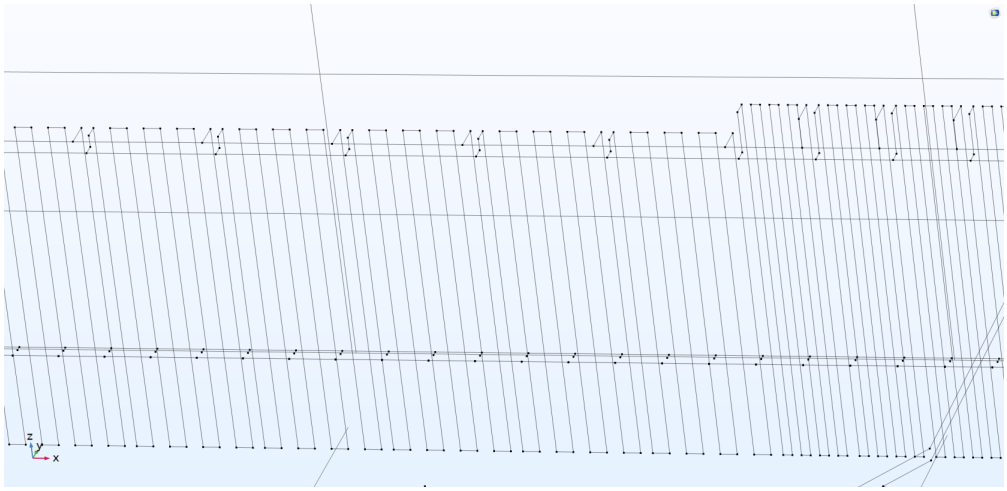

Figure 4.6 – Visualisation of the shape of the slurry walls loops as well as the primary and secondary circuit

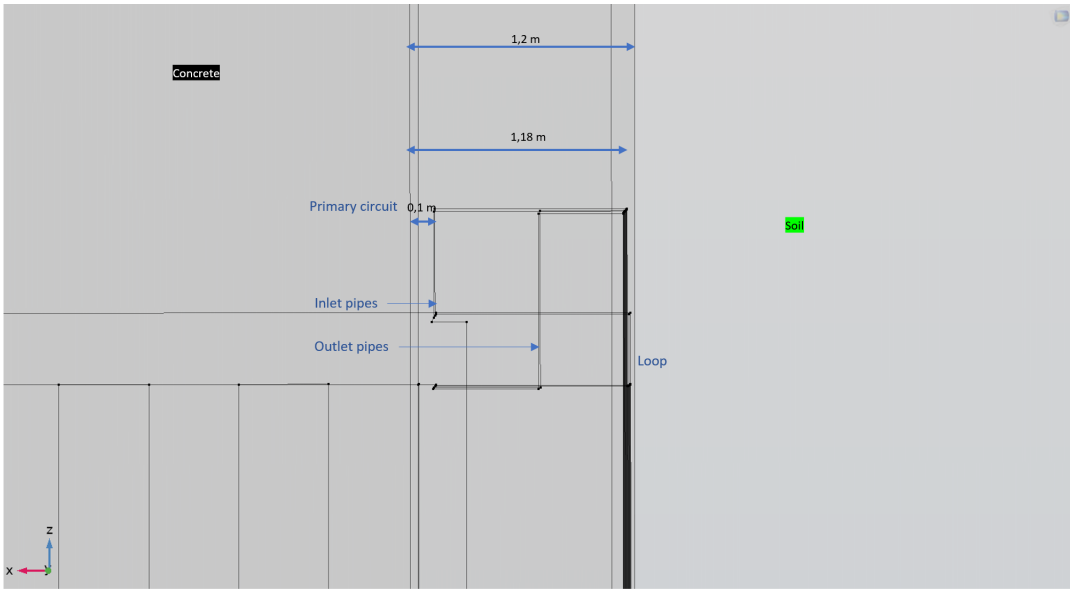

Figure 4.7 – Zoom in on the geometry of the secondary and primary circuits on the wall

Figure 4.8 aims to demonstrate the difference between the provided field values and the values implemented in the model. The provided data should be interpreted with caution as it periodically includes values that are dependent on the position of the loops in relation to the collectors. This is not the case in the model. The green curve in this graph indicates the difference between the model values and the expected length. When the value is negative, it means that the model has a shorter length than expected. On the contrary, if the value is positive, the model has a longer loop length than expected. The average of these differences is equal to 0.38 m, which indicates that, overall, the excess and deficient lengths are close. Annex A.3 on page vi represents the data used to form the model. The strictly respected values are the loop height and the size of the loop with the number of vertical pipes.

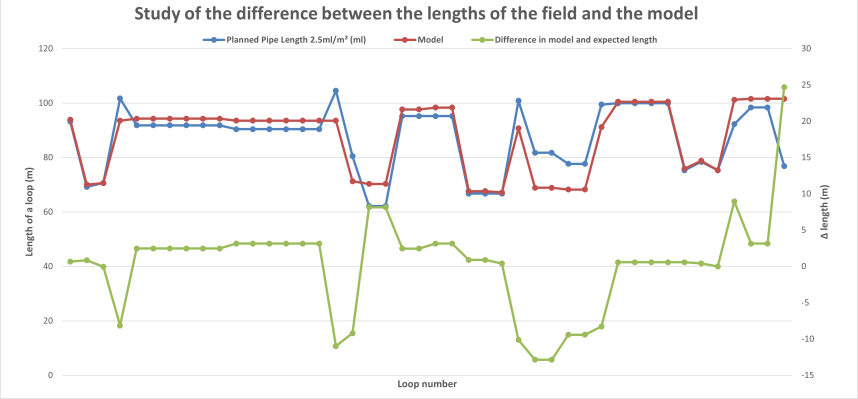

Figure 4.8 – Length difference between field and model values

4.2 Governing equation

In this part, a description of the equations used to resolve the numerical model is proposed. As described before, three different heat transfer mechanisms are involved in this model. Heat transfer within the ground, heat transfer within pipes and heat transfer within a solid.

Heat transfer in the soil The soil is considered as a two-phase medium with grains and pores filled with water under saturated conditions. Consequently, two equations must be used to solve for heat transfer within this medium, one for the solid grains and one for the water. However, it is possible to use the local thermal equilibrium assumption which assumes a temperature equilibrium at both solid and solid phase level, see Equation 4.1.

$$T_f = T_s = T \tag{4.1}$$

This assumption allows us to define an effective value for the parameters that depends on the properties of both the water and the solid, depending on the porosity of the medium. See equation 4.2

$$(\rho C_p)_{\text{eff}} = \epsilon \rho_f C_{p,f} + \theta_s \rho_s C_{p,s} \tag{4.2}$$

$$k_{\text{eff}} = \epsilon k_f + \theta_s k_s \tag{4.3}$$

The equation used to solve the heat variations in the soil is the heat conservation equation:

$$(\rho C_p)_{\text{eff}} \frac{\partial T}{\partial t} + \rho_f C_{p,f} \mathbf{u} \cdot \nabla T + \nabla \cdot (-k_{\text{eff}} \nabla T) = 0 \tag{4.4}$$

— θ is the solid matrix volume fraction;

— ϵ is the porosity;

— eff denotes effective;

— f denotes fluid;

— s denotes solid;

— u is the field velocity, which is interpreted as the Darcy velocity.

The blue term represents the heat transfer induced by the movement of groundwater. This term includes heat transfer due to a thermal gradient, but also heat transfer due to a difference in density [Dassargues, 2020].

The green term is the divergence of the conductive heat flow [COMSOL]. This term exists even if there is no movement of water [Dassargues, 2020]. It is this mechanism that governs the majority of heat exchangers, considering that the value of Darcy flow is very low (see next section).

The absence of a dispersion term in the equation indicates that this process is neglected. This assumption is acceptable due to the low contribution of dispersivity compared to the dominant conduction processes.

Heat transfer in concrete In concrete, the equation used to solve the heat transfer is:

$$(\rho C_p)\frac{\partial T}{\partial t} + \nabla \cdot (-k\nabla T) = 0 \tag{4.5}$$

where,

— ρ is the bulk density in (kg/m^3);

— C_p is the specific heat capacity (J/kg.K);

— k is the thermal conductivity of the concrete (W/m.K).

The coloured term in this equation represents the heat transfer due to a temperature gradient.

Heat transfer in pipes This equation represents heat transfer by conduction and convection in pipes for an incompressible fluid. The fluid model used is a Newtonian fluid.

The blue term represents the heat transfer in relation with the tangentiel velocity inside it.

The green term represents the heat transfer thanks to the gradient of temperature close to the pipes with the surface A.

The orange term on the right side corresponds to the heat dissipated due to friction caused by viscous shear [COMSOL].

In comparison with the other equation of conservation, all the term are linked with the cross-sectional area.

$$\rho A C_p \frac{\partial T}{\partial t} + \rho A C_p u \nabla \cdot \mathbf{T} = \nabla \cdot (Ak\nabla \mathbf{T}) + \frac{1}{2} f_D \frac{\rho A}{d_h} |u^3| + Q_{\text{wall}} \tag{4.6}$$

Where,

— ρ is the fluid density of the fluid inside the pipes (kg/m^3);

— A is the pipe cross-sectional area (m^2);

— C_p is the specific heat capacity of the fluid inside the pipes (J/kg·K);

— $\mathbf{T}$ is the temperature of the fluid inside the pipes (K);

— d_h is the inner diameter of the pipe (m);

— f_D is the Darcy friction factor of the pipes;
— u is the tangential velocity of the fluid inside the pipes (m/s);
— k is the thermal conductivity of the plastic tube (W/m·K);
— Q_{wall} represents external heat exchange through the pipe wall (W/m);

$$Q_{\text{wall}} = (hZ)_{\text{eff}}(T_{\text{ext}} - \mathbf{T}) \tag{4.7}$$

where,
— h is the heat transfer coefficient (W/m^2·K);
— Z is the wall perimeter (m);
— T_{ext} is the temperature outside the pipes (K).

4.3 Parameters of materials

The parameters described in this section are specific to the mediums studied (soil, concrete, and water), and they are not the "effective" values described above.

Soil As described in the previous chapter, the geology around the station is mainly bedrock. The latter is composed of fractured shale with more or less sandstone. On the document [Terrasol, 2015] some test has been made on the different samples of rock in order to characterise the geology. The results show that the characteristics of the rock are variable depending on the depth studied. In addition, the samples studied were collected before the start of construction work and therefore the construction of the station has disturbed the terrain, which may lead to different parameter values than those described.

— The bulk density is chosen by using the values found by the extracted sample in the investigated area of the model. The sample closest to this condition was found at a depth of 23 m, it consists of a shallowly fractured sandstone shale and has a bulk density of 2650(kg/m^3).
— The thermal conductivity has not been measured in the laboratory; therefore, the value used is a theoretical value based on literature research. First of all, dry shale has a thermal conductivity value between 1.5 and 3.5 (W/(m·K)) [Dassargues, 2020]. Since the model conditions are saturated, this will result in an increase in thermal conductivity. However, the value of the bulk density indicates that the porosity is low and so the impact of water will decrease. For a first approximation, a value of 1.5 (W/(m·K)) is chosen. A parametric study will be conducted in order to refine this value.
— The heat capacity of a dry shale is found between 890 and 1110 (J/kg.K) [Dassargues, 2020]. The value of 1100 is chosen has a first approximation (J/kg.K).
— Laboratory tests provide a rock porosity of 0.03. This is the value chosen in the model.
— Hydraulic conductivity of shale is between 10^{-9} and 10^{-13} (m/s) according [Dassargues, 2020]. The value of this parameter is important in order to characterise the groundwater flow. In a first approximation the chosen value is put equal to 10^{-9} (m/s) but it has to be studied with a parametric test.

Concrete

— The density of the concrete is set equal to 2400 kg/m^3. According to the norme NF EN 206+A2/CN, concrete has a density ranging from 2000 to 2600 kg/m^3 [Guiraud and Daubilly, 2022]. Therefore, since the exact density of the concrete on the site is not known, the chosen value is a reasonable assumption for initial estimations.

— The thermal conductivity of concrete varies due to different factors, including density. The thermal conductivity can be determined based on the concrete density [Iman et al., 2018]. In this case, it leads to:

$$k = 0.0625e^{(0.0015\times 2400)} = 2.29(W/(m.K)) \tag{4.8}$$

This value is consistent with laboratory tests conducted on the concrete used, which estimated its thermal conductivity to be between 2.2 and 2.3.

— The heat capacity at constant pressure of concrete has a value between 800 and 1400 (J/kg.K). The chosen value is based on the density of the concrete. According to [Shafigh et al., 2018], a reasonable average value is 780 (J/kg.K).

— Concrete porosity is not a simple parameter to measure. However, this parameter is often very low [Alsayed and Amjad, 1996]. Consequently, a zero porosity will be imposed in the model. Imposing this assumes the absence of water flow in this medium in the model. Indeed, in the field, concrete is protected by layers of waterproofing that prevent the presence of water flow inside.

Water The water parameters are pre-set parameters in COMSOL. Indeed, each parameter is linked to a function that depends on the temperature in the pipes. For more detailed information, please refer to the documentation on the COMSOL website.

	Concrete	Soil
Bulk density (kg/m^3)	2400	2650
Thermal conductivity (W/(m.K))	2.29	1.5
Heat capacity at constant pressure C_p (J/kg.K)	780	1100
Porosity (-)	0	0.03

Table 4.3 – Summary of the physical parameters used in the model

In the model this is important to notice that an approximation of a homogeneous and isotropic soil and concrete is chosen.

Heat transfer coefficient This parameter depends on various factors such as air speed, humidity level, temperature, thermal conductivity of the concrete, etc. [Guo et al., 2011]. Therefore, it is extremely difficult to determine. As a first assumption, a value of 4 will be imposed. This value is chosen because it is necessary to have a low value given the temperature inside the station (between 11 and 15°C). However, this parameter will be the subject of a parametric study to determine its impact on the results obtained.

4.4 Boundary Condition

As a first assumption, a homogeneous initial condition of a temperature of 13°C is imposed throughout the entire domain and in the pipes. This value is chosen based on the results of the TRT indicate an initial temperature of 13 °C.

Boundary conditions are also imposed on the 6 sides of the model. Firstly, for the top face representing the surface in contact with the outside, a uniform temperature of 11°C is imposed. This condition is due to the average temperature between October and November in Rennes [ClimateData]. The other 5 faces, which represent faces in contact with the ground, have

a constant imposed temperature of 13°C. The temperature of 13°C is chosen to correspond with the theoretical value of the temperature of soil at a depth of 25 m and with the data received from the thermal response test. The model has been constructed so that the boundary temperature has as little influence as possible on the results related to the circulation of water in the geothermal circuit.

In addition, the walls inside the station have a transient imposed temperature. These temperatures are the ambient temperature data measured during the thermal response test. The value of the measure ambiant temperature and the smoothed temperature is visible on Figure 4.9.

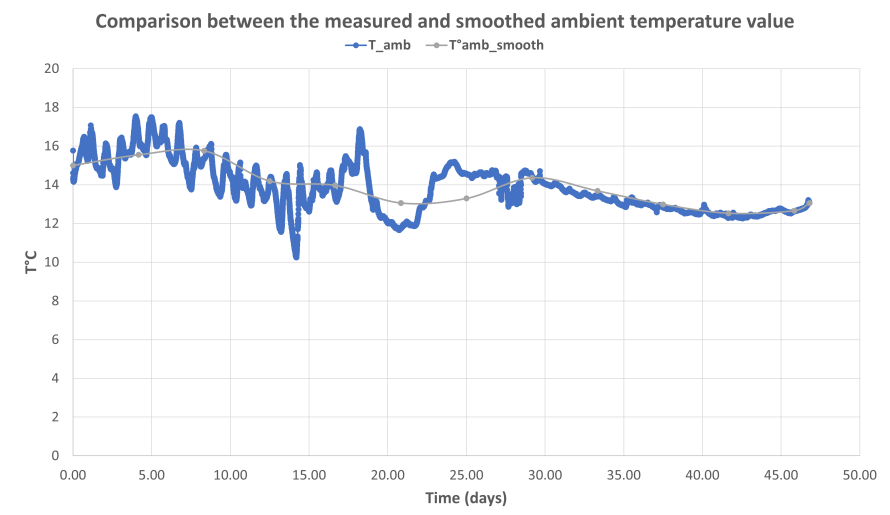

Figure 4.9 – Temperature ambiant recorded and smoothed

Figure A.2 represents the values of the temperature injected into the input of the circuit. These figures represent both the measured values and the smoothed values. The smoothed value are the curves introduced in the model to reproduce the thermal response test.

Similarly, Figure A.3 represents the values of the water temperature after passing through the entire circuit. This figure also includes both the measured values and the smoothed values. The smoothed values will be used to validate the results obtained with the numerical model.

There are several reasons for smoothing this data. To begin with, it allows us to obtain a reduced number of input data, thus reducing the computational load. In addition, introducing a variable data set into a model can lead to stability or convergence problems. This is because numerical models have difficulty accommodating sudden changes in variables.

4.5 Mesh

The mesh has a maximum size of elements equal to 2.8 m and a minimum size of 0.12 m. The mesh has a volume of 163,600 m^3 and is composed of both tetrahedra and triangles. In order to validate the accuracy of this mesh, the study of the mesh element quality is done.

4.5.1 Mesh Element Quality

The mesh element quality is important in order to validate a model. Table 4.4 indicates three different criteria that are used to quantify the quality of a mesh [COMSOL]. The values for those criteria are between 0 and 1, and a value of 1 means a high quality of the mesh. A low-quality mesh element leads to problems of convergence and inaccurate results.

The Skewness This measure evaluates the angle between two edges in an element and compares it with the angle of two edges in a corresponding ideal element. The average of this indicates that the quality of the mesh is acceptable. The equation used is Equation 4.9, where θ is the angle over an edge, and θ_e is the angle of the corresponding edge in an ideal element.

$$1 - \max\left(\frac{\theta - \theta_e}{180 - \theta_e}, \frac{\theta_e - \theta}{\theta_e}\right) \tag{4.9}$$

The Maximum Angle This measure is based on the largest angle in the element. If this angle is smaller than the largest angle of the corresponding ideal element, the quality is equal to one. If it is not the case, the quality shows how much larger this angle is in comparison with the ideal element. This value also indicates a good quality of the mesh.

Growth Rate This is a measure of local, anisotropic growth rate. It is a value that compares the maximum and minimum growth rate of a study element with respect to its neighboring elements. Therefore, the parameter indicates whether in a certain direction the neighboring element has a strongly different size compared to the neighboring elements in other directions. If the value is equal to 1, it means that the growth is identical in all directions, indicating no anisotropy in the mesh. The equation used is Equation 4.10.

$$\frac{min(s(E), s(E_a))}{max(s(E), s(E_a))} \tag{4.10}$$

With, s(E) the area of an element E and $s(E_a)$ the area of an neighbour element in the spatial direction a.

	Minimal quality of element [-]	Average quality of element [-]
Skewness	0.02032	0.6363
Maximum angle	0.03106	0.7246
Growth rate	0	0.5747

Table 4.4 – Summary of the mesh element quality

4.6 Solveur

Resolution of the matrix The general solver used is "MUMPS" (MUltifrontal Massively Parallel sparse direct Solver). This method aims to resolve large linear systems with a specific method for minimizing padding. It is multithreaded. A detailed explanation of how to solve linear matrices with this solver is beyond the scope of this work. For more information, please refer to the following links : https://mumps-solver.org/index.php.

Time step The method used to determine the time step is the implicit method of Backward Differentiation Formula (BDF). This method is known for its stability but also for its sensitivity to the "damping effect." Consequently, it is advisable to have highly smoothed inputs to avoid this phenomenon.

The time step has been imposed as strict in the model, meaning that the solver is forced to compute the solution at a certain time step, which is set to 1 day. In practice, the initial time step is 0.001 days and is increased to 1 day when stabilised. For the rest of the simulation the time step will be 1 day, except during phase changes when it will drop to a value of 0.001 in order to manage this change correctly [COMSOL].

Chapter 5

Calibration of the model

The aim of this section is to describe the various steps taken to increase the model's degree of complexity. To begin with, the model was built without the collector circuit. To do this, an identical inlet temperature was imposed at each loop inlet. The output temperature is calculated by taking the average of the output temperatures of each active loop in the circuit.

The second step consisted of adding the collector circuit, which connects all the loops in the circuit in parallel. The final step was to add groundwater flow to the model. This way, the model became sufficiently complex to reproduce field reality.

Next, a parametric study of the parameters introduced into the model is presented. This study not only calibrates the model with the thermal response test but also examines the impact of the various model parameters. After this calibration, the final model with all the calibrated parameters is studied in order to precisely understand the results.

5.1 Successive model improvements

The three results presented in this section are obtained using the parameters from Table 4.3 on page 41 described in previous Chapter. It is important to note that in this chapter, all results will be obtained with a temperature input. In the next chapter, the input is replaced by an input calculated according to a requested power and the results are still validated.

5.1.1 Without collector circuit and groundwater flow

Figure 5.1 represents the results obtain without the collector circuit and the groundwater flow. As there is no collector circuit, a measurement was taken at the output of each active loop to average these values. The green curve in Figure 5.1 represents the average temperature value at the output of each active loop. This green curve is contextualized with three other curves to correctly understand the results.

Firstly, the black curve represents the value of the circuit output temperature measured in the field during the thermal response test. The pink curve represents the water inlet temperature. The blue curve is the smoothed value of this measurement and is also used as input for the model. Additionally, the various phase changes taking place during the simulation are visible, helping to understand the changes in the curves' slopes. A full explanation of the results is given at the end of this chapter, on page 50. This result shows that this first approximation, even if incomplete, gives a result that is consistent with the expected results.

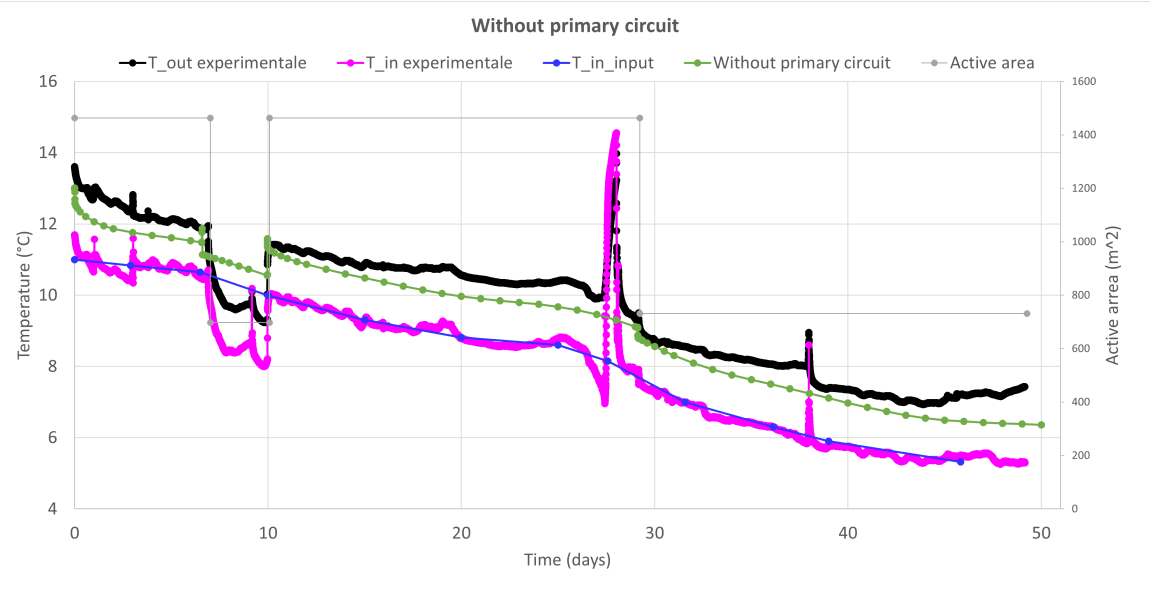

Figure 5.1 – Results without collector circuit and groundwater flow

5.1.2 With collector circuit

The second step was to make the model slightly more complex by adding the collector circuit. Figure 5.2 compares the temperature value at the circuit outlet with and without the collector circuit. It's important to note that the red curve shows the value of the water temperature at the model outlet, while the green curve shows the average value of the outlet temperature in each active loop of the circuit. The results show that the addition of the collector circuit introduces a constant temperature increase of 0.2°C throughout the model. This slight increase in temperature is due to the fact that the collector circuit is placed in the wall 10 cm from the inside of the station. In this warmer environment, the water heats up slightly.

In addition, the results indicate that the environment around the station is too insulating and not conductive enough, as shown by the fact that the numerical results are lower than the experimental results.

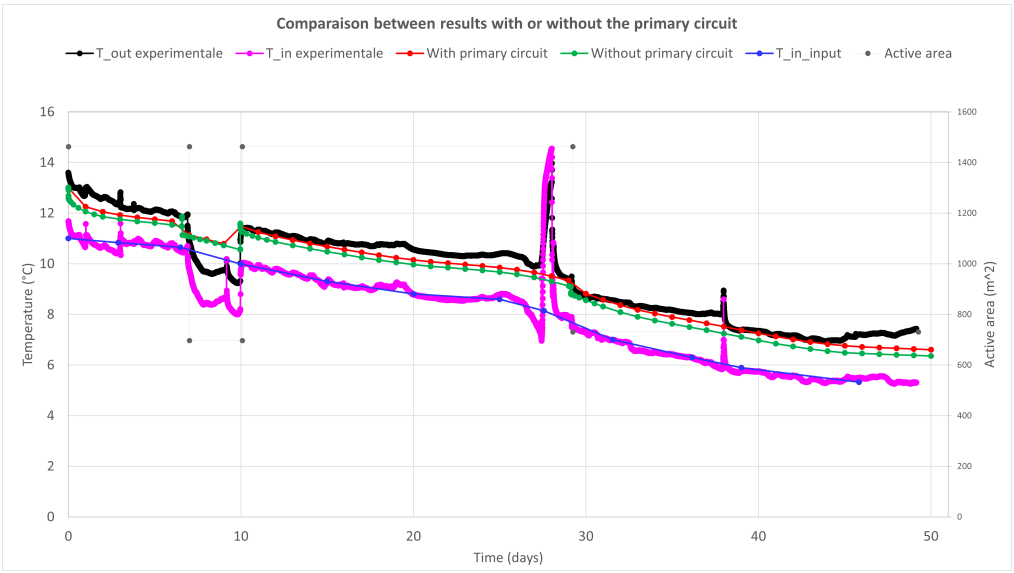

Figure 5.2 – Comparison between the outlet temperatures of the model with the primary circuit (red) and without the primary circuit (green).

5.1.3 With groundwater flow

As a reminder, there are no on-site measurements of groundwater flow in the soil. However, the description of the geology describes the presence of shale that becomes slightly sandstone from a depth of 18 m (the full description of the geology is presented on page 25). In this type of environment, if there is groundwater flow, it is mainly linked to the presence of fractures in the environment.

Darcy flow approximation As described in the parameter description on page 40, the hydraulic conductivity of the shale ranges from 10^{-9} to 10^{-13} (m/s). Moreover, Figure 3.4 on page 25 shows that groundwater is drained by the river "la Vilaine" in a northerly direction. The isopiets shown in this Figure, will be used to estimate the Darcy flux present. The difference in isopiets between the river "la Vilaine" and the nearest isopiet to the station is 5 m. These two measurement points are 1000 m apart. This leads to equation 5.1 shown below, with the highest permeability value chosen.

$$q = 10^{-9} \cdot \frac{5}{1000} = 5 \cdot 10^{-12} (m/s) \tag{5.1}$$

Figure 5.3 shows the results obtained with the addition of this Darcy flux. With a Darcy flux of such low order of values, it is negligible, the red curve merges perfectly with the blue curve.

Figure 5.3 – Impact of the add of a darcy flux

5.2 Calibration

In this section, a parametric study of the different variables is conducted to examine their impact and enhance the obtained results. The studied parameter is : the thermal conductivity of the soil and the concrete, the heat transfer coefficient of the wall, the hydraulic conductivity of the soil and the initial temperature of the soil.

5.2.1 Study of soil thermal conductivity

Figure 5.4 displays the results obtained with varying thermal conductivity of the soil. These values demonstrate that the influence of this parameter on the results is negligible, although

there is a slight increase in its impact towards the end of the simulation. Therefore, a thermal conductivity of 3 (W/(m K)) is chosen for future simulations.

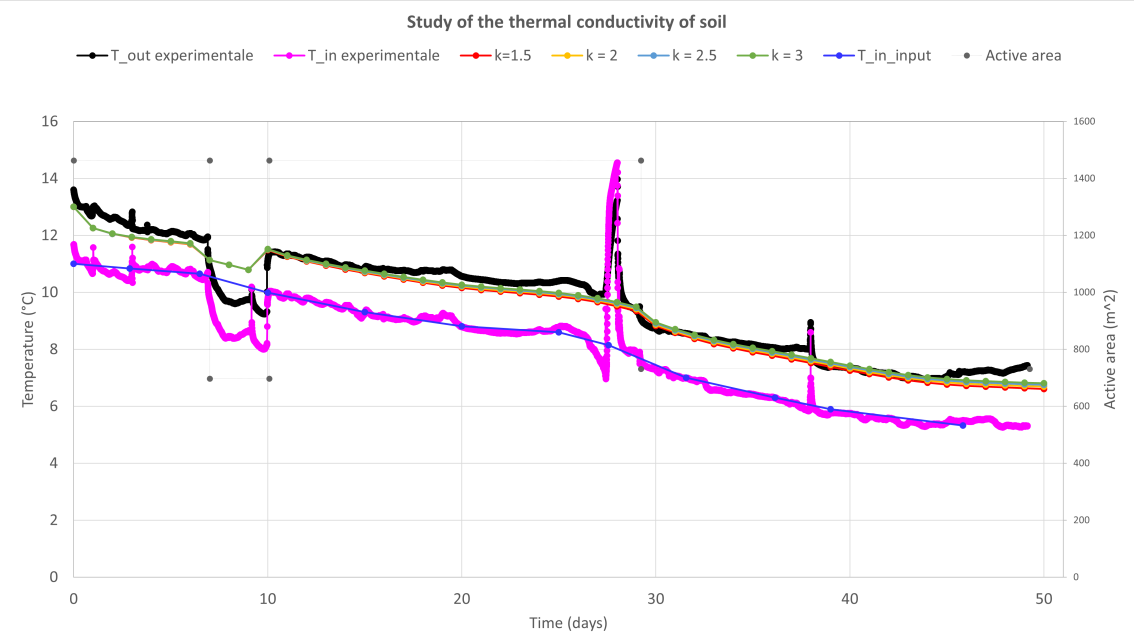

Figure 5.4 – Study of the thermal conductivity of the soil

5.2.2 Study of the heat transfer coefficient

The heat transfer coefficient describes the interaction between the air inside the station and the wall in contact with this air. Figure 5.5 shows the results obtained with different heat transfer coefficients. The variation of this parameter has a negligible effect on the overall result. For future simulations, a heat transfer coefficient of 3 $(W/(m^2.K))$ is chosen.

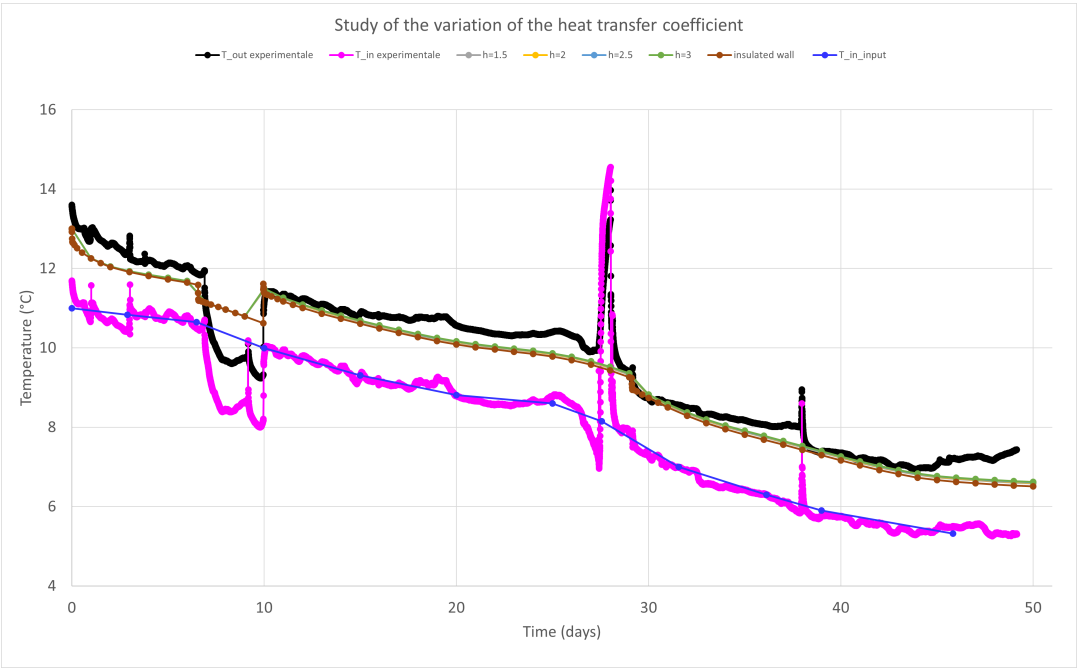

Figure 5.5 – Study of the heat transfer coefficient

5.2.3 Study of the temperature of soil

Figure 5.6 shows that the initial temperature of the soil has an impact in the beginning of the simulation but this impact decrease with time. This is due to the fact that over time the soil near the station has a lower temperature than the temperature passing through the pipes, so the temperature at this point is more uniform, whatever the initial soil temperature. The best results are obtained with a soil temperature of 14°C.

A soil temperature of 14°C at a depth of 25.5 m is quite high, but can be justified by two different arguments. Firstly, as the Cleunay station is located in a city, it may be subject to urban heat island effects, which lead to higher ground temperatures [Changnon, 1999] [Hendel et al., 2016]. In addition, the same initial temperature was used for the Jules Ferry station study, which seems to suggest that it was also consistent with the model's results. [Di Donna et al., 2021].

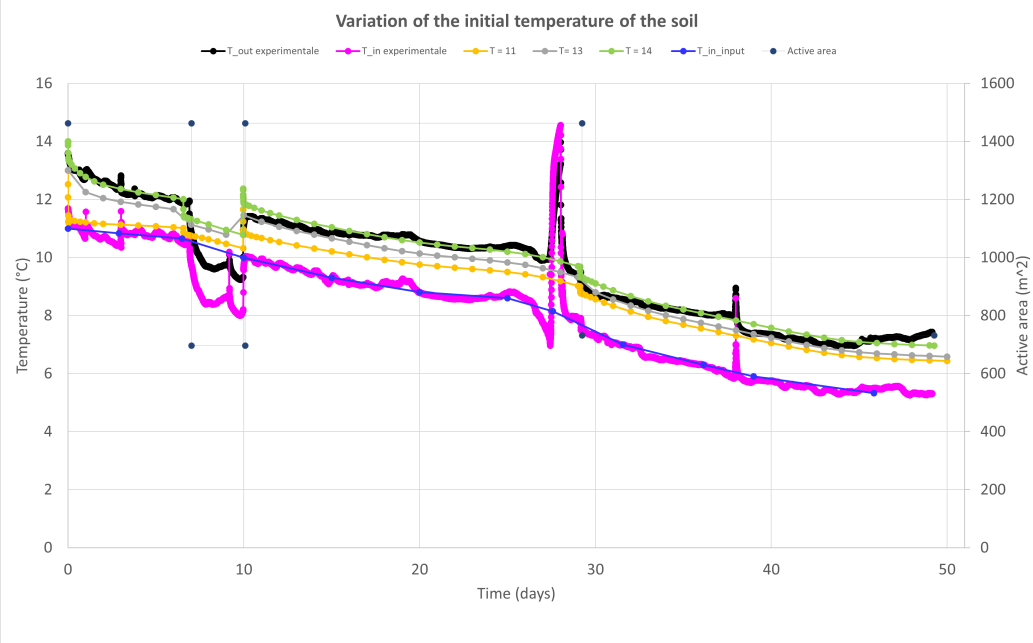

Figure 5.6 – Variation of the initial temperature of the soil

5.2.4 Study of the Darcy flux

Figure 5.7 shows the results obtained with Darcy flux of different orders of magnitude.

A higher Darcy flux means a greater displacement of water in the soil, which means that the water in the porous medium is more involved in heat exchange. This has the effect of making the soil more dissipative, resulting in a smaller reduction in soil temperature at points close to the wall.

To investigate this, a measurement point was placed in the ground 50 cm from the slurry wall on the south side of the station. At the end of the simulation (after 49 days), this measurement showed that for a Darcy flux of the order of 10^{-12} and 10^{-8} (m/s), the temperature at this point drops to a value of 8.5°C. If the flux is of the order of 10^{-4}, the same point will have a value of 12.8°C. This explains why the results are identical at the beginning of the simulation, but why there is a difference after 10 days. Indeed, at the start of the simulation, the soil has the same temperature regardless of the Darcy flux. Then, as the water passes through the pipes, the soil temperature close to the pipes decreases. Depending on whether the soil is more or less dissipative, the temperature will fall more or less. If the Darcy flux is high, the ground will be

more dissipative and so the temperature will fall less locally. Conversely, if the Darcy flux is low, the ground is less dissipative and the temperature falls more near the pipes.

For the next simulation, a Darcy flux equal to 5.10^{-12} (m/s) is choosen, this Darcy flux is considered has negligible but it is the most coherent choice thanks to the geology present.

Figure 5.7 – Study of the Darcy flux

5.2.5 Study of the thermal conductivity of concrete

Figure 5.8 represents the comparison between different values of the thermal conductivity of concrete. The difference can be consider has negligeble. Therefore, for future simulations, a thermal conductivity of 2.29 (W/(m.K)) will be utilized because it was the values calculated.

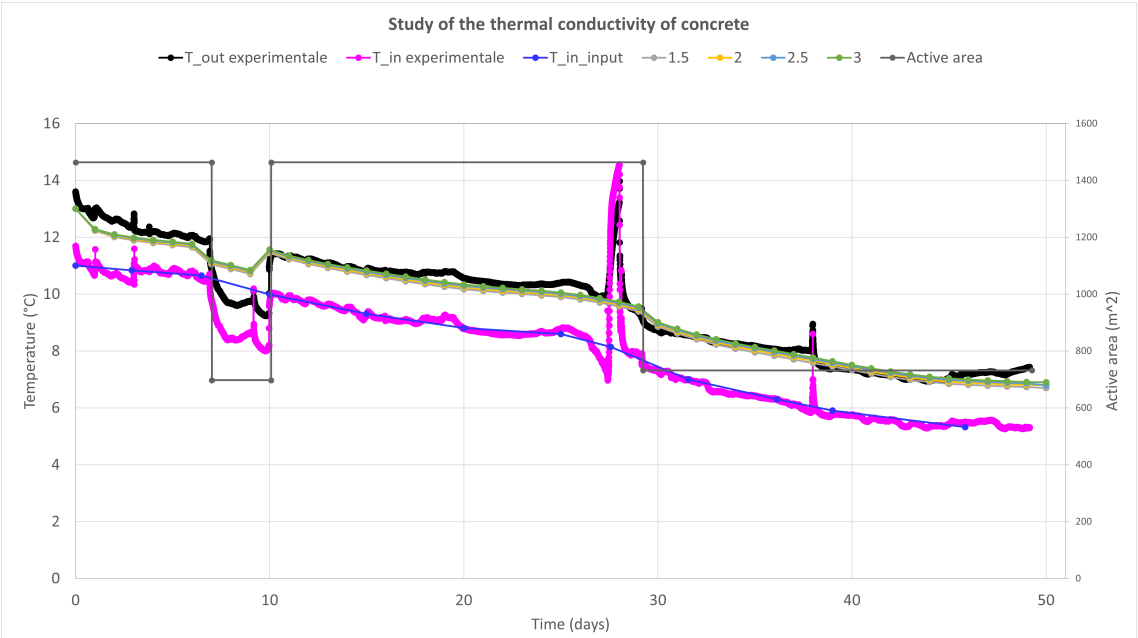

Figure 5.8 – Variation in the thermal conductivity of concrete

5.3 Description of the results

Figure 5.9 shows the results obtained with the changes made to all the parameters, thanks to the calibration. This theoretical result compares satisfactorily with the experimental result.

Between days 7 and 10, the pink curve shows a decrease in water temperature at the circuit inlet. However, this is not reflected in the water temperature imposed at the model inlet (blue curve). On-site, this drop in temperature is linked to the closing of the cast walls and the need to reduce the inlet temperature to keep extraction power constant. Although this effect is not included in the model, it is nevertheless reflected in the results obtained, as the brown curve shows a local decrease in temperature over this period.

This local decrease is linked to the closing of part of the circuit, which is expressed in the model by a change in the velocities inside the pipes within the model. Indeed, as seen on Figure 3.11 on page 31, the velocities of the water inside the pipes is calculated in function of the active pipes and the flowrate measured. This Figure show an increase of the the tangentiel velocity for this period. This is why, even if the model do not take into account the drop in temperature for this period, there is still a slight drop in temperature at this time, this is the change of the velocity inside the pipes. This also explains why the temperature drop in the results is so abrupt.

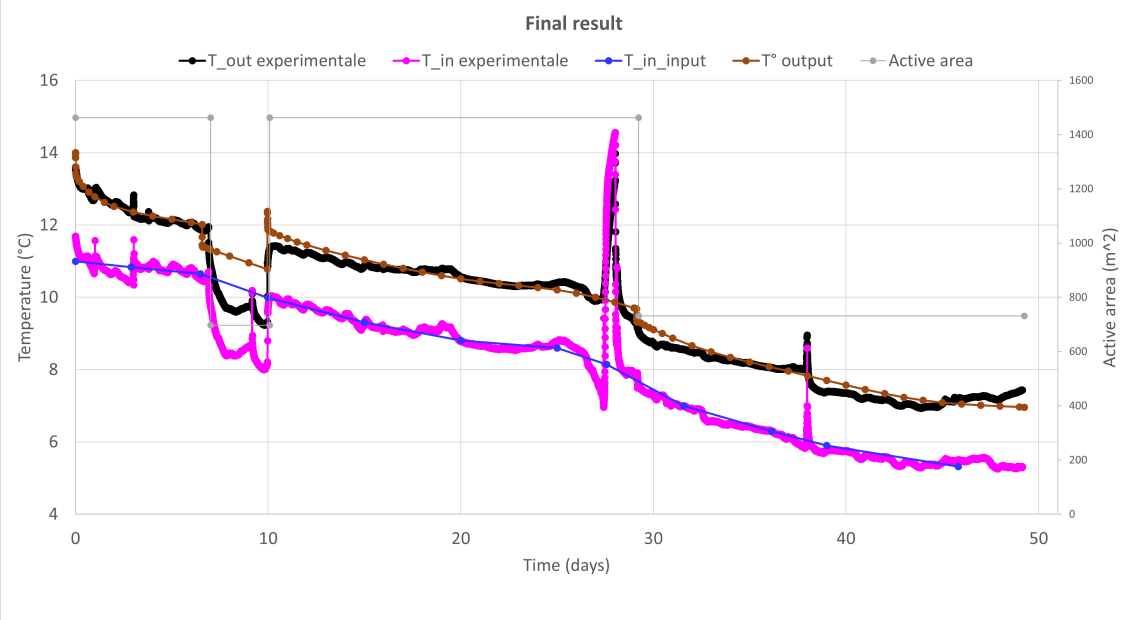

Figure 5.9 – Final result thanks to the calibration

5.3.1 Comparison between slab loop and wall loop

The aim of this section is to study the differences in behavior between the loop in the slab and in the cast wall. To this end, four loops are studied, two in the wall and two in the slab. The four loops studied are as follows:

- "Wall South" is a loop in the wall, called P02C112;
- "Wall North" is loop in the wall, called P08C15;
- "Slab South" is the sixth loop on plot 1 of the slab;
- "Slab North": is the penultimate loop in the slab of the plot 6.

Figure 3.7 on page 28 allows visualizing the position of the studied loops thanks to the description above. Moreover, Table 5.1 indicates the state of activation of those loops for the different phases. The names "south" and "north" used to characterize the loops come from the fact that the loops are situated at the south or north of the station.

	Phase 1	Phase 2	Phase 3	Phase 4
Wall South	Activate	Desactivate	Activate	Activate
Wall North	Activate	Desactivate	Activate	Desactivate
Slab South	Activate	Activate	Activate	Activate
Slab North	Activate	Activate	Activate	Desactivate

Table 5.1 – Summary of the activation phase of the studied loop

Study of the outlet of each loop Figure 5.10 indicates the difference of temperature at the outlet of the studied loops. It is noticeable that when all the loops are active and the result is stabilized, there is a difference of 1°C between the water temperature at the outlet of a loop in the slurry walls or in the slab. This can be explained by several factors.

Firstly, the loops studied in the slurry walls has a length of ± 90 m long (the length varies for each loop), whereas the slab loops are 78 m long. The slurry walls have more than 10 m of additional heat exchange, which will increase the heat extracted. In addition, the shape of the loops between the cast walls and the slab will also have an effect. In fact, the shape of the loops in the "U"-shaped slurry walls will result in a smaller temperature drop at wall level, as the pipes are spaced further apart than in the case of the slab and snail-shaped loops. This effect will be studied below in the following paragraph because this is linked with the soil of temperature.

In addition, this graph shows that when a loop is deactivated, the temperature will rise to the temperature of the ground near the loop. In fact, the green curve shows that when the loop is deactivated in the fourth phase, the temperature within the loop undergoes an initial rapid rise, linked to the temperature of the surrounding environment. This temperature then stabilizes at around 12°C. This leads to a temperature increase of 2°C over 4 days. The purple curve doesn't show the same effect. The temperature of the pipes will not increase, but simply stabilize. This effect may seem inconsistent, but in reality, it describes another problem.

Indeed, Figure 5.11 shows that loops at rest will experience a different temperature rise depending on whether they are located in the cast walls or in the slab. In fact, the loops in the cast walls will first warm up in the middle (the point furthest from the cold zones coming from the collector circuits) and then propagate towards the ends. The slab loops, on the other hand, will first heat up in the central part of the station, then propagate towards the extremity of the station in contact with the collector circuit, resulting in a local temperature reduction at this point. Moreover, the "Slab North" loop is the penultimate loop on the plot, and will therefore be subject to a zone effect linked to the corner and a greater temperature drop. This will slightly bias the results.

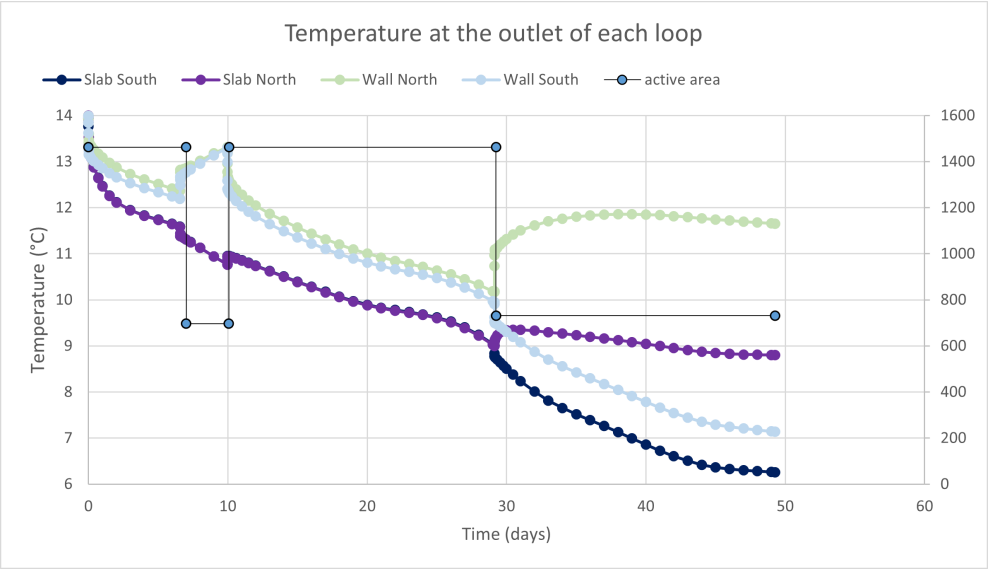

Figure 5.10 – Study of the outlet of each studied loop

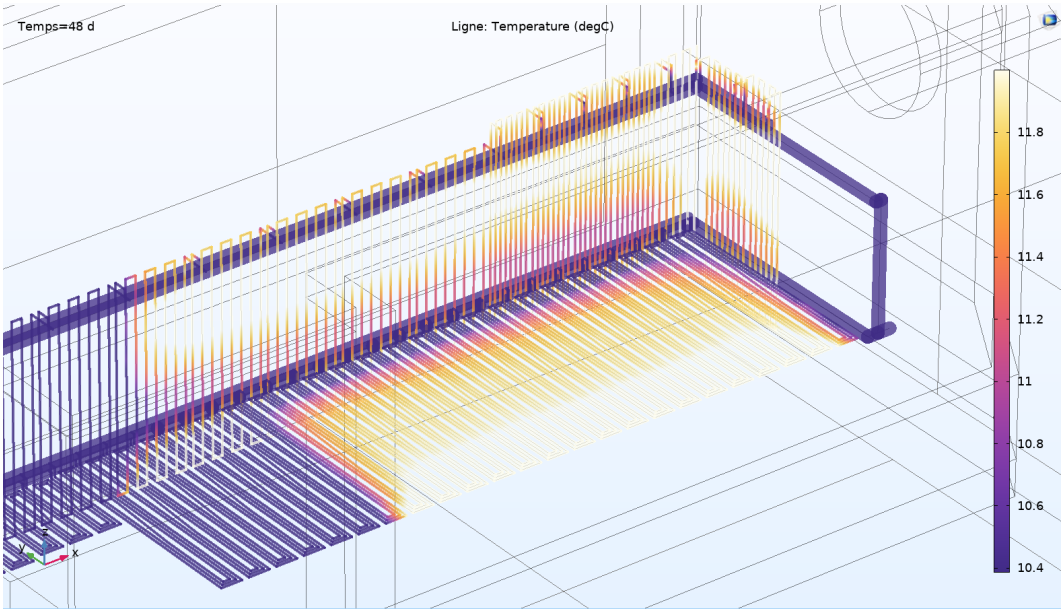

Figure 5.11 – Study of loop behavior at rest

Study of the temperature of the soil close to the loop Figure 5.12 shows four soil temperature measurements at the four loops studied. Measurements taken at the slab level show a temperature up to 0.6°C lower than the ground temperature at the slurry wall level. This is a symptom of the slab geometry extracting more heat than the cast wall geometry, leading to a lower ground temperature. However, it should be noted that during the fourth phase, the two zones where the loops have deactivated will have a temperature tending towards 12°C.

Figure 5.13 allow to see the distribution of temperature close to the station at the end of the simulation. The decrease of the temperature close to the loop are visible and also the decrease of the temperature when there are only the collector circuit.

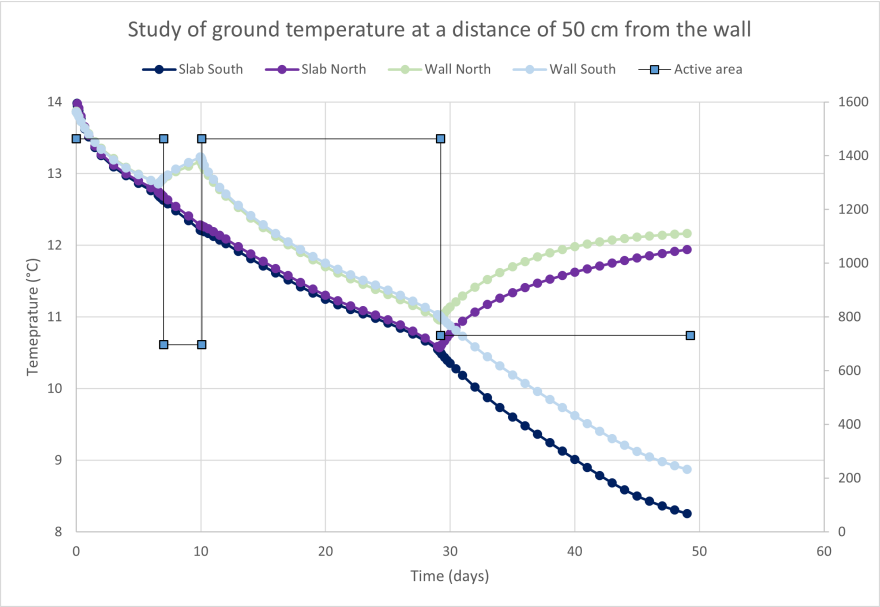

Figure 5.12 – Variation of the temperature of the ground close to the loop

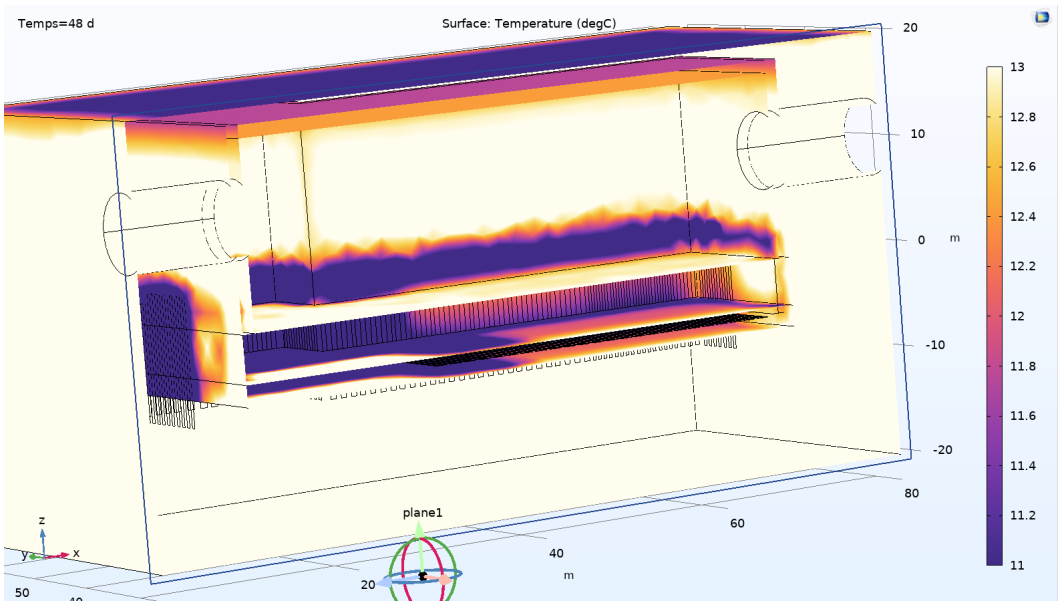

Figure 5.13 – Visualiser of distribution of temperature inside the station

Study of the Delta T Figure 5.14 indicates the difference of ΔT between the loop in the slurry wall and in the slab. Only the stabilized phases are of interest for the analysis.

In phase 3, the loops have a difference of 2°C between the loop inlet and outlet. The slab loops, on the other hand, have a temperature difference of 1°C. This difference, as mentioned above, is mainly due to the different geometry, but also on a smaller scale, due to a loop length 10 m shorter in the case of the slab.

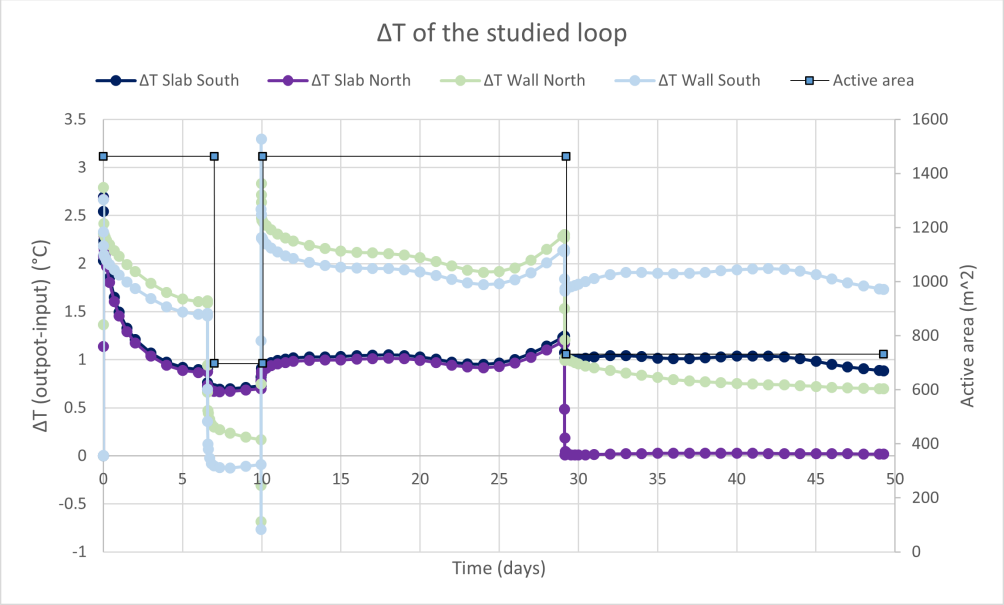

Figure 5.14 – Study of difference between the outlet and the inlet of the loop

5.4 Conclusion of the chapter

This chapter describes the effects of the various parameters governing this model. The parameters that have a significant effect on the results are the presence or absence of Darcy flow and the soil temperature. Other parameters such as the thermal conductivity of the soil and concrete and the heat transfer coefficient have little influence.

A closer examination of the results using the calibrated model highlighted the differences between the thermal behaviour of the slurry walls and the slab. The slab loops have a shape and length of pipe per m^2 that results in a greater reduction in soil temperature than the temperature around the slurry walls. At 50 cm from the loops, the difference is 0.6°C, while at the outlet of the loops the difference is up to 1°C.

In addition, the loops in the cast walls and in the bottom do not react in the same way when the flow in the pipes stops. Indeed, it's possible to see that the slab loop at the centre of the station is the first to heat up because the eastern part of the loop is not active and so the temperature is highest there. On the other hand, the slurry walls heat up through the central part of the loops.

Chapter 6

Thermal Study of the Cleunay Station

The aim of this final chapter is to study the thermal behavior of the metro station during one year's use. To do this, a search of the scientific literature was carried out to obtain a benchmark for the data to be introduced. This research led to an article written by [Attia et al., 2020], which studies electricity and gas consumption in primary and secondary schools.

To perform this one-year simulation, the first step is to change the model from temperature input to power input. This step is followed by a description of the one-year simulation which describes the type of building to be heated.

The next step is to study the results obtained. This study will focus first on the heat extraction period and then on the rest period of the station. This rest period is studied according to two scenarios. The first scenario is a rest period with no heat injection and no cooling of the building, while the second scenario is cooling of the building with free cooling.

This chapter concludes with a discussion of future studies to be carried out in order to obtain a more precise description of the thermal behavior of this station.

6.1 Input of power

The first step in performing a theoretical simulation of the model is to change the model input from temperature to power. Indeed, in the field, what can be imposed is a certain power and the input temperature of the water will only be a function of this power.

As a reminder, in the field, the temperature at the outlet of the circuit is measured before passing through a heat pump, which imposes a temperature reduction of a certain ΔT on the water. The heat pump then extracts a certain amount of energy, which is set by the user. The temperature of the water is measured after it has been through the heat pump and it is these measurements that have been input into the input model so far.

This means that the model must be modified to take into account the effect of the heat pump, with the user's power demand as input. To do this, the model takes a measurement at the circuit outlet and then calculates the temperature imposed on the input by the equation 6.1.

$$T_{input} = T_{output} - \frac{P}{\rho.C_p.Q} \tag{6.1}$$

With,

— T_{input}, the input temperature of the geothermal circuit (in K);

— T_{output}, is the temperature at the outlet of the geothermal energy circuit (K). ;
— P, the power asked at the heat pump (kW);
— ρ the density of the fluid inside the pipes, which is water (in kg/m^3);
— C_p the heat capacity of water (J/kg.K);
— Q, the flow rate of water inside the pipes (m^3/h).

Figure 6.2 represents the results obtained with this new input. The power and the flow rate imposed on the model comes from the thermal response test measurements. The values entered are shown in Figure 6.1. These results are compared with the experimental results. The results obtained are satisfactory and validate the use of power as an input.

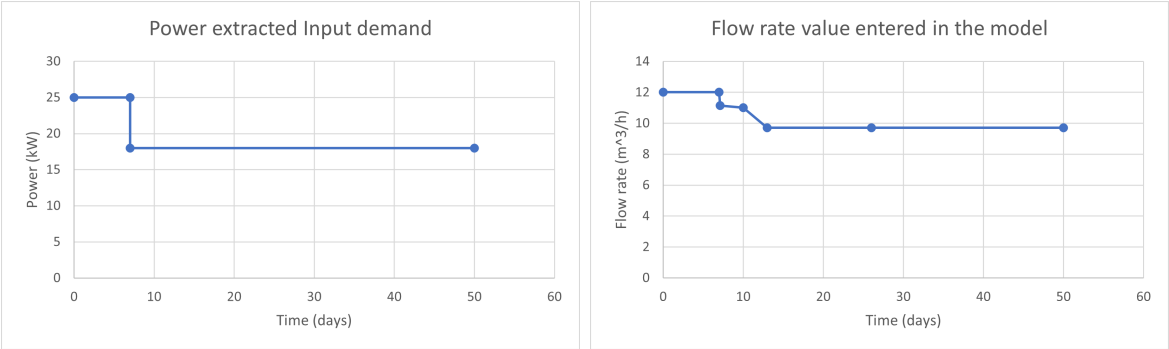

Figure 6.1 – Power and flow rate input

However, it can be observed that at the beginning of the simulation, there is a difference between the pink curve and the dark blue curve. This is due to the initial phase of the thermal response test, which is less stable in comparison with the others. Indeed, as explained in the report sent by the company that carried out the thermal response test, it is stated that this period is characterized by a calibration of the probes and by a reversal of the direction of the water in the loops. Moreover, these fluctuations weren't correctly taken into account in the power and flow data entered in order to smooth out the data entered in input as much as possible. As a result, this first period leads to less reliable measurements than the others.

Compared with the final results obtained in the previous section (Figure 5.9 on page 50) phase 2, which begins on day seven and finish on day 10, is better represented in this case. This is due to the fact that this simulation did not use the smooth input temperature but calculate it according to the power asked. Consequently, the drop in temperature at this point is due to both the drop in power demand, the drop in flow rate and the closure of part of the circuit. Indeed, as explained in the previous section, closing the slurry walls causes the temperature at T_{out} to fall. This is because the only temperature recovered is that leaving the slab loops, which are cooler.

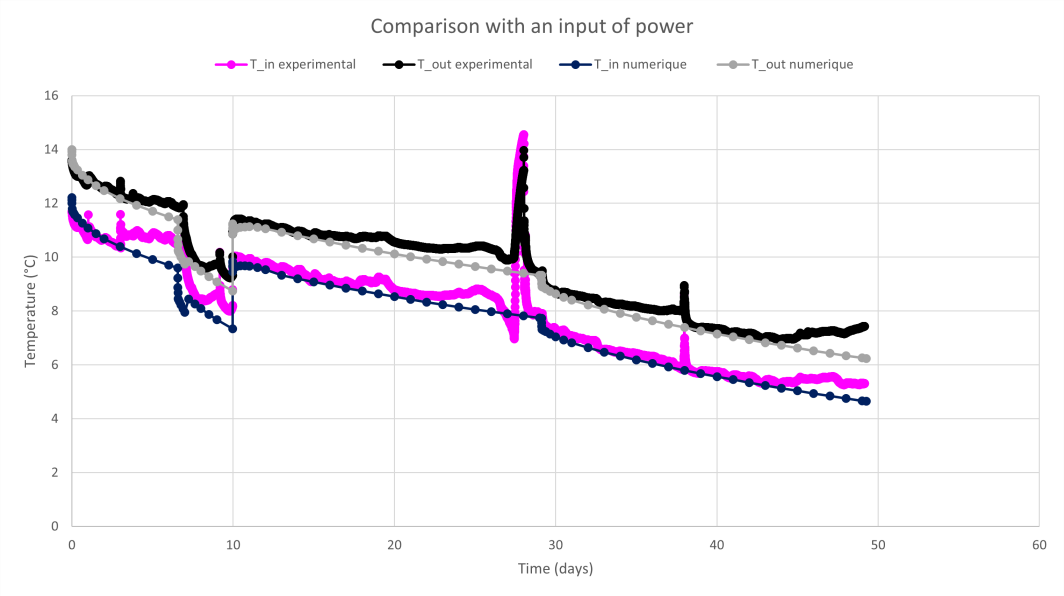

Figure 6.2 – Comparison between experimental and numerical thermal response test results. The numeric results are calculated using an input temperature corresponding to the power demand.

6.2 Description of the theorical simulation

In order to determine how much energy needs to be extracted from the station's soil, reference data from the [Attia et al., 2020] article will be used. This article provides an idea of the energy consumption of an elementary school in Belgium and the variations in consumption over the different months of the year. The data used will only concern heating, not the production of electricity. Figure 6.3 will be used as a reference. This Figure shows the heating consumption in kWh of an elementary school per m^2 of school space.

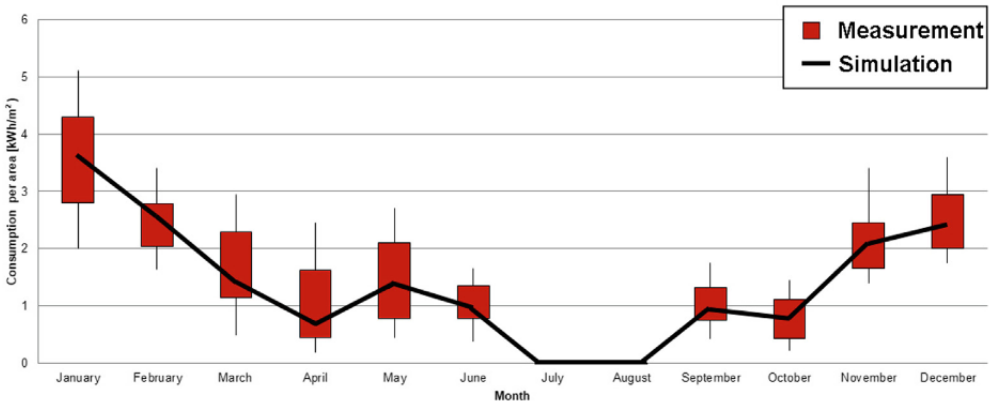

Figure 6.3 – Surveyed and simulated monthly gas use of the primary school [Attia et al., 2020]

Figure 6.4 was created with the aim of obtaining a maximum value for the power that could be extracted from the ground, and therefore a maximum limit for the type of building that could be heated with this type of structure.

In order to do this, tests were carried out in advance to determine the maximum value of the potential that could be extracted from the ground. This maximum value would then be used as a reference point for the other points. The value of 63.5 kW was therefore chosen as the

maximum value, the peak of demand. The other values in the graph were chosen in relation to this peak, taking into account the variability of the measured values, represented by the red blocks in the Figure 6.3. An exception was made for the month of June, where a rest period of 3 months was imposed in order to obtain sufficient visibility on the behaviour of the station at rest.

This Figure 6.4 represents the power (in kW) that will be extracted from the ground by the heat pump, and it is this graph that will be input into the model.

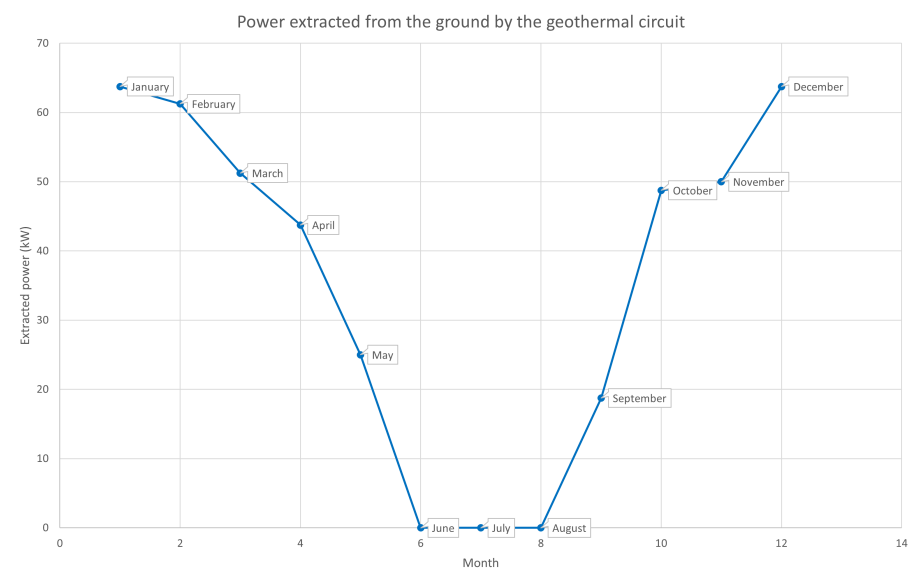

Figure 6.4 – Power extracted from the ground by the model

Heating period In order to be consistent with the data used as a basis, it is necessary to introduce an heating period and a rest period for each week. Since the simulation is based on the heating of an elementary school, the schedules used will be the same as those studied in the article. That is, a heating period from 7 am to 6 pm. During nights and weekends, the system will be stop. It will be interesting to study the thermal behavior of the soil during these rest periods. However, school vacations have not been taken into account.

The simulation is divided into two parts. The first part begins in September and ends in May (See Figure 6.5). The second part consists of simulating the remaining months of June, July, and August. Dividing the simulation into two allows for two distinct scenarios for the station's rest period.

Converting energy into power Figure 6.4 and Figure 6.3 do not provide the same information. The first Figure indicates the power to be extracted through geothermal equipment, while the second figure represents the energy consumption per m^2 of the building. To relate the two, the duration of the heating period must be taken into account. For each month, the energy extracted from the soil is calculated. An example of this calculation is shown for the month of September.

Between September and October, the energy required from the system increases from 18.5 kW to 48.75 kW (Figure 6.5). The simulation will start in September, at the end of the rest period. In addition, the assumption that September begins with a Monday is also introduced. This will have an impact on the precise number of hours of operation of the geothermal system, which in consequent will equal to 242 hours of operation.

Furthermore, the equation of the straight line linking September and October is as follows:

$$y = 0.0417x + 18.75 \tag{6.2}$$

This equation is used to calculate the energy produced during the operating period of the geothermal system.

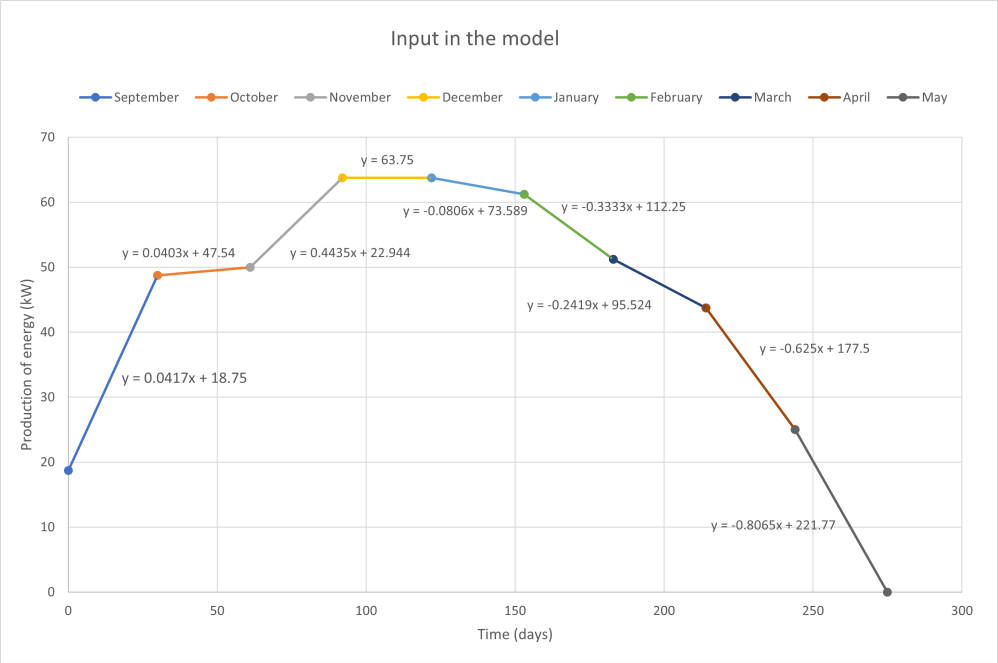

Figure 6.5 – Visualization of the power input in the model and the equation for each linear interpolation.

By integrating this equation with the bounds of the duration of the month (in hours), [0 ; 720], a total energy production of 24 309 kWh over the month is obtained. However, this result is the energy production if the geothermal circuit were running continuously, which is not the case. Consequently, it is also necessary to enter the ratio between the total number of hours in September and the number of hours of system activation, see equation 6.3:

$$\frac{720}{242} = 2.9[-] \tag{6.3}$$

This ratio can then be used to divide the total production to obtain the production over the number of effective hours:

$$\frac{24309}{2.9} = 8170\text{kWh} \tag{6.4}$$

This ratio allows us to switch between continuous production over a month and production for a given hour. The value of 8170 kWh obtained is therefore the total product energy for the month of September.

The calculation described above is reproduced for the other months, but is not transcribed, given that the operation is identical. The results obtained for each month can be seen in Table 6.1.

	Operating time (h)	Output power(kWh)
September	242	8170
October	253	12497
November	220	12937
December	253	15608
January	242	15093
February	220	13248
March	242	11473
April	242	8374
May	231	2890

Table 6.1 – Energy generated per month in the simulation

Adding up these different values, this leads to an annual production of 100.3 MWh. However, this value does not include the COP of the heat pump. In the case of geothermal circuits, this coefficient varies from 3.5 to 4 [Laloui and Rotta Loria, 2020]. The following equation, equation 6.5, is used to convert the energy extracted from the soil into the energy actually delivered to the building.

$$E_{building} = E_{soil}.\frac{COP}{1 - COP} \tag{6.5}$$

$E_{building}$ is the energy supplied to the building and E_{soil} is the energy extracted from the ground by the heat pump. With a COP of 4, the energy actually supplied to the building will be equal to 133 MWh.

Referring to the article [Attia et al., 2020], it says that for a school, we can estimate consumption at 14 kWh/m^2/year. Using this rule, this means that a school of 9 300m^2 can theoretically be heated if the COP is equal to 4.

The following section will therefore examine the station's thermal behavior in the face of the heat extraction described above.

6.3 Study of thermal behavior during the heating period

As a reminder, the calibrated results only concern the western part of the station. Consequently, the simulation will only activate the western part of the geothermal plant. The flow rate is constant and equal to 12 (m^3/h). The velocity inside the pipes is constant and equal to 0.17 (m/s) in the loop and 0.36 (m/s) inside the collector circuit. This data is the same as the data initially input during the thermal response test, see Figure 3.11 on page 31.

Figure 6.6 and Figure 6.8 represent the variation of temperature at the input and output.

It can be seen that in Figure 6.6, there are blank spaces on the curve. This corresponds to the weekends and so when the station is at rest. Moreover, there are also blank spaces between each day, although they are not visible. Figure 6.7 shows a zoom on the input and output temperature for the first two weeks of simulation. This pattern is repeated throughout the year before the summer holidays.

Inlet temperature limit Between January and December, when energy consumption is at its highest (15 600 kWh), the inlet temperature exceeds the permitted limit of 0°C. Despite the presence of an anti-freeze agent in the water in the pipes, a minimum inlet temperature must be imposed to avoid structural problems. This safety margin could, for example, limit the

inlet temperature to 2°C. The specific limit required in this case is not known. As a result, the system is unable to meet the peak energy demand in December and January. To meet these exceptional demands, the system could, for example, be coupled to another gas heating system.

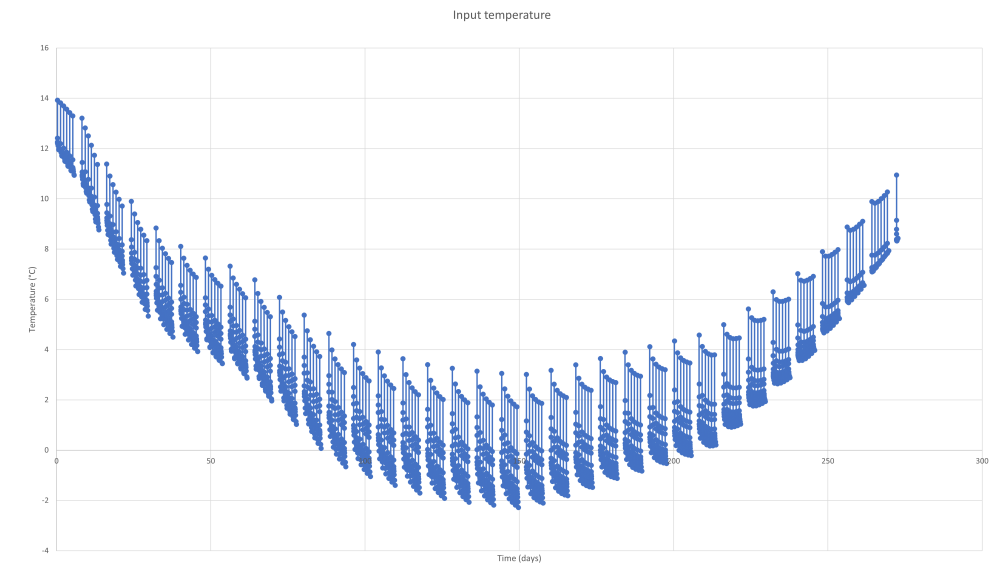

Figure 6.6 – Input temperature in the model, calculated with equation 6.1

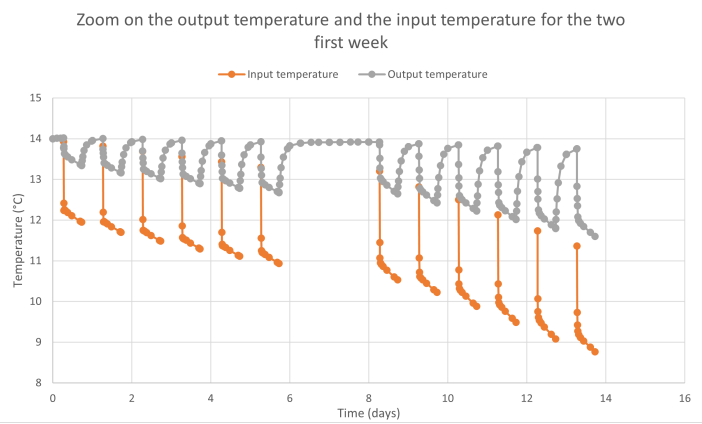

Figure 6.7 – Zoom in on the input and output temperatures for the first two weeks.

Temperature at the output of the station Figure 6.8 represents the temperature at the outlet of the station. This graph shows some surprising results, given that the temperature difference at a given moment will vary by 9°C, from a temperature of 3°C to a temperature of 11°C. This effect is actually a biased measure on the model, linked to the position of the T_{out} point in the model.

Indeed, Figure 6.9 shows this point in relation with the equipment of the station. This point is the end of the collector circuit and is located in the middle of the station's north phase. As a result, this point is not surrounded by loops in the slurry walls or slab which mean that the temperature close to this point decrease not so much that the other. As a result, what we see in the results is that when the temperature inside the pipes is subjected to a flow, the temperature will decrease at the outlet temperature of the other pipes. However, when the system stops and its flow becomes zero, the temperature will rise very quickly in relation to the temperature

of the ground around this point, which has cooled down much less than the other parts of the station. This effect will be confirmed with the description below.

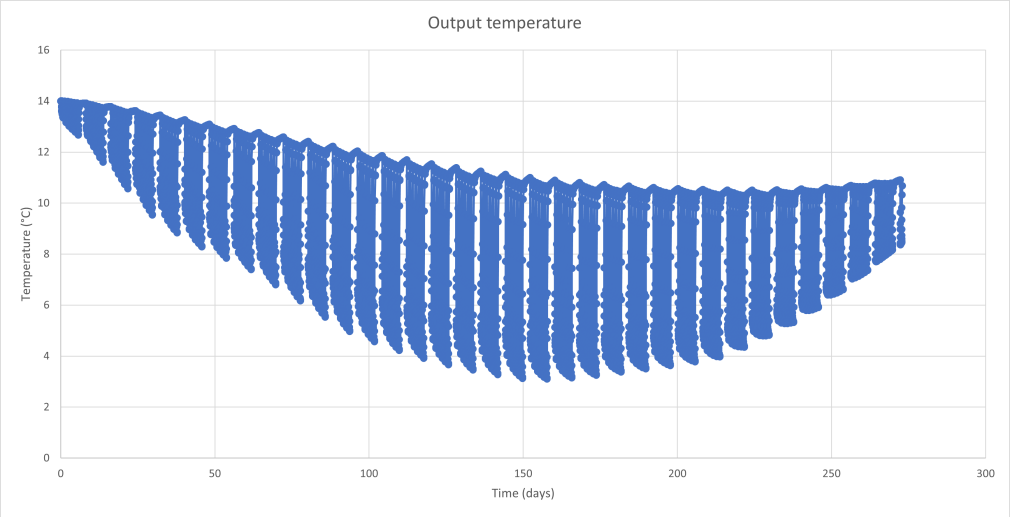

Figure 6.8 – Output temperature during the heating phase

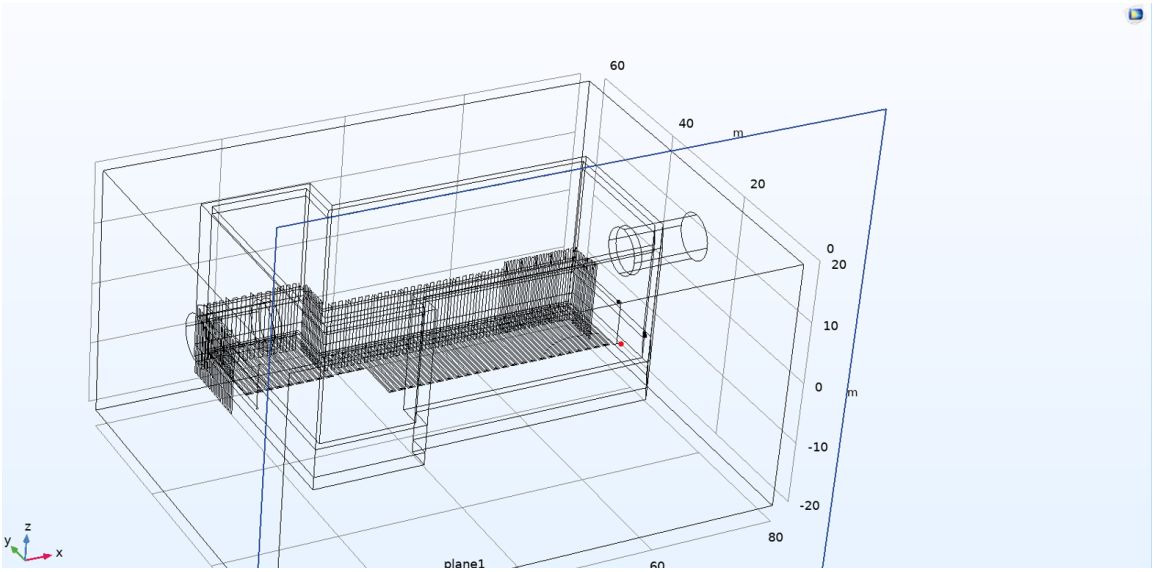

Figure 6.9 – Visualisation of the output (red point) in relation with the loop inside the station

Comparison between temperature inside the slab and inside the slurry wall Figure 6.10 represents the temperature at the outlet of a loop in the slab and in the slurry wall. When compared to the temperature values in Figure 6.8, the results are consistent with expectations.

During the weekend, rest period, the temperature at the outlet of the slurry walls increases by 4°C, while the temperature at the outlet of the slab increases by 2°C. The difference in these values is due to the fact that the temperature of the slurry walls is higher than that of the slab. This effect will be examined in more detail in the following paragraph, as it is related to the distribution of temperature in the soil.

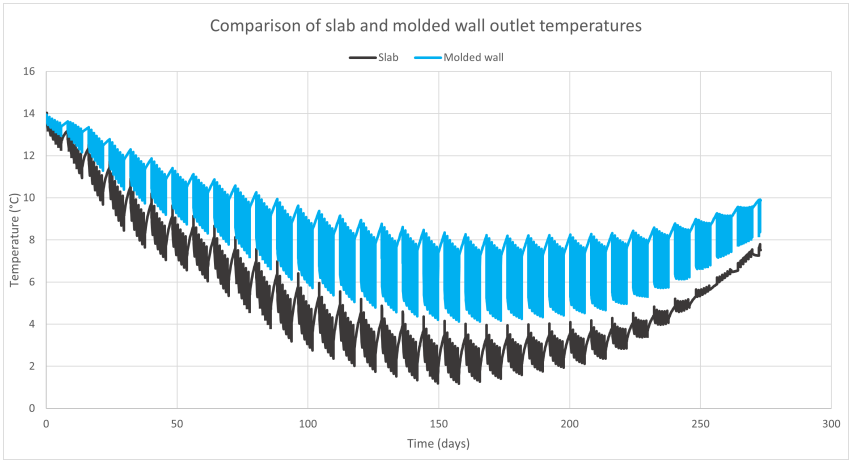

Figure 6.10 – Comparison between the outlet temperature at the slab and at the slurry wall

Study of the temperature on the soil Figure 6.11 study the temperature of the soil at four different points on the ground. Those points are situated at the location to the 4 points studied describeb on the previous section 5.3.1 page 50. Two points are located close to the slurry wall and the two others are located below the slab. The name used are : PM south, PM north, Slab south, Slab north. Those four different points is then studied at different distance from the station.

At a distance of 50 cm from the loops, the soil that will experience the most cooling is the soil beneath the slab loops with the lowest temperature of 4°C. The lowest temperature at this distance in the slurry wall is equal to 6°C. This means that the maximum temperature difference between the slab and the slurry wall is equal to 2°C. Moreover, it can be noticed that for the slab, there is no distinction between the north and the south which is not the case with the measure close to the slurry wall.

The explanation for this phenomenon is that the measurement point on the south side is located on a face with only 4 loops in total, whereas the measurement point on the north side faces a wall with 10 loops. In other words, the wall will experience a greater drop in temperature in the north due to its colder surroundings.

At a distance of 1.5 m from the loops, the same type of result is observed. This is consistent with the fact that the set of imposed parameters is homogeneous and isotropic. However, the farther the measurement point is from the loops, the less the results are influenced by cutoff moments.

Let's return to the analysis of the previous Figure 6.10. As a reminder, all loops in this model are parallel. This means that the entire model has an identical inlet temperature (to within 0.01°C as there is a very slight rise in the temperature of the water in the primary circuit). However, Figure 6.10 shows that the outlet temperature of the loop is different between slab and slurry wall. The water will heat up less in the slab pipes for several reasons. Firstly, the length of the pipes is different (a difference of up to 10m). Secondly, the positioning and shape of the pipes means that there is a greater length of pipe per m^2 in the slab, which leads to a greater reduction in soil temperature. As a result, the water passing through the slab has a length that allows for a shorter heat exchange and a cooler environment.

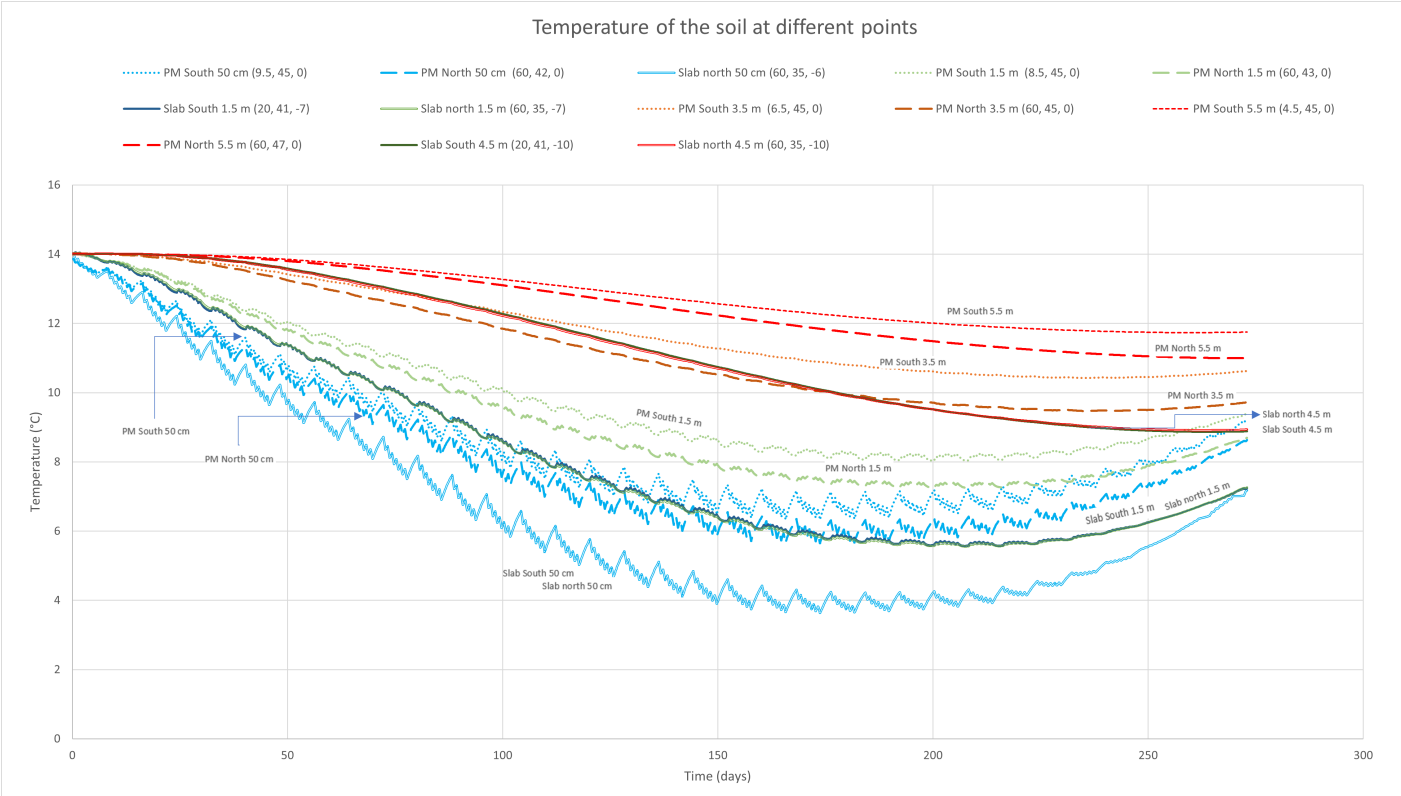

Figure 6.11 – Comparison of the temperature on the soil close to the loop of the slurry wall and the slab

6.4 Study of thermal behavior during months of rest

The final stage of this study consists of investigating the station's behavior during the three months after undergoing the heating cycle described above. This study will take the form of two scenarios. The first scenario involves studying the station without heat injection. Scenario 2, on the other hand, describes the behavior of the soil in response to free cooling.

6.4.1 Scenario n°1: no building cooling

Figure 6.12 shows the temperature distribution in the soil without cooling. The station is at rest for three months. The only mechanisms involved in temperature variation within the station are temperature gradients.

It can be seen that the temperature at the slab remains lower in comparison to the temperature at the slurry wall even after the rest period. Indeed, after the three months, the maximum temperature below the slab is around 9.5 and 10 °C, which is 4 degrees lower than the temperature of the soil before the heating period. This indicates that the station has not sufficiently recovered to be able to reproduce the same heating cycle without causing cooling of the soil in future years.

In conclusion, it would not be possible to use a heating cycle as shown below without geocooling because there would not be a sufficient increase in temperature to extract enough power for the next cycle and this would cause a temperature imbalance which would worsen over time. If geocooling is not used, it is absolutely necessary to reduce the power extracted to avoid this phenomenon.

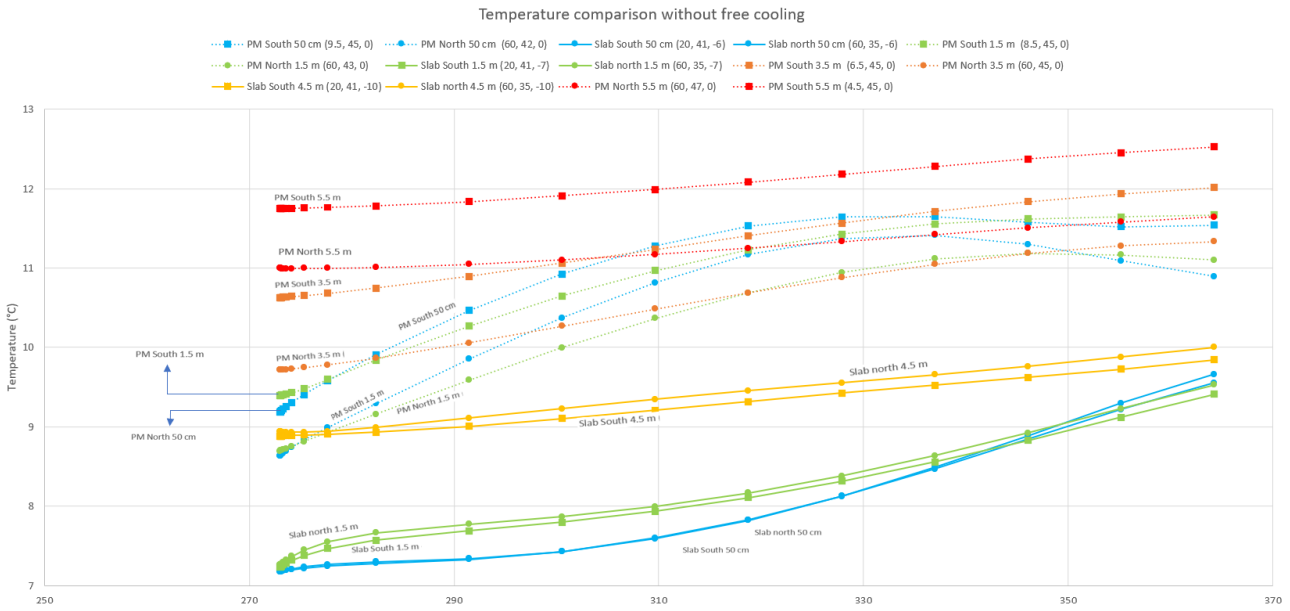

Figure 6.12 – Study of the thermal behavior of the station without free cooling

6.4.2 Scenario n° 2: building cooling

To estimate the cooling required for the fictitious school studied, the article [Attia et al., 2020] is referenced again. In this article, it is proposed that a cooling energy of 5 kWh per m^2 is required. This value must then be converted into power by adding the duration of the cooling period. The equation to be solved is as follows, with x representing the power needed:

$$x \cdot (365 - 273) \cdot 24 = 5 \cdot 9300 \tag{6.6}$$

The left-hand side of the equation multiplies the power by the duration of the three months and multiplies by 24 to convert into hours. The right-hand side of the equation multiplies 5 by the calculated surface area of the fictitious school (9300 m^2) in order to obtain a value in kWh.

By solving this equation, we find that the power to be injected is 21 kW. To simulate this heat re-injection, a constant power -21 kW of has simply been introduced into the calculation of T_{in}. With a separate circuit, the cold water circulates in the building to be reheated and is then re-injected into the ground.

Figure 6.13 shows the results obtained. Compared with the results without geo-cooling, the results are more homogeneous depending on the location studied (slurry walls or slab). It can be seen that the ground in the direct vicinity of the loops (blue curves) is naturally the hottest. At this point the temperature will even rise to 16°C. At a distance of 1.5 m, the temperature rises from 7°C to 14°C. From 4.5 m from the loops, whether for the invert or the slurry walls, the soil did not reach the initial temperature of 14°C. In order to determine the extent of the problem, several heating cycle simulations should be carried out to determine whether there is a local cooling effect on the floor over the years.

In conclusion, if geocooling is used with this re-injection power, additional simulations would be required to determine the possibility of extracting the heat required. Indeed, it is absolutely necessary to determine whether the extraction/injection cycle would be sufficiently balanced to avoid serious problems in the future.

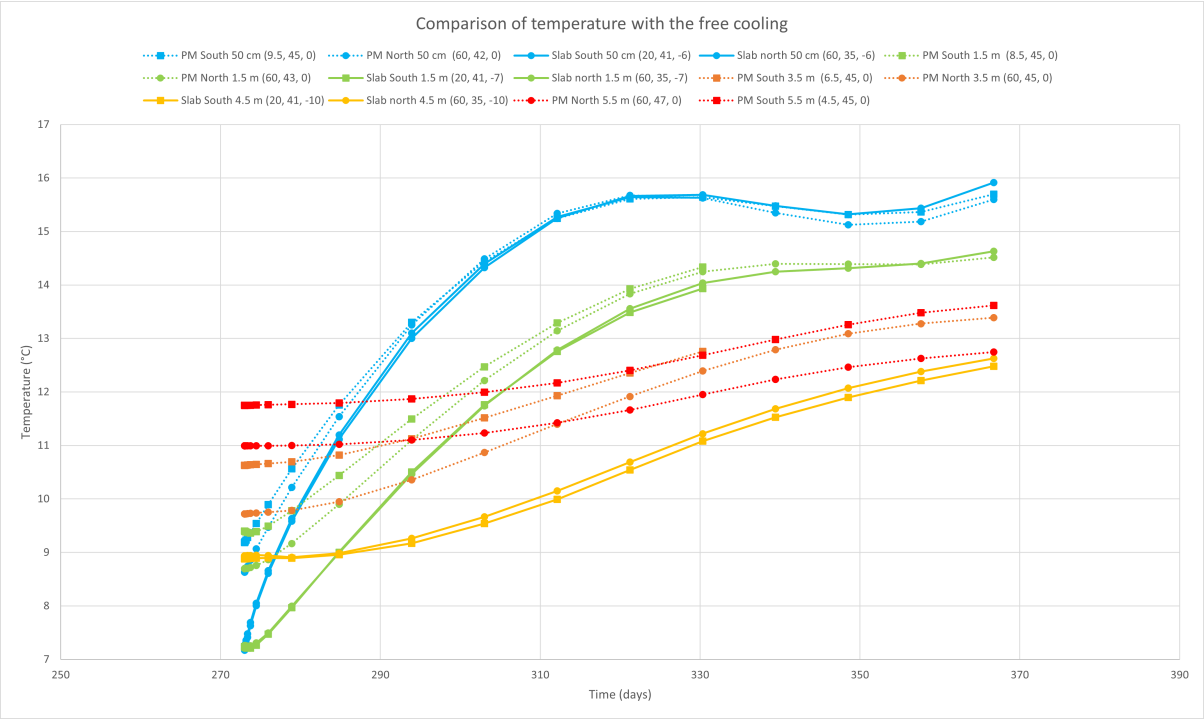

Figure 6.13 – Study of the thermal behavior of the station with a free cooling of the school

Figure A.4, A.5 and A.6 show the distribution of temperature inside the Cleunay station after the three stage presented.

6.5 Further researches

The study of the geothermal equipment at Cleunay station will continue next year with the THERMETRENNES research programme. This section suggests a number of ideas for completing the work already carried out.

To begin with, it is necessary to study the thermal behavior of the station with the entire geothermal equipment activated. So far, only the western part has been activated, either in the TRT test or in the building simulation. The model that was created was built with the pipes from the east part. This change will, of course, lead to variations in the results obtained and in the conclusions that can be drawn regarding the power that can be extracted from the ground.

Another aspect would be to simulate the actual buildings that we want to heat on-site using this geothermal equipment. This work has been carried out on a fictitious building to provide orders of magnitude for the values that can be extracted from this structure, but it is not representative of reality. In fact, each type of building has its own heating requirements, so the heat that can be exploited will differ from one application to another. Currently, the station is still not being used to heat buildings. As a result, it is not possible to obtain real data to feed into the model.

In the study of geothermal structures, an important aspect is the financial cost of installation and operation. Therefore, it would be interesting to carry out a cost comparison between the installation of equipment for an energy geosystem and a conventional geothermal well, whether it is an open or closed system. These data would provide concrete order of magnitude in terms of financial cost, which may allow future projects to choose this type of structure if the conditions are favorable. Currently, the number of concrete applications of energy geosystems

is limited. Moreover, this comparison can be extended to include the cost of heating with gas or other traditional ways of heating in order to determine the point at which this type of heating becomes more expensive than geothermy.

This study must also necessarily be complemented with the analysis of the deformation of the structure and the soil due to temperature variations during both the heating and cooling periods. Indeed, a structure that is heated will create expansion, and conversely, if it is cooled [Soga and Rui, 2016]. This mechanism needs to be precisely studied in order to determine the maximum limit of heat extraction from the ground before it has a negative impact on the structure.

When using geothermal energy, it is extremely important to pay attention in order to avoid cooling or heating of the ground during the different heating and cooling cycles. Indeed, if more energy is extracted from the ground, the soil will gradually cool down, initially leading to a decrease in the coefficient of performance but potentially resulting in locally cold zones where the system can no longer be used. Similarly, if the injected energy is excessive, the temperature of the ground will increase, and at some point, it will no longer be suitable for cooling a building because the temperature will be too high [environnement, 2020].

Chapter 7

Conclusion

Energy geostructures are geostructures such as foundation piles, diaphragm walls, tunnels, etc. equipped with heat exchangers to recover the heat naturally present in the ground. The number of these technologies built and in operation in the world is still very small. To help develop and promote these technologies, the "thermetrennes" research program has been set up to provide feedback on four new stations fully equipped with heat exchangers in the city of Rennes.

The Cleunay metro station is one of the stations studied, and is fully equipped with heat exchangers, both in its slurry walls and in its slab. In all, the station is equipped with 2950 m^2 of heat exchangers. These are made on polyethylene pipes with an internal diameter of 20.4 mm. The geothermal equipment is located at a depth of between 20 and 25 m. The geology has been described by 7 boreholes drilled on site near the station. At this point the geology is shale with sandstone and will generate extremely low groundwater flow, but there have been no on-site measurements to quantify this flow.

In November 2019, a thermal response test was carried out to obtain data that will be useful for calibrating the model. This thermal response test was divided into four different phases depending on the model's active zone. Thanks to this thermal response test, a sensitivity study of the parameters introduced into the model was carried out. It was found that parameters such as the heat transfer coefficient, which is a difficult parameter to estimate given the complexity of the physics it represents, did not have a significant influence on the results. Similarly, the thermal conductivity of concrete and soil have little influence on the results obtained. The parameters with the greatest influence are the hydraulic conductivity value and the initial soil temperature.

Once this model had been calibrated on the basis of the various tests carried out, an analysis of the use of this geothermal circuit to heat an elementary school of 9 300 m^2 was carried out. Over a period of 9 months, with a heating cycle of 11 hours per day, an attempt was made to extract 100.3 MWh of energy from the ground. The results obtained show that the geothermal system will not be able to meet peak demand in December and January, and will need to be coupled with another type of heating.

This heating cycle was followed by a rest period during which no more heat was extracted. This rest period will be studied in two scenarios. The first scenario is simply a study of the temperature distribution around the station without the use of geocooling. These results show that it is not possible to extract the amount of heat from the ground, as the ground temperature drops too sharply and fails to return to its initial values. In the second scenario studied, the rest period is accompanied by a period of free cooling. Reference data is used to reproduce this free cooling. According to these data, a power of 21 kW was chosen for the three months of rest.

In the vicinity of the wall, the temperature increased to 16°C. However, the temperature was 12.5°C at a distance of 5.5 m from the station. This shows that the soil temperature distribution is not homogeneous and that it is difficult to predict how this temperature distribution would behave in the face of repeated cycles.

These different results show that the particularity of this station is the presence of a very weak underground flow (order of 10^{-12} (m/s)). As a result, when the soil is at rest, temperatures will vary very slightly. This is because heat exchange is governed by conduction which means governed by the presence of thermal gradients. This effect is visible because when heat is injected into the ground, there is mainly an accumulation of hot water around the station but little distribution within it. As a result, this station needs to be carefully considered in the heating/cooling balance, as its characteristics are favourable to temperature disequilibrium over time.

In order to provide a more complete study of the Cleunay station, this work should be complemented by several additional studies. There are many aspects to be studied, as this technology is still in a state of development, but two main aspects will be presented here. Firstly, this thermal study of the station should be complemented by a study of the mechanical deformation of the structure caused by these heating and cooling cycles. This would provide additional data to determine the maximum power that can be extracted from the station. Another interesting aspect to consider is the long-term financial benefits of this type of structure. This information could be used to estimate the costs of future projects and perhaps help to democratise them.

Bibliography

S. H. Alsayed and M. A. Amjad. Strength, water absorption and porosity of concrete incorporating natural and crushed aggregate. *Journal of King Saud University - Engineering Sciences*, 8(1):109–119, 1996. ISSN 1018-3639. doi: https://doi.org/10.1016/S1018-3639(18)30642-1.

Atlas climatique du Canada. Gaz à effet de serre . URL `https://atlasclimatique.ca/gaz-effet-de-serre`.

S. Attia, N. Shadmanfar, and F. Ricci. Developing two benchmark models for nearly zero energy schools. *Applied Energy*, 263:114614, 4 2020. doi: 10.1016/j.apenergy.2020.114614. URL `https://doi.org/10.1016/j.apenergy.2020.114614`.

P.. Ball. A Review of Geothermal Technologies and Their Role in Reducing Greenhouse Gas Emissions in the USA. *Journal of Energy Resources Technology*, 143(1), 09 2020. ISSN 0195-0738. doi: 10.1115/1.4048187. URL `https://doi.org/10.1115/1.4048187`. 010903.

P. Bayer, G. Attard, P. Blum, and K. Menberg. The geothermal potential of cities. *Renewable and Sustainable Energy Reviews*, 106:17–30, 2019. ISSN 1364-0321. doi: https://doi.org/10.1016/j.rser.2019.02.019.

P.J. Bourne-Webb, T.M. Bodas Freitas, and R.A. da Costa Gonçalves. Thermal and mechanical aspects of the response of embedded retaining walls used as shallow geothermal heat exchangers. *Energy and Buildings*, 125:130–141, 2016. ISSN 0378-7788. doi: https://doi.org/10.1016/j.enbuild.2016.04.075.

H. Brandl. Energy foundations and other thermo-active ground structures. *Géotechnique*, 56 (2):81–122, 2006. ISSN 0016-8505.

Brugeo. Shallow geothermics. URL `https://geothermie.brussels/en/the-principles-of-geothermics/shallow-geothermics`.

CartesFrance. Carte du relief de rennes. `http://www.cartesfrance.fr/Rennes-35000/carte-Rennes.html`. Accessed: 2023-02-16.

S. A. Changnon. A rare long record of deep soil temperatures defines temporal temperature changes and an urban heat island. *Climatic change*, 42(3):531–538, 1999. ISSN 0165-0009.

C. Clauser and M. Ewert. The renewables cost challenge: Levelized cost of geothermal electric energy compared to other sources of primary energy – review and case study. *Renewable and sustainable energy reviews*, 82:3683–3693, 2018. ISSN 1364-0321.

ClimateData. Climat rennes (france). URL `https://fr.climate-data.org/europe/france/bretagne/rennes-343/#climate-table`. Accessed: 2023-04-04.

Multiphysics COMSOL. Reference manual. URL `https://doc.comsol.com/6.1/docserver/#!/com.comsol.help.comsol/helpdesk/helpdesk.html`.

A. Dassargues. *Hydrogéologie appliquée: science et ingénierie des eaux souterraines*. Dunod, 2020. ISBN 2100794345.

A. Di Donna, F. Emeriault, L. Demongodin, and J-F. Gobichon. Aspects géotechniques et énergétiques des géostructures thermoactivespplication à un cas d´étude réel. *Rev. Fr. Geotech.*, (164):4, 2020. doi: 10.1051/geotech/2021001.

A. Di Donna, F. Loveridge, M. Piemontese, and M. Barla. The role of ground conditions on the heat exchange potential of energy walls. *Geomechanics for Energy and the Environment*, 25:100199, 2021. ISSN 2352-3808. doi: https://doi.org/10.1016/j.gete.2020.100199.

Brussels environnement. La géothermie à Bruxelles, 2020. URL `https://environnement.brussels/pro/gestion-environnementale/renover-et-construire/la-geothermie-bruxelles`.

GIEC. Synthesis report of the ipcc sixth assessment report (ar6). *Géotechnique*, 2023.

P. Guiraud and B. Daubilly. Norme béton NF EN 206+A2/CN (2022) : classification des bétons, 2022.

L. Guo, L. Guo, L. Zhong, and Y. Zhu. Thermal conductivity and heat transfer coefficient of concrete. *Journal of Wuhan University of Technology-Mater. Sci. Ed.*, 26:791–796, 08 2011. doi: 10.1007/s11595-011-0312-3.

M. Hendel, P. Gutierrez, M. Colombert, Y. Diab, and L. Royon. Measuring the effects of urban heat island mitigation techniques in the field: Application to the case of pavement-watering in paris. *Urban climate*, 16:43–58, 2016. ISSN 2212-0955.

A. Iman, S. Payam, A. Hassan, Z. Fitri Bin, and M. Norhayati Binti. Thermal conductivity of concrete – a review. *Journal of Building Engineering*, 20:81–93, 2018. ISSN 2352-7102.

InfoTerre. Cartes géologiques. URL `https://infoterre.brgm.fr/page/cartes-geologiques`. Accessed: 2023-02-17.

A. Kawuwa Sani, R. Martand Singh, T. Amis, and I. Cavarretta. A review on the performance of geothermal energy pile foundation, its design process and applications. *Renewable and Sustainable Energy Reviews*, 106:54–78, 2019. ISSN 1364-0321. doi: https://doi.org/10.1016/j.rser.2019.02.008.

L Laloui and Rotta Loria A. F. Chapter 1 - energy and geotechnologies. In *Analysis and Design of Energy Geostructures*, pages 3–19. Academic Press, 2020. ISBN 978-0-12-820623-2. doi: https://doi.org/10.1016/B978-0-12-816223-1.00002-3.

L Laloui and A. F. Rotta Loria. Chapter 2 - energy geostructures. In *Analysis and Design of Energy Geostructures*, pages 25–65. Academic Press, 2020. ISBN 978-0-12-820623-2. doi: https://doi.org/10.1016/B978-0-12-816223-1.00002-3.

D. P. Nicholson, Q. Chen, and M. Pillai, A.and Chendorain. Developments in thermal pile and thermal tunnel linings for city scale gshp systems. 2013.

W. Noriaki and W. Koichi. Effective thermal conductivity of packed beds. *Journal of Chemical Engineering of Japan*, 2(1):24–33, 1969. doi: 10.1252/jcej.2.24.

S. Pinson and V. Bault. Profondeur des entités hydrogéologiques et évaluation des contraintes à l'infiltration des eaux pluviales urbaines sur le territoire de rennes métropole projet phoebus. rapport final. brgm/rp-68599-fr, 74., 45 ill., 3 ann. 2019.

RennesMétropole. Métro ligne b - Rennes Métropole - Accueil. URL http://www.metro-rennes-metropole.fr/accueil. Accessed: 2023-02-17.

P. Shafigh, P. Asadi, and N. Binti Mahyuddin. Concrete as a thermal mass material for building applications - a review. *Journal of Building Engineering*, 19:14–25, 2018. ISSN 2352-7102. doi: https://doi.org/10.1016/j.jobe.2018.04.021.

Bretagne SIGES. Thermetrennes. URL https://sigesbre.brgm.fr/THERMETRENNES-Suivi-et-analyse-du-comportement-energetique.html. Accessed: 2023-05-08.

K. Soga and Y. Rui. Energy geostructures. In Simon J. Rees, editor, *Advances in Ground-Source Heat Pump Systems*, pages 185–221. Woodhead Publishing, 2016. ISBN 978-0-08-100311-4. doi: https://doi.org/10.1016/B978-0-08-100311-4.00007-8.

Terrasol. Tout / station cleunay geotechnique note d'hypothèses géotechniques, 2015.

D. Waboso and M. Gilbey. Cooling the tube. *Tunnels and Tunnelling International*, pages 36–39, 2007.

W. Wei, Li. Xianting, and Y. Tian. *Absorption Heating Technologies: Efficient Heating, Heat Recovery and Renewable Energy*. Springer Singapore Pte. Limited, Singapore, 2019. ISBN 9789811504693.

J. Zannin, A. Ferrari, M. Pousse, and L. Laloui. Hydrothermal interactions in energy walls. *Underground Space*, pages 1–12, 2020.

Appendix A

Annexes

A.1 Piezometric survey campaign A1SC12

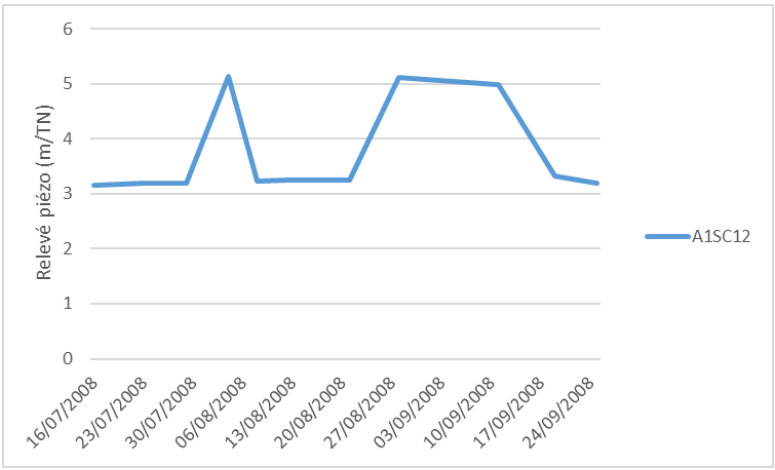

Figure A.1 – Piezometric height in the A1SC12 during 70 days

A.2 Log of a drilling close to the Cleunay station

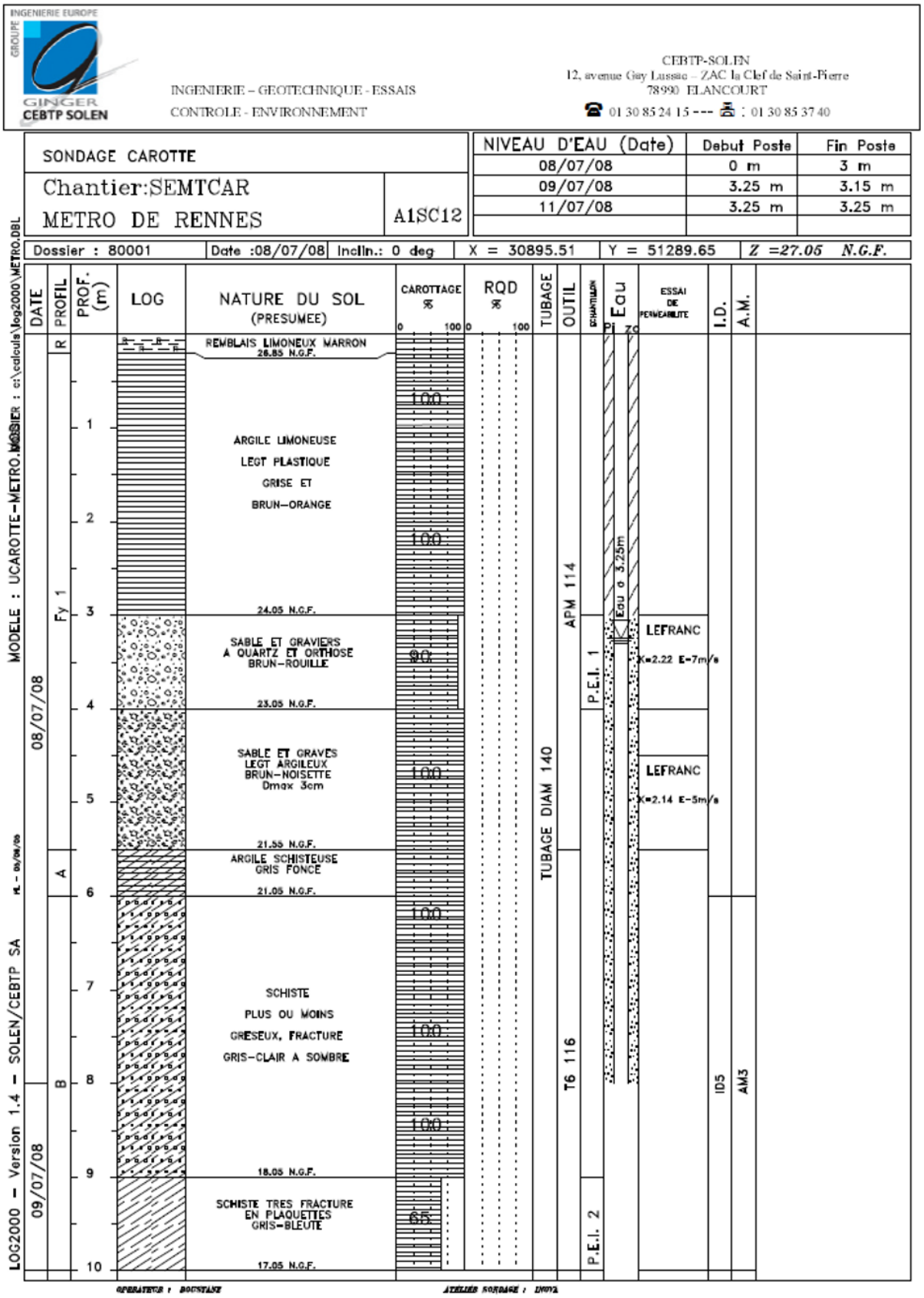

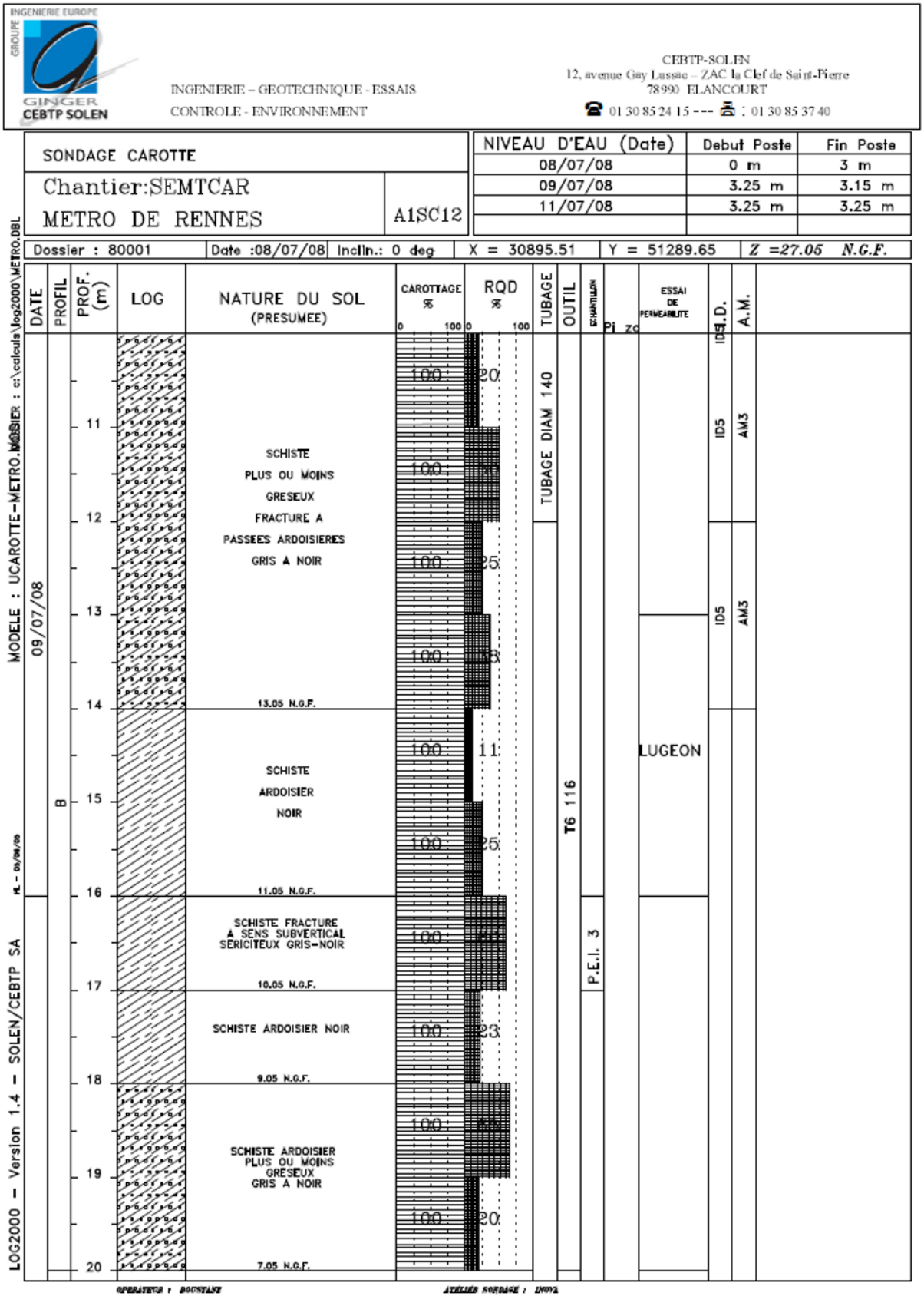
INGENIERIE EUROPE
GROUPE
GINGER
CEBTP SOLEN
INGENIERIE – GEOTECHNIQUE - ESSAIS
CONTROLE - ENVIRONNEMENT
CEBTP-SOLEN
12, avenue Guy Lussac – ZAC la Clef de Saint-Pierre
78990 ELANCOURT
01 30 85 24 15 --- 01 30 85 37 40
SONDAGE CAROTTE
Chantier:SEMTCAR
METRO DE RENNES
A1SC12
NIVEAU D'EAU (Date)
Debut Poste
Fin Poste
08/07/08
0 m
3 m
09/07/08
3.25 m
3.15 m
11/07/08
3.25 m
3.25 m
Dossier : 80001
Date :08/07/08
Incl.: 0 deg
X = 30895.51
Y = 51289.65
Z =27.05 N.G.F.
DATE
PROFIL
PROF. (m)
LOG
NATURE DU SOL (PRESUMEE)
CAROTTAGE %
RQD %
TUBAGE
OUTIL
ECHANTILLON
Pi
Qc
ESSAI DE PERMEABILITE
I.D.
A.M.
MODELE : UCAROTTE-METRO.MODELE : c:\calculs\log2000\METRO.DBL
LOG2000 – Version 1.4 – SOLEN/CEBTP SA
09/07/08
B
SCHISTE PLUS OU MOINS GRESEUX FRACTURE A PASSEES ARDOISIERES GRIS A NOIR
13.05 N.G.F.
SCHISTE ARDOISIER NOIR
11.05 N.G.F.
SCHISTE FRACTURE A SENS SUBVERTICAL SERICITEUX GRIS-NOIR
10.05 N.G.F.
SCHISTE ARDOISIER NOIR
9.05 N.G.F.
SCHISTE ARDOISIER PLUS OU MOINS GRESEUX GRIS A NOIR
7.05 N.G.F.
TUBAGE DIAM 140
T6 116
P.E.I. 3
LUGEON
ID5
AM3
OPERATEUR : BOUSTAINE
ATELIER SONDAGE : LYON

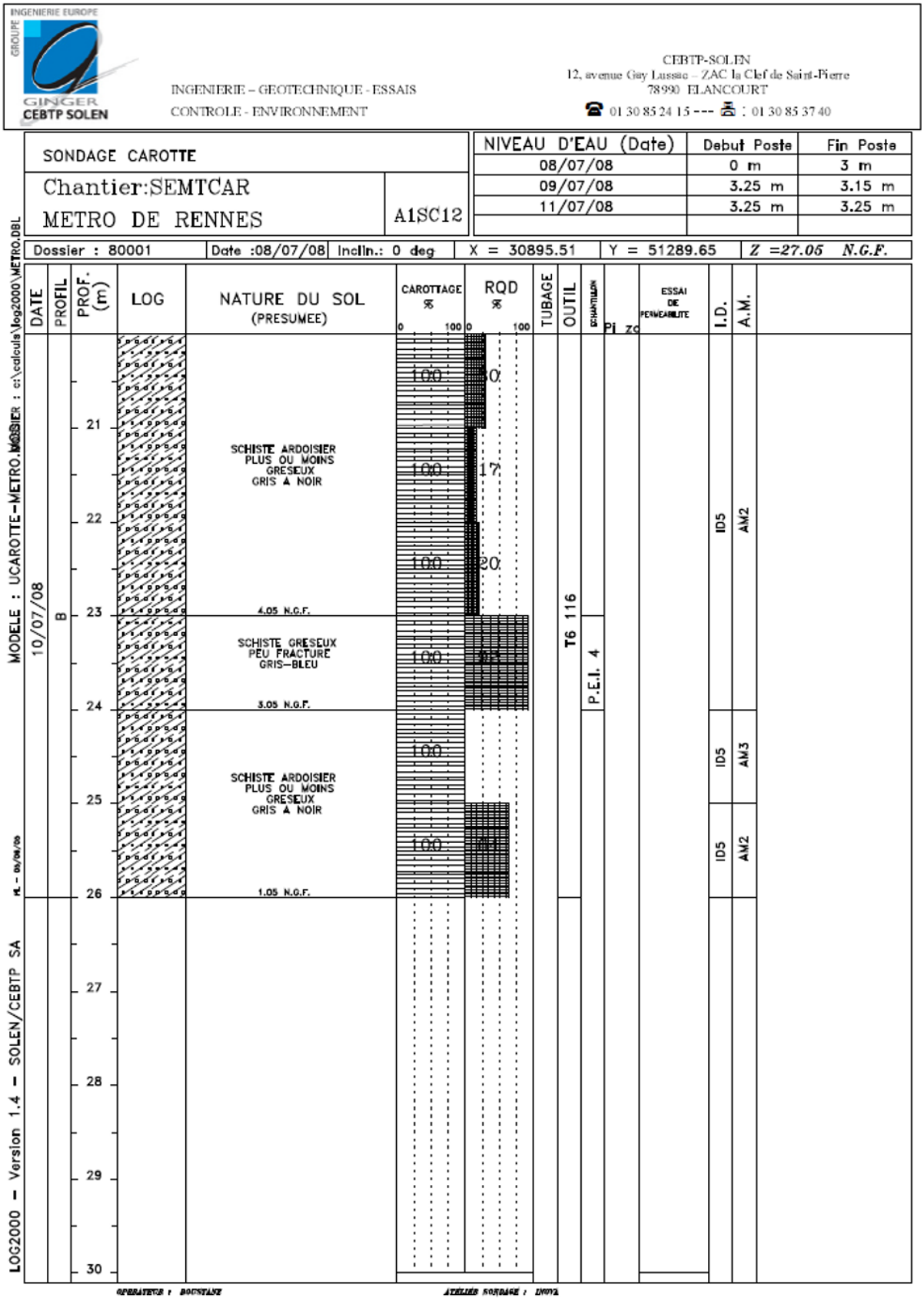
INGENIERIE EUROPE
GROUPE
GINGER
CEBTP SOLEN
INGENIERIE – GEOTECHNIQUE - ESSAIS
CONTROLE - ENVIRONNEMENT
CEBTP-SOLEN
12, avenue Guy Lussac – ZAC la Clef de Saint-Pierre
78990 ELANCOURT
01 30 85 24 15 --- 01 30 85 37 40
SONDAGE CAROTTE
Chantier:SEMTCAR
METRO DE RENNES
A1SC12
NIVEAU D'EAU (Date)
Debut Poste
Fin Poste
08/07/08
0 m
3 m
09/07/08
3.25 m
3.15 m
11/07/08
3.25 m
3.25 m
Dossier : 80001
Date :08/07/08
Inclin.: 0 deg
X = 30895.51
Y = 51289.65
Z =27.05 N.G.F.
DATE
PROFIL
PROF. (m)
LOG
NATURE DU SOL (PRESUMEE)
CAROTTAGE %
RQD %
TUBAGE
OUTIL
ECHANTILLON
Pi
Zc
ESSAI DE PERMEABILITE
I.D.
A.M.
10/07/08
B
SCHISTE ARDOISIER PLUS OU MOINS GRESEUX GRIS A NOIR
4.05 N.G.F.
SCHISTE GRESEUX PEU FRACTURE GRIS–BLEU
3.05 N.G.F.
SCHISTE ARDOISIER PLUS OU MOINS GRESEUX GRIS A NOIR
1.05 N.G.F.
T6 116
P.E.I. 4
ID5
AM2
ID5
AM3
ID5
AM2
MODELE : UCAROTTE-METRO.MDB
FICHIER : c:\calculs\log2000\METRO.DBL
LOG2000 – Version 1.4 – SOLEN/CEBTP SA
OPERATEUR : BOUTAHAR
ATELIER SONDAGE : INOVA

A.3 Summary of the differences between the theoretical lengths provided and the lengths laid down in the model

Cage	Width(m)	Height (m)	Area (m^2)	(m) length loop	Vertical pipe	Model (m)
C01	3.3	11.3	37.29	93.225	8	93.9
C02A	2.45	11.3	27.685	69.2125	6	70.05
C02B	2.5	11.3	28.25	70.625	6	70.575
C03	3.6	11.3	40.68	101.7	8	93.55
C04	3.25	11.3	36.725	91.8125	8	94.285
C04	3.25	11.3	36.725	91.8125	8	94.285
C04	3.25	11.3	36.725	91.8125	8	94.285
C04A	3.25	11.3	36.725	91.8125	8	94.285
C04B	3.25	11.3	36.725	91.8125	8	94.285
C04B	3.25	11.3	36.725	91.8125	8	94.285
C05	3.2	11.3	36.16	90.4	8	93.55
C05	3.2	11.3	36.16	90.4	8	93.55
C05	3.2	11.3	36.16	90.4	8	93.55
C05A	3.2	11.3	36.16	90.4	8	93.55
C05B	3.2	11.3	36.16	90.4	8	93.55
C05B	3.2	11.3	36.16	90.4	8	93.55
C06	3.7	11.3	41.81	104.525	8	93.55
C07	2.85	11.3	32.205	80.5125	6	71.3
C08	2.2	11.3	24.86	62.15	6	70.3
C08	2.2	11.3	24.86	62.15	6	70.3
C09	3.2	11.9	38.08	95.2	8	97.65
C09	3.2	11.9	38.08	95.2	8	97.65
C09A	3.2	11.9	38.08	95.2	8	98.35
C09A	3.2	11.9	38.08	95.2	8	98.35
C10	2.45	10.9	26.705	66.7625	6	67.65
C10A	2.45	10.9	26.705	66.7625	6	67.65
C10B	2.45	10.9	26.705	66.7625	6	67.15
C11	3.7	10.9	40.33	100.825	8	90.7
C12	3	10.9	32.7	81.75	6	68.9
C12	3	10.9	32.7	81.75	6	68.9
C13	2.85	10.9	31.065	77.6625	6	68.25
C13	2.85	10.9	31.065	77.6625	6	68.25
C14	3.65	10.9	39.785	99.4625	8	91.19
C15	3.25	12.3	39.975	99.9375	8	100.5
C15	3.25	12.3	39.975	99.9375	8	100.5
C15A	3.25	12.3	39.975	99.9375	8	100.5
C15B	3.25	12.3	39.975	99.9375	8	100.5
C16A	2.45	12.3	30.135	75.3375	6	75.9
C16B	2.45	12.8	31.36	78.4	6	78.8
C16C	2.45	12.3	30.135	75.3375	6	75.3375
C18	3	12.3	36.9	92.25	8	101.2
C19	3.2	12.3	39.36	98.4	8	101.55
C19A	3.2	12.3	39.36	98.4	8	101.55
C20	2.5	12.3	30.75	76.875	8	101.55

A.4 Comparison of measured and smoothed data

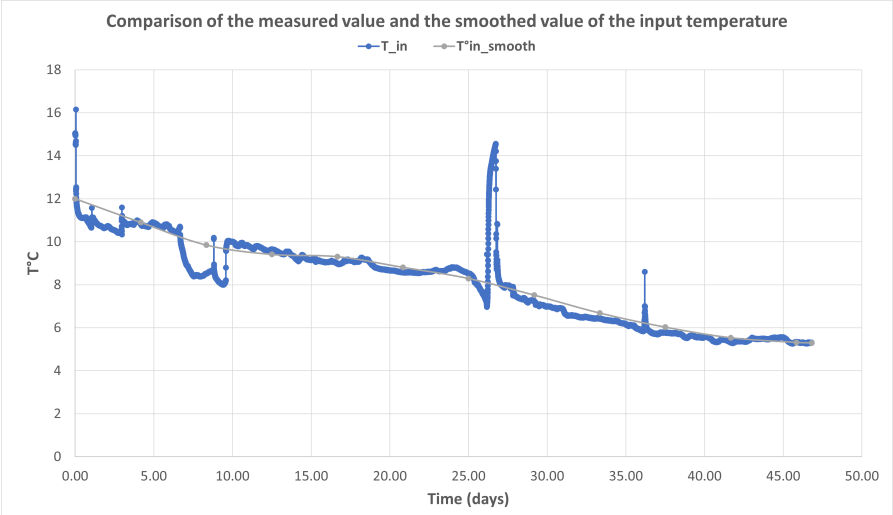

Figure A.2 – Input temperature recorded and smoothed

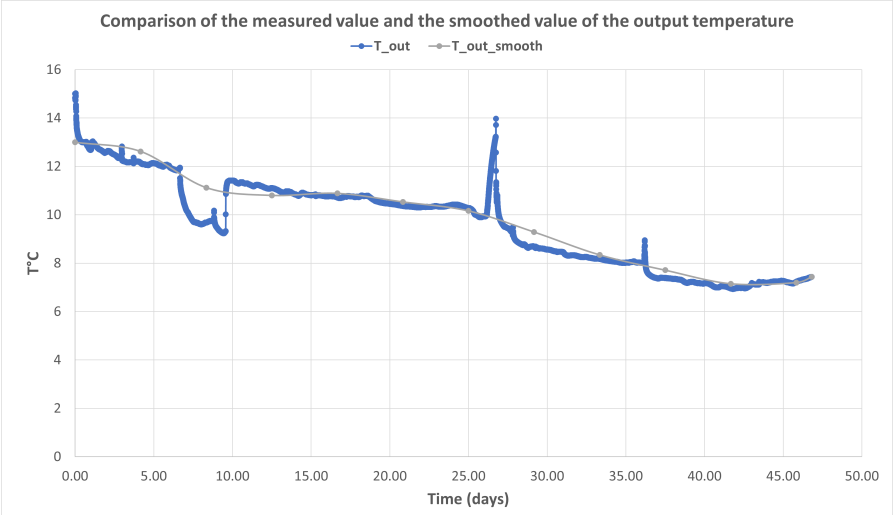

Figure A.3 – Output temperature recorded and smoothed

A.5 Temperature distribution in the station after heating a school

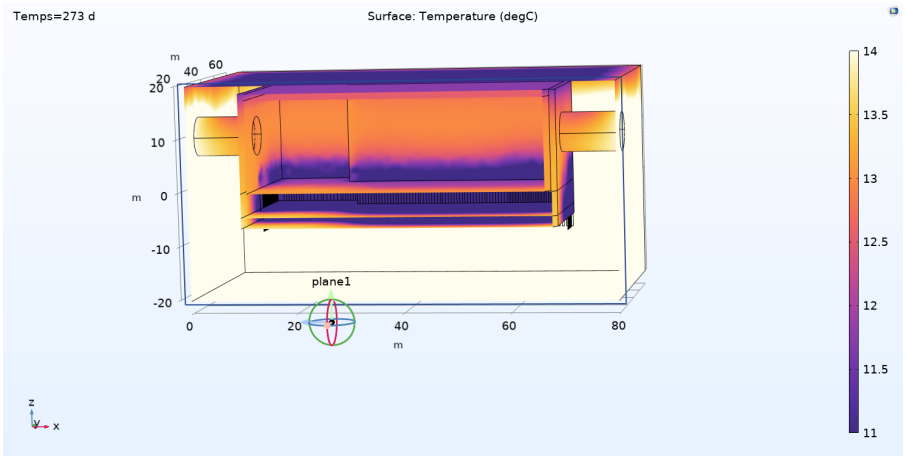

Figure A.4 – After the heating period

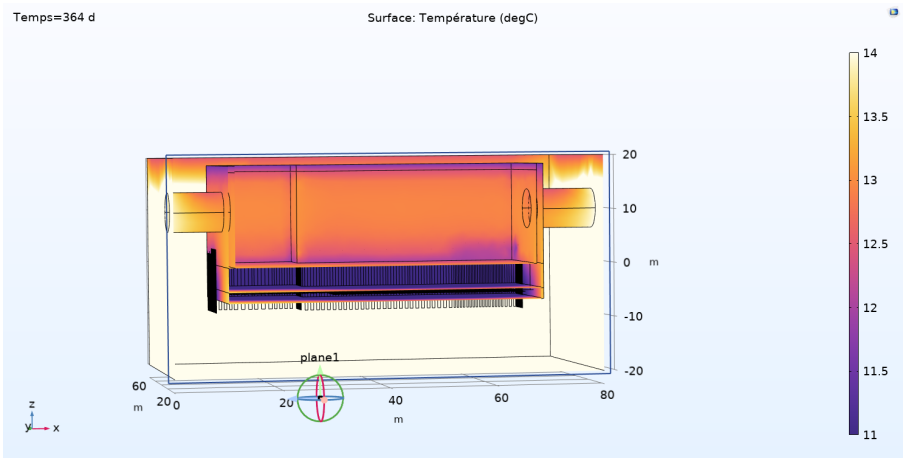

Figure A.5 – After the rest period without free cooling

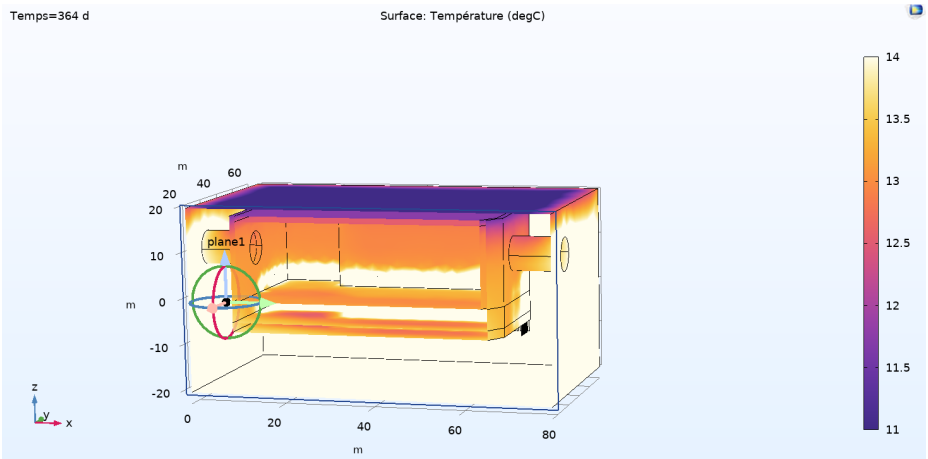

Figure A.6 – After the rest period using geocooling